Università degli Studi di Ferrara

DOCTORAL COURSE IN
CHEMICAL SCIENCES

CYCLE XXXVII

COORDINATOR Prof. Alessandro Massi

LIPID-BASED NANOSYSTEMS: GREEN NANOTECHNOLOGIES FOR PHYTOCOMPOUNDS TOPICAL ADMINISTRATION

Scientific/Disciplinary Sector (SDS) CHIM/09

Candidate
Dott. Bondi Agnese

_____
(signature)

Supervisor
Prof. Esposito Elisabetta

_____
(signature)

Year 2021/2024

UNIONE EUROPEA
Fondo Sociale Europeo

Ministero dell'Università e della Ricerca

PON RICERCA E INNOVAZIONE 2014 - 2020

REACT EU

CONTENTS

1. INTRODUCTION

1.1. SKIN STRUCTURE

The skin is the outermost epithelial tissue which forms an effective barrier between the body and the environment, preventing the invasion of pathogens and repelling chemical and physical aggressions, as well as avoiding the loss of water and solutes [1]. In addition, the skin has a role in homeostasis, regulating body temperature and blood pressure and acts as an important sensory organ [2]. Skin's stratified structure is organised in three main layers: epidermis, dermis and subcutaneous tissue or hypodermis (Figure 1).

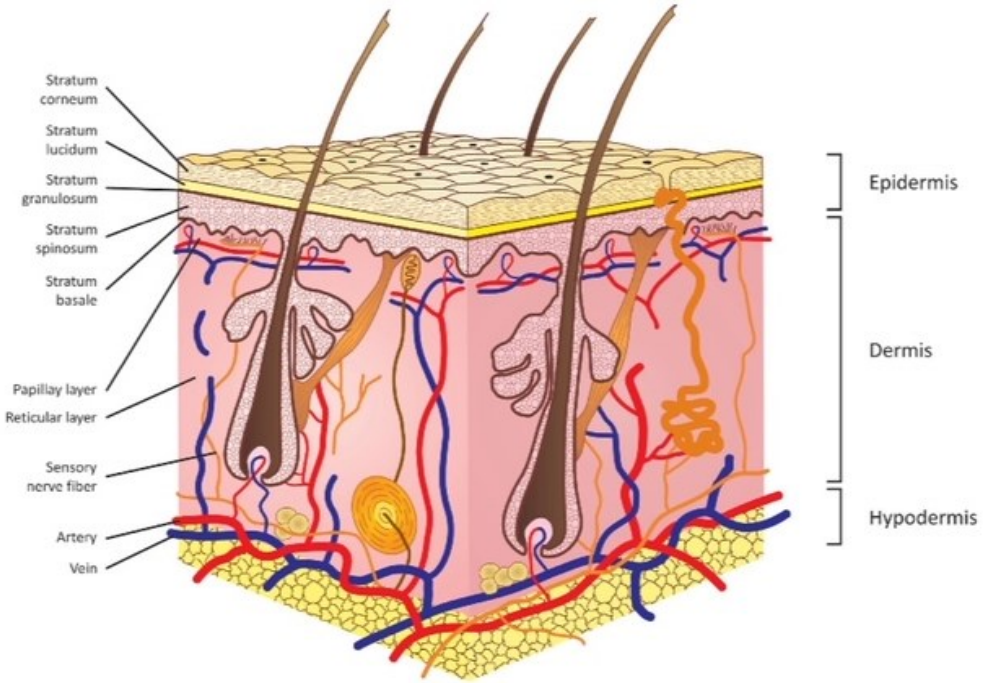

Figure 1. Schematic representation of skin structure [3].

1.1.2. EPIDERMIS

The epidermis is the outermost layer, exposed to the external environment. It is a stratified squamous keratinized epithelium, organized in different layers. Starting from the inside towards the surface of skin, these layers are: the *stratum basale*, *stratum spinosum*, *stratum granulosum*, *stratum lucidum* (not present in thin skin), and *stratum corneum* [4]. The principal cell type within the epidermis is the keratinocyte, and the different epidermal layers represent the differentiation of the keratinocytes proceeding from the deepest to the superficial layers [5]. During their differentiation, keratinocytes lose their nucleus and cytoplasmatic organelles, their cytoplasm becomes filled with keratin filaments and layers

of insoluble proteins and lipids are arranged on the inner surface of the plasma membrane to form a cornified lipid envelope [6].

Other less-abundant and nonepithelial cells are the melanin-producing melanocytes, tactile Merkel cells and antigen-presenting Langerhans cells [4].

Stratum basale or *stratum germinativum* is composed of stem cells called basal cells, which divide to form keratinocytes then begin migrating superficially, contributing to epidermal renewal. Renewal of epidermis takes 15 to 30 days, and it is influenced by age, region of the body, and other factors [4]. The next layer is the *stratum spinosum*, the thickest layer of epidermis, whose name derives from the fact that keratinocytes in this layer form intercellular attachments via protein channels called desmosomes. The attachments are responsible for this layer's spiny appearance beneath the microscope [5]. Cells contain nuclei, and the production of tonofilaments increases. These tonofilaments cluster together into bundles, forming tonofibrils as the cells migrate towards the surface [4]. Proceeding towards the surface we find the *stratum granulosum*, so called because of the keratohyalin granules visible in the cytoplasm [5]. These granules consist of filaggrin and other proteins related to the keratins of the tonofibrils. The cells are flattened and still have nuclei. In addition, small lamellar granules (lamellar bodies) are present in the cytoplasm, whose lipid content is released by exocytosis into the extracellular space. The lipids derived from the lamellar bodies are subsequently modified and rearranged into intercellular lamellae positioned approximately parallel to the cell surface [4,7]. The *stratum lucidum*, whose name derives by its translucent appearance under a microscope, is visible only in area of thick skin. It consists in a thin layer of extremely flat, highly refractive eosinophilic cells with thick cell membranes and rarely visible nuclei [4]. Finally, there is the *stratum corneum*, which, although only 10-15 cells deep, acts as the skin's primary barrier [2]. Here, keratinization is completed and cells, the so called "corneocytes", are flat and anucleate; their cytoplasm is filled with keratin filaments and surrounded by a cornified envelope. Corneocytes are embedded in a hydrophobic matrix composed of a mixture of lipids (ceramides, free fatty acids, cholesterol and cholesterol esters) arranged in multiple lamellar layers. Its function is to counteract the loss of water and salts from the skin and avoid the penetration of hydrophilic substances [7]. The *stratum corneum* structure has been described as a brick wall in which the corneocytes represent the "bricks" in a matrix (or "mortar") of intercellular lipids, and the desmosomes acts as molecular rivets between the cells [2]. *Stratum corneum* physical and biochemical properties enables it to protect the underlying living layers from chemical and physical injuries and attack by microorganisms. Additionally, these properties

permit selective absorption of compounds and the prevention of excessive loss of water from the body [6].

1.1.3. DERMIS

The dermis lies between the epidermis and subcutaneous tissue. It is a layer of connective tissue that, unlike the epidermis, is highly vascularized and provided with a network of lymphatic vessels. Several structures and appendages are found or originate in this site, including hair follicles, nerve endings sweat and sebaceous glands [2]. The dermis is about 2 – 5 mm in thickness and consists mainly of collagen and elastin fibrils that provide support and elasticity embedded within a mucopolysaccharide matrix. It can be divided in two indistinct layers: the superficial one is the papillary layer, and the deeper one is the reticular layer [4]. The primary cell type are fibroblasts, responsible for the synthesis and the renewal of extracellular matrix [7] but there are also mast cells involved in immune and inflammatory response, and melanocytes responsible for pigment production [2].

1.1.4. SUBCUTANEOUS TISSUE

The subcutaneous tissue or hypodermis is the deepest layer, which in most cases consists largely of adipose tissue. It is attached to the deep fascia or periosteum and provides thermal insulation, protection from mechanical insults and acts as energy storage [4,7].

1.2. TOPICAL DRUG DELIVERY

The topical application of substances on the surface of the skin for therapeutic purposes has a very ancient history. Nowadays, there is a very wide variety of products on the market for the topical application of active molecules designed to have a local or systemic action. Specifically, skin delivery can be classified into two types: dermal and transdermal drug delivery [8]. Dermal delivery involves administering a drug directly onto the skin, which is also the site of action, increasing the local concentration of the drug while reducing systemic undesired effects. In contrast, in the case of the transdermal delivery, the active compound is intended to reach the bloodstream and be absorbed and then exert a systemic activity.

Dermal and transdermal ways of administration represent interesting alternatives to the conventional oral route. In fact, it is possible to avoid problems such as first-pass metabolism, adverse gastrointestinal environment, side effects and poor patient compliance, as well as allowing, in many cases, a prolonged release of the drug [2,9].

However, the skin, as an effective barrier, represents a challenge for scientists who work in the field of transdermal drug delivery. Precisely, *stratum corneum* is the main responsible for the barrier properties of human skin and for this reason limits drug transition through the skin [10,11]. Moreover, there are a number of physiological factors that can influence the characteristics of the skin barrier and thus its permeability. These include age, ethnicity, gender, anatomical site of application and skin disorders [2].

It is important to consider that, in order to reach the systemic circulation, it is sufficient for the active compound to reach the dermis, a richly vascularised area where most of the molecules that pass through the outer epidermis are rapidly diluted and transported away by the bloodstream. This washout allows to maintain a concentration gradient which represents the driving force for drug delivery through the skin [10].

1.2.1. ROUTES THROUGH THE EPIDERMIS

A molecule applied to the skin surface has three main ways to cross the epidermis: through the skin appendages or across the continuous *stratum corneum*, which can occur via transcellular or intercellular route (Figure 2).

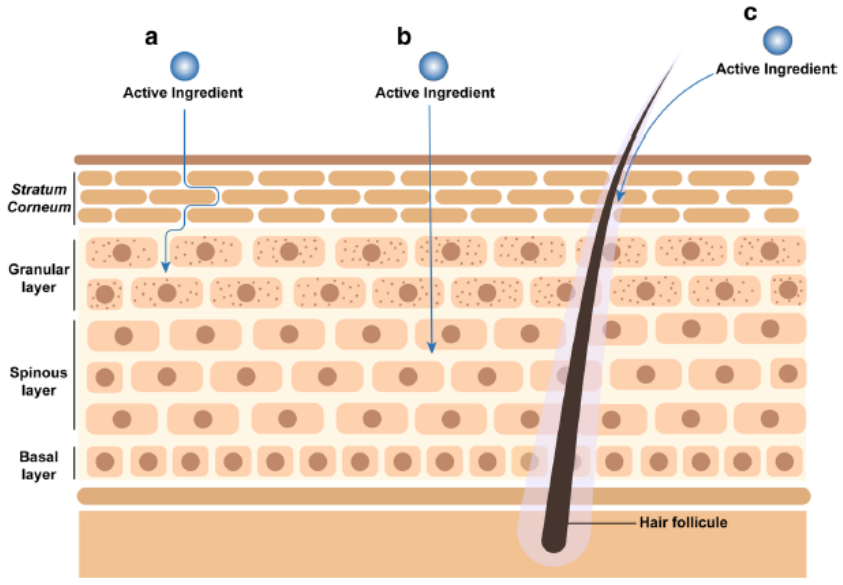

Figure 2. Illustration of the three main pathways of active compounds through the epidermis: (a) intercellular route, (b) transcellular route and (c) appendageal/follicular route [12].

The appendageal route is based on crossing the epidermis via skin appendages such as hair follicles or sweat glands. In this case molecules will partition into sweat or sebum before diffusing against the outflow from the glands. Although this pathway represents a potential preferential route through the epidermis, sweat glands are filled with aqueous sweat and the follicular glands with lipoidal sebum; moreover, the area these structures occupy on the

surface of the skin is relatively small (0.1-1%). This route is particularly interesting for the delivery of nanosystems to hair follicles, where they could accumulate drugs and release them into the systemic bloodstream [8].

The transcellular route involves passing the molecule through the corneocytes of the *stratum corneum*. Specifically, it first requires the molecule to partition into the polar environment of the corneocytes, whose cytoplasm is filled with keratin. It then diffuses through them and partitions into the intercellular lipid bilayers. Therefore, crossing essentially requires a repeated partitioning between the polar environment of the corneocytes and the lipophilic domains surrounding the corneocytes [2,10].

Lastly, the intercellular route requires the molecule to partition into the lipid bilayers of the extracellular domain between the corneocytes, and then diffuse via a tortuous direction across the mortar of the "brick wall" [10].

It must be taken into account that these pathways are not mutually exclusive, as most compounds likely penetrate the skin through a combination of these routes, with the contribution of each pathway depending on the physicochemical characteristics of the permeant molecule [2].

1.2.2. FACTORS AFFECTING THE PERMEATION

The permeation process involves several stages: it begins with the release of the active molecule from the vehicle, followed by its diffusion through the *stratum corneum*. Subsequently, the molecule crosses the aqueous environment of the viable epidermis and can be absorbed into the blood circulation. Certainly, all of these steps are highly dependent on the solubility and diffusivity of the permeant within each environment. Additionally, as mentioned before, the characteristics and condition of the skin, including its hydration, can influence the ability of a molecule to be absorbed.

Due to the predominantly hydrophobic nature of the *stratum corneum*, more lipophilic compounds are expected to cross it more easily than hydrophilic molecules. However, they may encounter difficulties in crossing the aqueous layers of the living epidermis or the hydrophilic domains of extracellular matrix of *stratum corneum*. Ideally, the partition coefficient (log P) should be in the range from 1 to 4, even if it is observed that some more lipophilic molecules, can also be effectively delivered [10].

Another relevant parameter is the size of the molecule. As a general principle, permeants selected for topical and transdermal administration generally tend to be less than 500 Da.

This “500 Dalton rule” is based on the fact that all common contact allergens and pharmacological compounds applied on the skin show a molecular weight under 500 Da [13].

In addition, drugs applied to the transdermal route of administration should have a melting point below 200 °C and not be irritating or immunogenic [14].

Hence the extent to which the transdermal route of administration is still prohibitive for many active molecules [15].

From a technological point of view, several strategies have been used to facilitate the penetration of an active compound across the skin barrier. These include not only traditional formulations like creams, ointments, or gels but also, for example, transdermal patches. Nevertheless, the active compunds that are appropriate for this type of administration must have a low molecular weight, be lipophilic, and be effective at low doses [15]. Moreover, there is a second generation of transdermal delivery systems which include the use of chemical penetration ehnancers or physical methods enhancing the skin permeability like iontophoresis and non-cavitational ultrasound. In addition, new transdermal technologies such as microneedles, thermoablation, microdermabrasion, electroporation and cavitational ultrasound have been developed [13,15].

However, although effective, many of these methods are still invasive as they are associated with skin irritation or pain, so they do not guarantee adequate patient acceptability [6]. For this reason, nanoparticulate drug delivery systems have shown great potential for dermal and transdermal drug delivery over the past years [8].

1.3. LIPID-BASED NANOSYSTEMS

Nanotechnology-based products are becoming increasingly relevant in the medical field, both for diagnostic and therapeutic applications [16,17] due to their ability to improve bioavailability of drugs and enable the delivery of active compounds that would otherwise not be usable in therapy. They also offer the opportunity to reduce the invasiveness of certain treatments and minimise side effects [14]. In general, they represent innovative delivery systems designed to overcome the limitations associated to traditional pharmaceutical forms and make therapies more effective and acceptable to patients.

Nanocarriers employed for drug delivery include: polymer-based nanoparticles, solid nanoparticles (such as iron oxide, gold, silver and other metal-based nanoparticles), carbon-based nanoparticles (i.e. carbon nanotubes), lipid-based nanoparticles, nanovesicles, nanoemulsions [17].

Among these, lipid-based nanosystems are of particular interest. First of all, because of their composition: essentially based on biocompatible and biodegradable lipids, they are able to prevent unwanted toxicity or accumulation phenomena. They also offer a number of advantages, including effectiveness in encapsulating lipophilic-poor soluble molecules as well as, in most cases, hydrophilic drugs. Besides, they are able to achieve a controlled release of the drug and to protect it against environmental degradation. Furthermore, the lipid composition is particularly suitable for topical application, due to its similarity to the intercellular lipids of the *stratum corneum* [6,11,18,19]. In addition, their occlusive effect increases the hydration and elasticity of the skin, facilitating drug permeation [8].

In addition, the use of natural, biocompatible and biodegradable lipids not only reduces the potential occurrence of adverse effects, but they can also be included in the "green economy", a sustainable approach for both producers and consumers [18]. Moreover, the production methods generally do not involve the use of toxic organic solvents and high energy, in accordance with the intention of reducing energy consumption and making production more sustainable on an industrial level.

Depending on the kind of nanosystem and its composition, it is possible to design lipid-based nanosystems to treat different skin disorders [8]. Specifically, lipid-based nanosystems comprise a wide variety of nanoplatforms, differing in composition and architecture, which are also closely dependent on the method of preparation. Particularly, lipid-core micelles, nanoemulsions, nanovesicles such as liposomes, transferosomes, ethosomes, transethosomes, or niosomes, and also nanoparticles, including solid lipid nanoaprticles, nanostructured lipid carriers, monoolein-based systems and cubosomes [13,18].

In the present doctorate project, three of these delivery systems were investigated more specifically: ethosomes, transethosomes and spongosomes.

1.3.1. ETHOSOMES AND TRANSETHOSOMES

Ethosomes (ET) are vesicular drug delivery systems which have been described for the first time by Touitou et al in 2000 [20] in order to overcome the limitations of conventional liposomes in delivering active compounds through the skin. Liposomes are nanovesicular

carriers typically composed of natural phospholipids such as lecithins, main constituent of most biological membranes, which have the ability to spontaneously self-assemble in aqueous media and to form bilayers delimiting aqueous compartments [11]. They have been extensively studied since the 1960s due to their advantageous characteristics for drug delivery. However, the potential of liposomes as a transdermal delivery system is limited by their inability to reach the deeper layers of the skin. In fact, the vesicles are supposed to remain relegated to the more superficial layers where, thanks to their affinity with the lipids of the *stratum corneum*, they can fuse and form a depot from which the active compounds are gradually released [19,21,22]. Some studies demonstrated that intact liposomes can reach the deeper layers only through skin appendages (hair follicles and sweat glands) [6,11]. Moreover, the use of liposomes is also limited by instability problems related to their constituents, which are based on phospholipids prone to oxidation and bilayer breakage, resulting in phase separation [13].

ET can therefore be considered as a second generation of liposomes, whose composition contains a high percentage of ethanol (20-45%), in addition to phospholipids and water. Ethanol exerts various effects on the physicochemical properties of ET: (i) it reduces vesicles size, (ii) it enhances the stability and flexibility with respect to classic liposomes, (iii) it increases the entrapment efficiency of both hydrophilic and lipophilic compounds, furthermore, (iv) it contributes to a negative surface charge to the system, preventing the vesicles aggregation and drug leakage [11,18,23]. The presence of ethanol is also crucial to allow penetration through the skin towards the deepest layers, not only because it greatly increases the flexibility and elasticity of the vesicles, as mentioned above, but also because of its well-known penetration enhancer behaviour, which synergizes that of phospholipids [12]. For these features, ET can be considered as transdermal vehicles, able to pass through *stratum corneum* and to reach the lower skin strata up to derma [13].

ET are effective in delivering both hydrophilic and lipophilic drugs under occlusive and non-occlusive conditions. Regarding drug arrangement in the molecular ultrastructure, it is assumed that the hydrophilic active compounds remain within the aqueous core, while the amphiphilic and lipophilic ones interact and intercalate within the lipid bilayer [12,22] as shown in Figure 3.

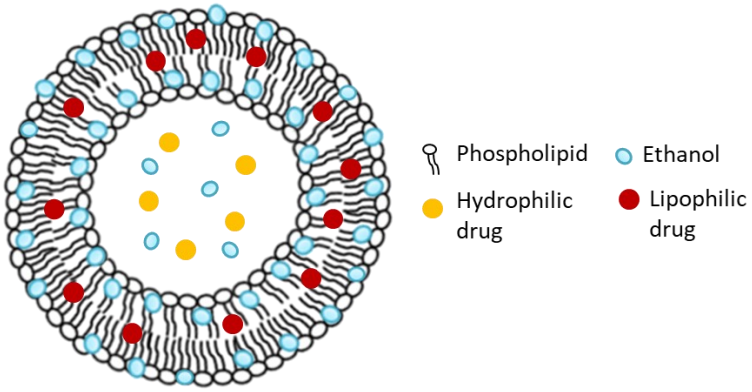

Figure 3. Schematic representation of the ethosomal vesicle showing the arrangement of active compounds according to their characteristics.

Transethosomes (TE) are a second generation of ET, first produced by Song et al. in 2012 [24] to further increase the permeability of nanovesicles, combining the advantages of ET with those of transferosomes. In the case of TE, the composition is enriched by the presence of an edge activator which can further increase the penetration ability, making the vesicles even more malleable than ET [6]. Edge activators may be glycerol or surfactants, molecules capable of intercalating in the lipid bilayer of the vesicle and altering its packing. This results in variations in terms of size, permeability and flexibility of the nanovesicles, which may also depend on the nature as well as the concentration of the edge activator [24,25].

Figure 4 schematically shows the comparison between ET and TE.

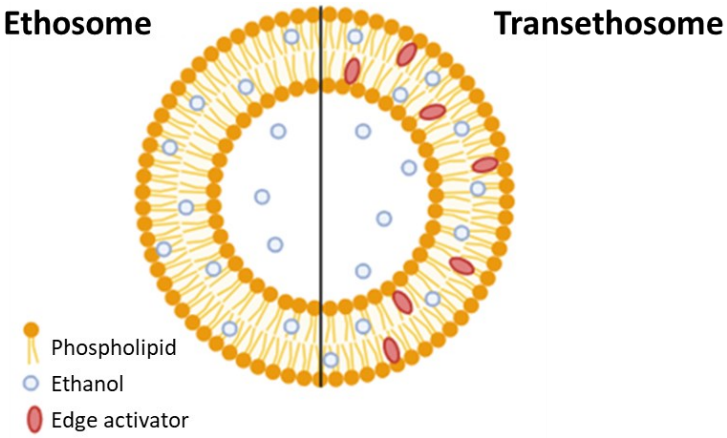

Figure 4. Schematic representation of ET and TE structure.

The mechanism of ET and TE penetration through the skin is still being studied. As anticipated, a key role is certainly played by the synergism between ethanol and the phospholipids, both acting as penetration enhancers. Touitou and colleagues suggested a penetration mechanism in which ethanol first disrupts the organisation of *stratum corneum* lipids, increasing its fluidity and permeability. Thus, ethosomal nanovesicles, made flexible

by the presence of ethanol, are able to penetrate through the lipid bilayers of the *stratum corneum*. Finally, in the deeper skin layers, the release of the drug occurs, due to the fusion of the nanovesicles with the skin lipids [20].

Recent works by Costanzo et al. [26] and Sguizzato et al. [25] have shown that both ET and TE can be found intact within the cytoplasm of different cell types (i.e. fibroblast, keratinocytes, myoblasts), without alteration in cell organelles, confirming good biocompatibility. Moreover, nanovesicles were never observed inside endosomes, suggesting that the cellular uptake does not take place by endocitic process. Internalisation can be assumed to occur by virtue of the vesicles' affinity for the plasma membrane and the penetration enhancer action of ethanol, which is able to disorder the plasmalemma region making contact with the nanocarrier, allowing the passage inside the cytoplasm. Transmission electron microscopy images also showed how nanovesicles are degraded following physiological pathways and, above all, how TE undergo more rapid degradation than ET, evidenced by an accumulation of lipid droplets in the cytoplasm. This phenomenon is a consequence of the presence of the edge activator (Tween 80 in the case of the study), which significantly affects the packing of the bilayer, making it more susceptible to cellular elimination pathways.

In addition, in recent work by Esposito et al. [27] ET and TE were tested through an ex vivo model consisting of human skin biopsies kept in a specific bioreactor able to maintain physiological conditions. Here again, the ability of the nanovesicles to penetrate through the skin is explained by virtue of their affinity for the intercellular lipids of the *stratum corneum* and the presence of ethanol, which makes them flexible and acts as a penetration enhancer. Entry into cells is hypothesised to occur by ethanol-mediated fusion. This study also evidenced the ability of ET to reach the deeper layers of the skin (papillary dermis) intact, while TE remained in the upper layers, probably undergoing faster degradation. Thus, the study showed that the ability to penetrate depends not only on the size and deformability of the nanoplatform, but also on its susceptibility to degradation pathways. Furthermore, it has been shown that nanovesicles cross the *stratum corneum* by the intercellular route and even penetrate the corneocytes, whereas the living layers of the epidermis are crossed mainly by the transcellular route. For this reason, the vesicles most susceptible to degradation are unable to reach the deep layers intact.

In the light of these findings, it is clear that the choice of ET or TE as a vehicle for active compounds must depend on the type of skin pathology to be addressed [27].

1.3.2. GLYCERYL MONOOLEATE LIQUID CRYSTALLINE PHASES – SPONGOSOMES

Glyceril monooleate (GMO) is a biodegradable and non-toxic unsaturated monoglyceride, classified as GRAS (generally recognized as safe) and it is included in the FDA Inactive Ingredients Guide [28]. Its structure consists in a long hydrophobic chain with a *cis* double bond at carbon 9 attached to a glycerol backbone by an ester that forms a polar head group (Figure 5A). This gives to GMO amphiphilic properties that allow the molecules to self-assemble in water into different liquid crystalline structures under varying conditions of temperature and concentration, known as "thermotropic" and "lyotropic" phases, respectively [29]. This aggregation is driven by the hydrophobic effect, which acts to minimise the interface between the hydrocarbon tails of the amphiphile and water [28,29]. In particular, once the concentration is equal to or greater than the critical micellar concentration, and the temperature is greater than the critical micellar temperature, amphiphilic molecules aggregate in water and give rise to micelles, spherical aggregates. [29]. As the concentration increases, more complex and ordered three-dimensional structures can be originated [30].

An important parameter influencing the formation of certain structures is the shape of the amphiphilic molecule which can be qualitatively described by the critical packing parameter (CPP). In the case of GMO, the *cis* double bond at the 9,10 position increases the steric hindrance of the hydrocarbon tail, leading to the formation of inverse micelles where the CPP value is above 1 [29].

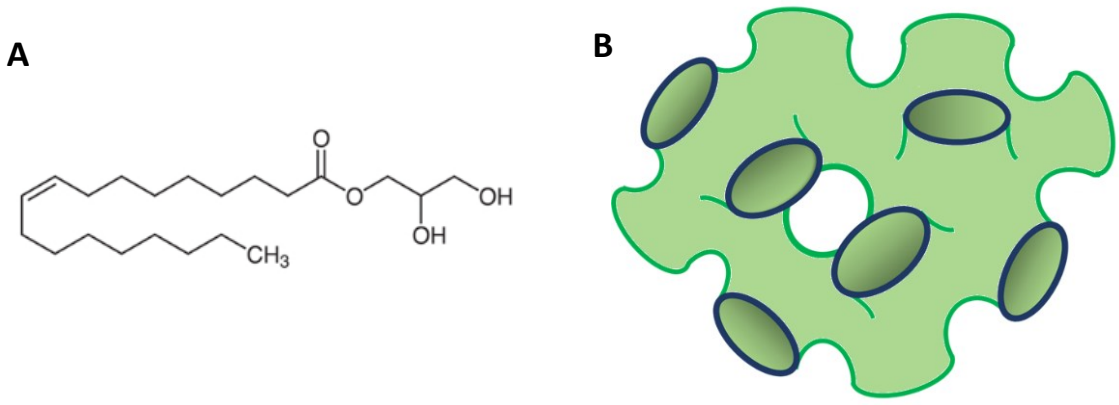

Figure 5. GMO chemical structure (A) and sponge L3 phase schematic representation (B).

In general, all of the lyotropic phases consist in three-dimensional assemblies in which lipid bilayers separate aqueous compartments in an ordered organisation that may be of varying complexity. Specifically, in the presence of water, the main lyotropic phases that an

amphiphilic molecule, like GMO, can originate are: lamellar (L), hexagonal (H) and cubic (Q) phases [31]. In addition, it is possible to find other two mesophases, such as sponge phase and ribbon phase [31].

Lipid polymorphism is of particular interest in a variety of different fields, from scientific to technological [29,31]. In particular, in recent years, liquid crystalline lyotropic phases have received particular attention for their excellent potential as drug vehicles due to their advanced characteristics, mainly associated with their well-organised and stable internal crystal structure, and have accordingly been studied as drug delivery systems for various routes of administration, including parenteral, oral, topical and transdermal route [30,31]. Their potential as drug delivery systems is also associated to their biocompatibility and biodegradability, efficacy in encapsulation of both hydrophilic and hydrophobic molecules, ability to control drug release, capability to protect the active compound against degradation and to improve its bioavailability, high versatility and easy and economic manufacture [31,32]. In this context, GMO is actually the most widely used lipid for the preparation of lyotropic liquid crystals for drug delivery [31].

Another advantage regards topical and transdermal administration. In fact, lyotropic phases are particularly suitable for topical administration of drugs both because of their structural similarity *stratum corneum* lamellar lipidic structure, but also because of the penetration enhancer activity of GMO [32,33]. Precisely, GMO is supposed to generate a temporary and reversible disruption of the lamellar structure of the intercellular lipids of the *stratum corneum* and, in this way, increasing intercellular lipid fluidity [28,34].

As mentioned before, the internal organization of lyotropic liquid crystalline phases allow the efficient solubilization of drugs with different polarities. Usually, hydrophilic drugs arrange themself in close proximity to the polar head groups or within the aqueous channel of a lipid bilayer. Conversely, lipophilic drugs are sequestered within the lipid bilayer itself, while amphiphilic drugs are preferentially located at the interface between the polar head groups and the lipid layer [30].

When lyotropic phases are dispersed in water, it is possible to originate liquid crystalline nanodispersions. In particular: lamellar phase gives rise to liposomes, whereas cubic phase and hexagonal phase maintain their integrity, forming cubosomes or hexosomes respectively [31]. Such colloidal dispersions can be prepared by homogenisation and/or the addition of stabilising surfactants, which enable the fragmentation and steric stabilisation of the bulk lyotropic phase into colloidal nanostructures and help prevent aggregation phenomena

[30,34]. In general, colloidal dispersions of lyotropic liquid crystalline phases possess advantages over bulk forms. Firstly, because they have a lower viscosity that ensures flexible preparation and handling, but also because they can be easily functionalized on the surface [34]. All this while maintaining the advantages conferred by an orderly internal organisation, including high loading capacity, control over the release of the active compound, increased drug bioavailability, etc. Even in the context of topical application, liquid crystalline nanodispersions retain the advantages of the bulk forms previously mentioned, to which greater skin hydration is added [34]. For this reason, they are widely studied and described in the literature as drug delivery systems for the treatment of various skin diseases [34].

In the present doctorate project, the liquid crystalline lyotropic phase referred to as “sponge phase” or “L3” has been investigated more deeply. Sponge phase is a bicontinuous and disordered cubic phase formed by a bicontinuous 3D network of lipid bilayers highly interconnected (Figure 5B). This phase is less ordered and more fluid with respect to cubic phases [29,31]. The colloidal dispersion of this lyotropic phase can be defined as “spongosomes” and represents an interesting drug delivery system, which has not yet been much investigated.

1.4. PHYTOCOMPOUNDS FOR SKIN DISEASES

Nature is an almost inexhaustible source of active molecules of potential interest in both therapeutic and cosmetic fields. Plants, in particular, represent a very rich resource of bioactives, usually produced as secondary metabolites to protect against adverse environmental conditions.

Also to be taken into account is that many of these bioactive molecules are often located in parts of the plant representing waste for the agro-food or textile industry. For this reason, the recovery of these resources could be an advantage not only to ensure greater sustainability of the production process, but also to identify new compounds of therapeutic interest.

Among the innumerable phytocompounds, carotenoids, vitamins, polyphenols, flavonoids, stilbenes etc. possess healthy properties [6,23]. Indeed, these molecules are usually characterised by multiple biological activities, including antioxidant, anti-inflammatory and antimicrobial, and may represent interesting alternatives to synthetic molecules, often associated with undesired side effects, for the prevention or treatment of dermatological conditions.

However, despite their high therapeutic potential, many of these bioactives cannot be employed due to their poor bioavailability, usually associated with reduced solubility and rapid metabolic degradation [6]. In addition, such molecules are often highly susceptible to degradation by external agents such as light, oxygen and high temperature, representing drawbacks for storage and even for the preparation of a medicinal formulation. Of course, all of these factors also affect their possible application for dermatological conditions. Specifically, the lipophilic nature of most of these natural compounds, added to the intricate structure of the skin barrier, hampers their delivery through the epidermis [6].

In order to overcome these problems, lipid-based delivery systems may represent a viable strategy. In fact, on the one hand they are able to optimise adverse chemical-physical characteristics of natural active compounds, such as solubility and biological stability. On the other hand, they can promote their bioavailability while enhancing their biological activity [35]. In the literature, numerous examples of the use of these nanotechnologies can be find, as a tool for natural active compounds delivery to treat various skin diseases and cosmetic issues [6,13,35,36].

In the present doctorate project, the following active molecules will be examined: curcumin, piperine, gossypin and genistein, in order to assess their potential for the treatment or prevention of skin disorders, once trapped in an appropriate drug delivery system.

1.4.1. CURCUMIN

Curcumin (CUR) is the main active component that can be found in the rhizome of *Curcuma longa* (Turmeric) and in other *Curcuma spp*. Turmeric has an ancient history of use in traditional Oriental medicine, particularly in Indian Ayurvedic medicine, for both topical and oral use to counteract a wide variety of disorders [37,38]. Nowadays, CUR is still widely studied for its numerous therapeutic properties, mainly related to its antioxidant and anti-inflammatory action. Moreover, it is marketed in several countries, inside a variety of different products, from the food to the cosmetics industry, not only for its medicinal properties but also as a preservative or colouring agent [39,40]. It has been approved by the US Food and Drug Administration (USFDA) as GRAS [40].

CUR is a low molecular-weight polyphenol, first chemically characterized in 1910, with the molecular formula of $C_{21}H_{20}O_6$ (Figure 6). It has a molecular weight of 368.37 and a melting point of 183 °C. The log P is estimated to be 3.29. CUR is relatively insoluble in water, but dissolves in acetone, dimethylsulphoxide and ethanol and belongs to the Biopharmaceutical Classification System (BCS) class 2.

CUR is a bis-α,β-unsaturated β-diketone and exists in two tautomeric forms: keto and enol. In acidic conditions (pH 3-7), the keto form predominates, while in basic environment (pH > 8) CUR exists mainly in enol form. In acidic environment, CUR acts as a strong H-atom donor, because keto form dominates and the heptadienone linkage between the two methoxyphenol rings contains a highly activated carbon atom, so the C–H carbon bonds on this carbon are very weak due to delocalisation of the unpaired electron on the adjacent oxygens [37,41]. Beside this, in enol form, prevalent in basic environment, CUR acts mainly as an electron donor but it is also more susceptible to degradation. Moreover, CUR is also found to degrade when exposed to UV-visible light [37].

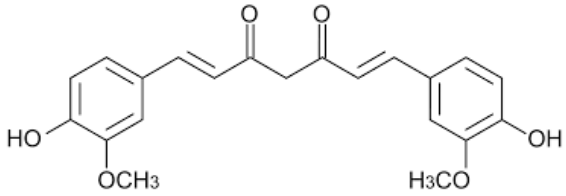

Figure 6. CUR chemical structure.

CUR has been shown to exert a wide range of therapeutical properties, mainly associated to its antioxidant and anti-inflammatory activity [40].

CUR antioxidant activity is carried out by several different mechanisms. At first, it acts directly as a radical scavenger, neutralizing both reactive oxygen and nitrogen species (ROS and RNS, respectively) and being able to protect biological membranes against peroxidative damage [40,42]. Besides, CUR can modulate the activity of catalase (CAT), glutathione peroxidase (GSH), and superoxide dismutase (SOD) enzymes which are active in the neutralization of free radicals; moreover, it can inhibit enzymes such as lipoxygenase (LOX) and cyclooxygenase (COX) and xanthine hydrogenase/oxidase which are often involved in ROS generating mechanisms [40]. Moreover, it is worth mentioning that among CUR products of degradation there are ferulic acid and vannilin which are well known for their antioxidant activity [42].

CUR possesses an anti-inflammatory activity because it is involved in the inhibition of induction of COX, LOX, and inducible nitric oxide synthase (iNOS) enzymes, consequently also the production of inflammatory mediators, and is also implicated in the suppression of nuclear factor (NF)-kB and tumor necrosis factor (TNF) [42].

Interference in these pathways also determines CUR's anti-cancer action and also effectiveness against other inflammatory-mediated diseases. In particular, CUR has also shown potential for the treatment of atherosclerosis, neurodegenerative diseases, HIV, liver

fibrosis, diabetes, metabolic syndrome, anxiety, infections and autoimmune diseases like rheumatoid arthritis [38,40,42].

Regarding skin conditions, CUR resulted to be effective for the treatment of atopic and iatrogenic dermatitis, wound care, acne, pruritus, psoriasis, skin aging, skin cancer and infections [38,43]. Therefore, its topical use for the treatment of dermatological/cosmetic disorders is particularly promising.

The main disadvantage of CUR use is associated with its poor solubility and bioavailability, which hinders its possible therapeutic application. Numerous papers in literature suggest that CUR possesses low absorption, biodistribution and rapid metabolism and elimination [39,40]. For this reason, cur has been the subject of several studies concerning its possible delivery through suitable drug delivery systems [43].

1.4.2. PIPERINE

Piperine (PIP) is an alkaloid (Figure 7) that can be isolated from several members of the *Piperaceae* family, including *P. nigrum* (black pepper), a commonly used spice. This plant contains 2-7.4% PIP, which is responsible for the characteristic sharp flavour and numerous health benefits [44]. In fact, due to the pharmacological effects of PIP, the plants of *Piperaceae* family have been used in traditional Ayurvedic medicine (in a formulation known as "Trikatu", consisting of black pepper, long pepper and ginger) to treat gastrointestinal disorders and improve digestion [45,46]. Moreover, this kind of plant was also employed for the alleviation of several other illnesses as antiseptic, diuretic, antibacterial and insecticidal [44,46].

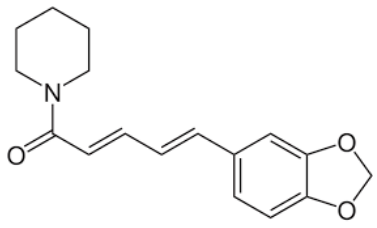

Figure 7. PIP chemical structure.

PIP was first isolated by Hans Christian Ørsted in 1819 and its chemical formula is $C_{17}H_{19}NO_3$ [46]. Molecular weight is 285.34 g/mol and it has the melting point of 128–130 °C. The log P value is 2.78 and it has poor solubility in water. According to FDA, PIP classified as GRAS [47].

Today, PIP is studied for its numerous therapeutic effects, which include: hepatoprotective, anti-diarrheal, antidepressant, immunomodulatory, analgesic, antioxidant, anticancer, antidiabetic, anti-obesity, cardioprotective, antiaging, antimicrobial, anti-inflammatory and anti-allergic [44,46].

In addition, PIP has been shown to increase the bioavailability of several co-administered drugs, including curcumin [45,46]. In particular, the bioenhancer behaviour of PIP is associated to several different mechanisms including inhibition of many enzymes involved in metabolism of xenobiotics such as many cytochrome P450 isoforms, hepatic arylhydrocarbon hydroxylse and UDP-glucuronyltransferase [45,48]. Furthermore, it inhibits p-glycoprotein efflux pump, preventing the elimination of drugs from several tissues, it reduces glucuronic acid intestinal production and stimulates the absorption by amino acid transporters [45,48]. PIP acts also indirectly by increasing intestinal blood supply, reducing acid secretion, improving emulsifying content of the gut and stimulating enzymes like gamma-glutamyl transpeptidase involved in transportation of nutrients to the intestinal cells [45].

Concerning skin application, PIP has also proven effective in treating inflammatory skin diseases, such as psoriasis [49] and it is also described in the literature as a natural penetration enhancer [50].

Despite its potential, the use of PIP in therapy is still limited by its low solubility and systemic absorption, in fact it belongs to class 2 of BCS [47]. In order to solve those drawbacks, many studies in literature describe the possibility to deliver PIP through innovative nanotechnological systems [47].

1.4.3. GOSSYPIN

Gossypin (GOS) is a flavanol glucoside (Figure 8) which can be found in roots and flowers of several hibiscus species, belonging to the *Malvaceae* family, including *H. esculentus*, *H. vitifolius*, and *G. indicum*.

GOS molecular formula is $C_{21}H_{20}O_{13}$, molecular weight is 480.4 g/mol and melting point is 229-230 °C. The presence of glucose makes the molecule soluble in water [51].

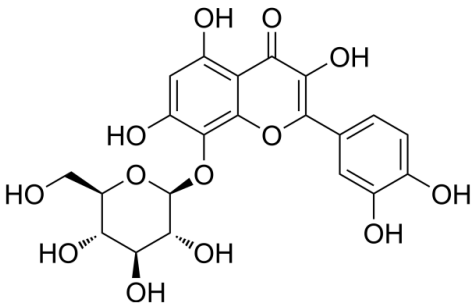

Figure 8. GOS chemical structure.

Nowadays GOS is employed in the chemical industry as a colourant in soaps, cosmetics, as well as dyes; and as insecticide and antioxidant [51].

Derived from traditional Chinese medicine, GOS has recently received extensive attention from researchers due to its wide range of therapeutical properties [52]. In particular, its therapeutical activities include: anti-diabetic, anti-inflammatory, antiviral, anti-allergic, effect on the cardiovascular system, central nervous system and gastrointestinal system, to which an antioxidant and anti-proliferative/anti-tumor power is added [51,52].

Antioxidant activity is associated to the radical scavenger action of GOS, as well as its ability to promote endogenous antioxidant systems levels (like SOD, CAT and glutathione) and counteract lipid peroxidation events [52].

On the other hand, the antitumour action is associated with GOS's ability to arrest the cell cycle and inhibit proliferation by intervening in a number of different pathways, including inhibition of NF-kB and TNF-induced matrix-metalloproteinase-9 (MMP9) expression [52]. In this context, GOS has been studied for the treatment of melanoma, the most aggressive and metastatic form of skin cancer [53,54]. However, in order to reach the deeper skin layers, as required for the treatment of this type of disease, encapsulation in an appropriate drug delivery system is necessary.

1.4.4. GENISTEIN

Genistein (GEN) is an isoflavone (Figure 9) which has been firstly identified in *Genista tinctoria L.*, from which its name is derived, but we can also find it in a wide variety of plants, including legumes, alfalfa and clover sprouts, cauliflower, broccoli, sunflower, barley, caraway and clover seeds. However, the main source of GEN is soybean [55].

GEN, whose molecular formula is $C_{15}H_{10}O_5$, has a molecular weight of 270.24 g/mol, melting point at 301.5 °C and log P value is 3.04, in fact is categorized as slightly soluble in

water [56]. In nature it is mainly found in its glycosylated form, (genistin) which is converted to the aglyconic form in the intestinal microbiota [57,58].

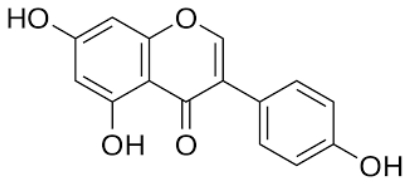

Figure 9. GEN chemical structure.

Regarding its biological activities, as an isoflavone, GEN is capable of exerting an estrogen-like action, due to the structural similarity with 17β-estradiol. Specifically, carbons 4 and 7 on GEN phenol rings are similar in structure and functionality to the phenol groups on 17β-estradiol, and this makes the isoflavone able to bind both α and β estrogen receptor isoforms. In addition, endocrine effects of genistein can be also associated to its main metabolite (-)-(S)-equol, a phytoestrogen generated by intestinal microbiota metabolism [55]. For those properties, GEN has been used as an alternative treatment for menopausal syndrome [59].

GEN biological activities, nevertheless, are not limited to this. Numerous studies have highlighted its antioxidant, anti-inflammatory, antimicrobial properties and pharmacological activities on diabetes and lipid metabolism [55].

About its antioxidant activity, several studies have highlighted the in vitro antioxidant power of GEN, even referred to other isoflavones [57,58]. Its action is essentially related to the polyphenolic structure of isoflavones, which can act as radical scavengers by donating hydrogen atoms and are also able to chelate metal ions [57]. Particularly relevant for the antioxidant activity are the hydroxyl group on C-4', of moderate importance that on C-5 and of negligible importance that on C-7, which could also be replaced by a glucose molecule. [57].

Additionally, GEN is widely studied for its chemopreventive and anti-cancer action, exerted through different pathways. It particular, GEN demonstrated a preclinical efficacy against various types of cancer including breast and lung cancers; brain tumors like neuroblastoma, pituitary cancer, glioblastoma; gastrointestinal cancers like pancreatic, colon, liver, gastric, esophageal, salivary gland and colon cancers, but also urinary tract and genitals cancers including kidney, prostate, uterine, ovarian and testicular cancers and also bone and skin cancers [55].

GEN exerts also a number of protective actions on the skin including: protection from the effects of UV radiation [59], antiaging effect, antioxidant action and stimulation of collagen synthesis [56].

Notwithstanding its high potential, GEN exhibits poor bioavailability, mainly due to its low solubility and rapid metabolic degradation. This obviously represents an obstacle to its therapeutic application both for systemic and topical use. For this reason, GEN represents the subject of numerous studies concerning its possible delivery through nanotechnological systems, whether polymeric, metallic or lipidic in nature, also with a purpose to promoting its bioavailability and permeation through the skin [56].

2. AIM AND ORGANIZATION OF THE THESIS

The aim of the present doctorate project was to study innovative nanosystems for the delivery of active molecules through the skin for the treatment of dermatological and cosmetic conditions, by virtue of the advantages offered by the topical route of administration. In particular, the focus is centred on active compounds of plant origin, known for their several therapeutic properties but also for their poor bioavailability. Therefore, the goal is to exploit the potential of lipid-based delivery systems to enable their topical application and enhance their action, while ensuring safety and biocompatibility.

Furthermore, one of the objectives of the research is to ensure the sustainability of the finished product as much as possible, in line with the principles of *green chemistry*. This was realised by selecting methodologies for the production of formulations that do not require the use of toxic organic solvents and high energy levels as well as excipients of natural origin.

Also to be taken into account is that the choice of investigating active principles of plant origin appears attractive for two main reasons. The first concerns the need to find new therapeutic alternatives to synthetic molecules, which are often associated with resistance phenomena or toxicity. The second involves the possibility of establishing a connection between the agri-food chain and the pharmaceutical industry through the use of plants as raw materials from which to obtain active compounds, in line with principles of *circular economy*.

The thesis is divided into 10 main chapters. After an introduction (chapter 1) focusing on the objectives and subjects of the research, the following chapters go into the merits of the experimental activity that has been undertaken. In particular, the research was divided into 4 main projects, each one with specific purposes.

Project 1 (chapter 5) describes the production and characterisation of ET separately loaded with CUR and PIP for their possible application in the prevention of skin damage caused by environmental pollutants, particularly diesel engine exhaust. The possible association of the two formulations (i.e. ET-CUR and ET-PIP) was investigated in vitro by antioxidant activity test. Moreover, biological activity was evaluated using an ex vivo model consisting of human skin biopsies that were exposed to diesel engine exhaust. A patch test was also performed on human volunteers to assess any irritation on the skin.

Project 2 (chapter 6) can be seen as a continuation of the previous one, since here again the aim is the use of CUR and PIP in the prevention of skin damage caused by exposure to

pollutants. However, in this case it was possible to produce and study the combination of the two drugs in a single nanoplatform based on GMO: spongosomes. First, a preformulatory study was carried out, in which a new preparation method to produce GMO dispersions was developed and the optimal formulation composition was selected. Then, formulations containing CUR and PIP, both separately and in combination in two different ratios, were produced and characterized. Finally, their activity was evaluated again employing an ex vivo model consisting of human skin biopsies exposed to diesel engine exhaust.

Project 3 (chapter 7) describes the production and characterisation of ET-gel formulation for the delivery of GOS, intended for the treatment of cutaneous melanoma. One of the objectives of the work was to investigate the method of ET preparation. Precisely, two different methods were compared: ethanol injection and water injection, in order to determine which would lead to the best formulation characteristics. ET dispersions were gelified using xanthan gum (X-Gum), whose percentage was selected by means of spreadability and leackage test. The antioxidant activity of gelified and non-gelified formulations was tested in vitro and their potentiality for melanoma treatment was evaluated on A375 melanoma cell line.

Project 4 (chapter 8) aimed at the delivery of GEN, a promising photo- and chemo-preventive agent intended for the protection against UV-induced skin disorders, particularly non-melanoma skin cancers. A preformulatory study was performed in order to identify the best vesicular vehicle (between ET and TE) and method of preparation. The selected formulation for GEN loading (i.e. TE) was characterised and its stability was evaluated in 90 days of storage. Subsequently, in order to facilitate its possible skin application, it was gelified with X-Gum. TE-gels, loaded and unloaded with GEN, were characterized and their antioxidant activity was assessed in vitro. Finally, patch test and tape stripping evaluations were executed on human volunteers, comparing vesicular gel formulation with plain X-Gum GEN gel.

In the end, chapter 9 reports the main conclusions and future perspectives concerning this research.

3. MATERIALS

3.1 ACTIVE COMPOUNDS

Curcumin (purity grade 94%) and piperine (purity grade 97%) were purchased from Merck Life Science S.r.l. (Milan, Italy). Gossypin (purity grade ≥ 95%) and Genistein (purity ≥ 98%) were purchased by Cayman Chemical Company.

3.2 EXCIPIENTS

The soybean lecithin (PC) (purity 92%) Epikuron 200 was purchased from Lucas Meyer (Hamburg, Germany) and employed in Project 1, while in Project 3 and Project 4 phosphatidilcholyne from soybean (PC) (purity 94%), acquired by A.C.E.F. Spa was employed. Glyceryl monooleate (GMO) was acquired from Ataman Chemicals (Instanbul, Turkey). Polysorbate 80 (polyoxyethylene sorbitan monooleate, Tween 80, TW80), sodium cholate hydrate (NaChol), casein sodium salt from bovine milk (NaCas) and xanthan gum (X-Gum) were bought from Merck Life Science S.r.l. (Milan, Italy).

3.3 OTHERS

Polytetrafluoroethylene (PTFE, Whatman®, Seoul, Republic of Korea) (pore size 0.2 μm), Nylon membranes (pore size 0.2 μm) and ® STRAT-M® membranes were purchased from Merck Life Science S.r.l. (Milan, Italy). Solvents were of an HPLC grade, and all other chemicals were of an analytical grade.

4. METHODS

4.1 NANOSYSTEMS PRODUCTION

4.1.1 PREPARATION OF ETHOSOMES AND TRANSETHOSOMES

Two different approaches for the preparation of ET and TE were studied, specifically "water injection" method and "ethanol injection" method.

Water injection method

Water injection method is based on the gradual addition of bidistilled water to an ethanolic solution of PC kept under magnetic stirring. Such a method had previously been developed by our research group [25,60,61] both for ET and TE preparation. In specific, PC solution is prepared in advance by solubilizing the lipid in ethanol at room temperature through magnetic stirring (IKA RCT basic, IKA®-Werke® GmbH and Co. KG, Staufen, Germany) to a final concentration of 30 mg/mL. In the case of TE, TW80, selected as edge activator, is added to the PC-ethanol solution in a concentration of 10 mg/mL by solubilization at room temperature.

The addition of water was performed drop by drop, continuously, on the ethanolic solution kept under magnetic stirring at 750 rpm up to a final 70:30 (v/v) water/ethanol ratio. Subsequently, the stirring was kept for 30 minutes. All steps were carried out at room temperature.

Drug-loaded formulations were prepared by the previous solubilization of the active compound in the ethanolic solution. In the case of photosensitive compounds, the preparation was carried out in the dark.

Ethanol injection method

Ethanol injection methodology differs from the previous one by reversing the mixing mode of the two phases. In specific, the PC-ethanol solution (30 mg/mL), eventually added of TW80 in the case of TE, was gradually added to the bidistilled water kept under magnetic stirring at 750 rpm, and once the addition was completed, the magnetic stirring was maintained for 30 minutes. Final water/ethanol ratio was always 70:30 (v/v). Entire procedure was conducted at room temperature. As previously described, drug-loaded formulations were prepared by the previous solubilization of the active compound in the ethanolic solution, and eventually performing the preparation protected from light.

4.1.2 GELS PREPARATION

Preparation of ET/TE gels

ET and TE vesicular dispersions were gelified using X-Gum. Precisely, one day after the preparation, ET or TE (loaded or unloaded with drugs), were viscosified by direct addition of X-Gum to the dispersion kept under magnetic stirring. In order to avoid lump formation, the addition was performed gradually and stirring was mantained until the system became uniform. Different concentrations of X-Gum were studied (i.e. 0.5, 0.75 and 1% w/w) both for ET and TE gelification. All of the steps were conducted at room temperature and protected from light in case of drug-loaded formulations.

Preparation of GEN gel

In the case of Project 4, a GEN X-Gum-gel was prepared as comparison with TE-gel formulation for in vivo tests. This gel was obtained by dispersion of the drug in water followed by the addition of X-Gum under magnetic stirring. Agitation was maintained until complete dispersion of the polysaccharide. The gel was prepared at room temperature and protected from light.

4.1.3 PREPARATION OF SPONGOSOMES

Preparation of spongosomes was performed by new method consisting on thin-film hydration followed by homogenization. First step consisted on GMO and NaChol solubilization in ethanol at room temperature. Subsequently ethanol was evaporated using rotavapor (Heidolf vv2000, Schwabach, Germany) at 60° C of temperature, leading to thin lipidic film formation. The film was hydrated with water (pre-heated at the same temperature) or NaCas water solution alternatively, and then vortexed for 5 min. Final step consisted on homogenization of the pre heated dispersion (60°C) using ULTRA-TURRAX T 10 basic (IKA WERKE) at 25000 rpm for 1 min. Subsequently, the formulation was cooled down to room temperature and water was added to restore any lost volume to final 5 mL.

In case of drug-loaded formulations, active compounds were previously solubilized in ethanol used in the very first production step.

4.2. NANOSYSTEMS CHARACTERIZATION

4.2.1 MORPHOLOGIAL CHARACTERIZATION

Transmission electron microscopy (TEM)

TEM analysis was employed for the evaluation of ET, ET-CUR and ET-PIP morphology (Project 1). Analyses were carried out at the University of Ferrara electron microscopy centre (CME).

Samples were negatively stained by depositing a sample drop on a TEM grid covered with a formvar film. The excess drop was removed after 1 min from the grid with filter paper to keep a thin veil of the sample on the supporting substrate. A drop of 2% phosphotungstic acid was placed on the grid for 1 min and then removed with filter paper to surround the nanosystems deposited on the grid and adhere to their surface. Then, the grid was observed with a TALOS L120C G2 Transmission Electron Microscope (Thermo Fisher Scientific, Eindhoven, The Nederland).

Cryo transmission electron microscopy (CRYO-TEM) – (Project 2)

The morphology of GMO dispersions (Project 2) was evaluated by Cryo-TEM. Analyses were performed by Dr. Markus Drechsler from Bavarian Polymer Institute (BPI), University of Bayreuth, (Germany).

This technique requires sample vitrification. Specifically, in order to vitrify the samples, a 2 μL droplet was put on a lacey carbon-filmed copper grid (Science Services, Munich, Germany) for 30 s. Subsequently, blotting paper was used to remove most of the liquid, resulting in a thin film stretched over the lace holes. The specimens were instantly shock frozen by rapidly immersing them into liquid ethane cooled to approximately 90 K by liquid nitrogen in a temperature-controlled freezing unit (Leica EMGP, Leica, Germany). All the steps of sample preparation were conducted at a controlled temperature.
A Zeiss/Leo EM922 Omega EFTEM Microscopy (Zeiss Microscopy GmbH, Jena, Germany) was employed to examine the vitrified specimens with reduced doses ≈1000–2000 e/nm^2 at 200 kV, keeping the samples at a temperature below 100 K. A CCD digital camera (Ultrascan 1000, Gatan, Munich, Germany) was used to record the Zero-loss filtered images (ΔE = 0 eV) and the GMS 1.9 software (Gatan, Munich, Germany) was employed to analyze the images.

Cryo transmission electron microscopy (CRYO-TEM) – (Project 3 and Project 4)

The morphology of ET and TE dispersions, prepared by the two different methodologies (Project 3 and Project 4) was evaluated by Cryo-TEM. In this case analyses were performed by Dr. Marc C.A. Stuart from University of Groningen (Netherlands).

3 µl of formulation was placed on a holy carbon coated grid (Quantifoil 3.5/1), blotted and vitrified in ethane (Vitrobot). Frozen hydrated grids were observed in a Tecnai T20 electron microscope operating at 200 keV. Images were recorded with a slow-scan CCD camera under low-dose conditions.

4.2.2 PHOTON CORRELATION SPECTROSCOPY (PCS)

PCS technique was employed to measure the size distribution of the nano-sized formulations. Thanks to this procedure, it is possible to derive the values of Z-Average, which is the mean hydrodynamic diameter, and Dispersity index (DI). The method is based on the correlation of the fluctuation of the intensity of scattered radiation from the sample to the particle size in the dispersed phase.

In specific, a Zetasizer Nano-S90 (Malvern Instr., Malvern, England) was employed for the analyses. The instrument is equipped with a 5 mW helium neon laser that produces a wavelength output of 633 nm. The analyses were conducted at 25° C with a 90° detection angle and 120 seconds equilibration time. The samples were diluted 1:10 (v/v) with bi-distilled water. Size distribution was obtained by the "CONTIN" method. Each analysis was carried out in triplicate from which the mean is derived.

4.2.3 ZETA POTENTIAL

Zeta potential (Z-potential) determination was performed using Zetasizer Pro (Malvern Instr., Malvern, England). This technique involves the measurement of scattering of incident laser light by moving particles according to their electrophoretic mobility. The instrument is equipped with a 4 mW helium neon laser that produces a wavelength output of 632.28 nm. The analyses were conducted at 25° C. The samples were diluted 1:10 (v/v) with bidistilled water inside plastic tube and then put (1 mL) inside cuvette DTS1070 (Malvern Instr., Malvern, England).

4.2.4 pH MEASUREMENT

Formulations' pH was measured using Crison Basic C20 pH meter (Crison Instruments,S.A., Alella, Barcellona, Spain) equipped with a pH 50 12 - Hach electrode.

4.2.5 SMALL-ANGLE X-RAY SCATTERING (SAXS)

SAXS technique was employed to investigate the inner supramolecular organization of nanosized dispersion. Experiments were performed at SAXS beamline at the Elettra Synchrotron in Trieste (Italy) thanks to the collaboration with Prof. Paolo Mariani (Università Politecnica delle Marche).

SAXS – Project 2

The wavelength of the incident beam was $\lambda = 0.154$ nm and the explored Q-range extended from 0.1 to 0.4 nm^{-1} (Q is the modulus of the scattering vector, defined as $4\pi \sin\theta/\lambda$, where 2θ is the scattering angle). Scattering data were recorded on a 2-dimensional Pilatus3 1M Detector and exposure times of 300 s per frame were used to avoid radiation damage. Samples were placed in a polycarbonate capillary with a diameter of 1 mm and measured both at 25°C and 37°C. Two-dimensional (2D) data were corrected for background, detector efficiency, and sample transmission and then radially averaged to derive I(Q) vs. Q curve. Errors were around 0.02 nm for the hexagonal lattice parameter and around the 5% for L3 data.

SAXS – Project 3 and Project 4

SAXS experiments were part of the CERIC proposal number 20242026. The samples were located in an apposite quartz capillary with a diameter of 1.5 mm thermostated within a KPR (Peltier heating/cooling) sample holder (Anton Paar, Graz, Austria) at 37°C. Two samples (ET_{WI} and $ET\text{-}GOS_{WI}$) were also measured in a wide temperature range (from 15 to 60°C, each 5°C). Each sample was irradiated by the X-ray beam with an exposition time of 10 seconds and by repeating 18 frames. Two-dimensional (2D) data were corrected for background, detector efficiency, sample transmission and then radially averaged to derive the differential scattering cross-section, more simply scattered intensity I(Q), as a function of the modulus of the scattering vector, Q, defined as $4\pi \sin\theta/\lambda$ (where 2θ is the scattering angle and λ the X-ray wavelength). The explored Q-range was between 0.1 and 5 nm^{-1}. The detector used for the measurement was a 2D Pilatus3 1M Detector System with a pixel size of 172x172 μm^2 and a discrete energy of 8 keV (corresponding to the beam wavelength of 0.154 nm). An additional Wide-Angle X-ray Scattering (WAXS) detector was used in Project 3 to simultaneously monitor diffraction patterns in the high-angle range from 8 to 17 nm^{-1}.

4.2.6 ANTIOXIDANT ACTIVITY EVALUATION

Different methods were used to assess the antioxidant activity of the formulations produced. All the experiments were carried out thanks to the collaboration with Prof. Anna Baldisserotto from University of Ferrara (Department of Life Science and Biotechnology).

FRAP (ferric reducing antioxidant power)

In case of Project 1, FRAP test was employed to test antioxidant activity of CUR and PIP loaded formulations. The test measures the reducing ability of antioxidants against Iron ions. It is a method based on electron transfer, in which iron ions change from Fe^{3+} to Fe^{2+}. Under certain pH conditions (3.6) and in the presence of TPTZ (2,4,6-tris(2-pyridyl)-s-triazine), these ions form complexes with different characteristics, in particular the reduced derivative (Fe^{2+}-TPTZ) takes on a blue coloration that exhibits a maximum absorption at 593 nm that can be measured spectrophotometrically. The reducing capacity of an antioxidant substance can then be measured as the change in absorbance of the solution containing the oxidant at the established wavelength by comparison with the change relative to a standard (e.g., Trolox, a water-soluble analogue of Vitamin E). Precisely, reaction is carried out by mixing 1.9 mL of FRAP reagent to 0.1 mL of sample appropriately diluted in methanol. Methanol was used as control. All samples were then incubated in the dark at 37 °C for 10 min, followed by a measurement of their absorbance at 593 nm with a UV-Vis spectrophotometer (UV-31 SCAN ONDA Spectrophotometer, Giorgio Bormac spectrophotometer Srl, Carpi (MO), Italy).

FRAP solution reagent should be prepared fresh each time and stored in an oven at 37 °C for the time of sample preparation. In particular, the reagent preparation involves the mixing of several components: 25 mL of the buffer solution, 2.5 mL of TPTZ and 2.5 mL of ferric chloride hexahydrate (10/1/1 ratio). Buffer solution is prepared by dissolution of 3.1 g of sodium acetate in 16 mL acetic acid and made up to 1 L with demineralized water; checking the final pH to be 3.6. TPTZ is 10 mmol/L solution of 2,4,6-tri(2-pyridyl)-5-triazine (TPTZ) in 40 mmol/L HCl, prepared by solubilization of 31.23 mg of TPTZ in 10 mL of 40 mmol/L HCl. HCl 40 mmol/L solution is previously prepared by diluting 3.3 mL of concentrated HCl and bring to volume of 1 L with demineralized water. Finally, ferric chloride hexahydrate solution is prepared dissolving 5.406 g $FeCl_3$ $6H_2O$ with demineralized water and made up to 1 L volume; final concentration is 20 mmol/L. Trolox was used as the standard for the calibration curve, so the results are expressed as μmol Trolox equivalent (TE) per gram of sample.

DPPH radical scavenging assay

DPPH assay was employed to test antioxidant activity of GOS-loaded formulations in Project 3. Using this assay it is possible to estimate of the ability of an antioxidant substance to convert the stable free radical DPPH to 1,1-diphenyl-2-picrylhydrazyl by hydrogen-donation. The reaction is monitored and measured by means of a UV-Vis spectrophotometer (UV/VIS ONDA Touch UV-31 Scan Spectrophotometer, Sinergica Soluzioni S.r.l., Milan, Italy), evaluating the reduction in absorbance at 517 nm, which corresponds to a colorimetric change from violet to light yellow, as described previously [62]. Solutions at different concentrations were prepared for each sample (SOL GOS, ET-GOS_{EI}, ET-GOS_{EI}-0.5%gel), and 0.750 mL of each of these solutions was added to 1.5 mL of DPPH in methanolic solution. From the calibration curve obtained for each sample, the IC50 (µg/mL) value is obtained, given as the mean of three independent experiments with standard deviation.

Photochemiluminescence (PCL) test

PCL test was selected in Project 4 to test the antioxidant activity of GEN-loaded formulations. The test is based on the reaction of a specific radical species, the superoxide anion ($O_2^{\bullet -}$), photochemically generated by UV radiation, with a compound capable of emitting chemiluminescence, according to the method of Popov and Lewin [63]. The marker used was luminol, a molecule that, oxidized by free radicals, emits light that can be measured with a special instrument (Photochem®, Analytik Jena, Leipzig, Germany). The presence of antioxidant substances in the mixture of the reaction deactivates the radical species by inhibiting the emission of chemiluminescence. PCL analysis is very fast and sensitive. Indeed, the application of two different analytical protocols, named ACW (antioxidant capacity of water-soluble compounds) and ACL (antioxidant capacity of lipid-soluble compounds) enables to evaluate the contributions to the total antioxidant capacity of both the water-soluble molecules and the fat-soluble one. The kinetic light emission curve, which exhibits no lag phase in ACL studies, was monitored for 180 s and expressed as micromoles of Trolox (selected as standard) per gram of sample. The areas under the curves were calculated using the PCL soft control and analysis software. As greater concentrations of Trolox working solutions were added to the assay medium, a marked reduction in the magnitude of the PCL signal and hence the area calculated from the integral was observed. This inhibition was used as a parameter for quantification and related to the decrease in the integral of PCL intensities caused by varying concentrations of Trolox. The observed inhibition of the signal was plotted against the concentration of Trolox added to the assay medium. The concentration of the added sample solution was such that the generated

luminescence during the 180 s sampling interval fell within the limits of the standard curve. At least two blank-measurements should be done (only reagents of ACL-kit without sample and/or Trolox): 2.3 mL of ACL-Diluent, 0.2 mL of Reaction buffer, and 0.025 mL of Luminol stock solution. Samples of TE_{EI}, TE_{EI} gel, SOL GEN, TE-GEN_{EI}, TE-GEN_{EI} gel were suitably diluted in methanol prior to analysis. The antioxidant assay was carried out in triplicate for each sample, and the results expressed as μmol Te/g.

4.3 GELS CHARACTERIZATION

4.3.1 SPREADABILITY TEST

The characteristics of the ET/TE gels were evaluated one day after the preparation through the spreadability test. The test is based on evaluating the area occupied by the formulation when a constant weight is applied on it. Precisely, 100 mg of gel were placed in the centre of a glass petri dish (3 cm diameter) and then subjected to pressure by a glass dish carrying a 50 g mass. Thereafter, 10 s were waited before measuring the diameter of the surface occupied by the formulation. Spreadability value (S) was measured following the equation:

$$S = m \times l/t \quad (1)$$

Where “m” is the applied weight (expressed in g), “t” is the application time (10 s), and “l” is the diameter (expressed in cm) of the area occupied by the gel. The trial was performed at room temperature, three times for each tested formulation.

4.3.2 LEAKAGE TEST

To test leakage and adhesion of ET/TE gels, it was evaluated their sliding ability on agar gels. Agar gels were previously prepared by agar solubilization (1.5 % w/w) in hot water (95 °C) under magnetic stirring. The hot agar solution was poured inside petri dishes (3 cm diameter) and allowed to cool. Once room temperature is reached, gelation of the solution occurs and it becomes suitable for the test. In parallel, gels were dyed by directly dissolving a spatula tip of coomassie blue (Merck Life Science S.r.l., Milan, Italy) into them.

The test is performed by placing 50 mg of formulation at one end of the agar slide and then positioning it vertically (90° angle with the supporting surface). The agar surface was pre heated at 32-35 °C to mimic physiological conditions. Afterwards, the distance travelled by the gel in 10 seconds is measured. Gel leakage, expressed as the running distance of the gel, was measured three times for each formulation.

4.3.3 RHEOLOGICAL ANALYSIS (PROJECT 4)

TE_{EI}, TE_{EI}-gel, TE-GEN_{EI} and TE-GEN_{EI}-gel (Project 4) were subjected to rheological analysis, performed by using an Anton Paar MCR702e MultiDriver Rheometer. Tests were performed thanks to the collaboration with Prof. Paolo Mariani (Università Politecnica delle Marche).

Each sample was placed between two appropriate cone-plate geometries (diameter 50 mm, cone truncation 0.1 mm and cone angle 1°). The parameter investigated through this technique was the viscosity (expressed as Pa·s) calculated as a function of the shear rate (expressed as 1/s). Measurements were performed on the samples at 25 °C and 37 C° and the humidity was 20 %. Both temperature and humidity were kept constant throughout the analysis.

4.4 DRUG QUANTIFICATION

4.4.1 ENTRAPMENT CAPACITY

In order to quantify the entrapment of the active agents within the nanocarrier, ultrafiltration method was employed. This method consists in the segregation of the particulate fraction and quantification of the associated drug through high-performance liquid chromatography (HPLC) analysis. In specific, one day after the preparation, 500 µL of colloidal dispersion underwent ultrafiltration (Spectrafuge™ 24D Digital Microcentrifuge, Infitek Inc., Spokane, WA, USA) using specific filters (Microcon centrifugal filter unit with YM-10 membrane, NMWCO 10 kDa, Sigma-Aldrich, St. Louis, MO, USA), at a centrifugal force of 4000 rpm for 20 min. The retentate samples were then diluted in ethanol (1:10 v/v) and agitated with a magnetic stirrer for 30 minutes in order to disrupt the nanostructures. An aliquot (100 µL) of the total dispersion was treated similarly to determine the actual drug content within the formulation. Prior to HPLC analysis, the disgregated samples were filtered using nylon syringe filters (0.22 µm). Finally, the entrapment capacity (EC), was calculated as:

$$EC = D/T_D \times 100 \quad (2)$$

In the equation, D represents the amount of drug retained by the vesicles, and T_D refers to the real drug content in the entire formulation.

4.4.2 HPLC ANALYSIS

The HPLC analyses were performed using Perkin Elmer Series 200 HPLC Systems (PerkinElmer, Waltham, MA, USA), equipped with a micropump, an auto sampler, and an UV detector. A stainless steel C-18 reverse-phase column (15 × 0.46 cm) packed with 5 μm particles (Hypersil BDSC18 Thermo Fisher Scientific S.p.A., Milan, Italy) was eluted under isocratic conditions at a flow rate of 1 mL/min with a mobile phase and wavelength selected depending on the drug as reported in Table 1.

Table 1. HPLC analysis conditions employed for CUR, PIP; GOS and GEN.

Drug	Wavelength (nm)	Mobile Phase	Retention Time (min)
CUR	360	MeOH/H_2O 80:20 (v/v)	2.3
PIP	243	MeOH/H_2O 80:20 (v/v)	2.7
GOS	260	CH_3CN/H_2O 30:70 (v/v) + TFA 0.1%	2.9
GEN	260	CH_3CN/H_2O 40:60 (v/v) + TFA 0.1%	4.1

4.5 PRELIMINARY STABILTIY STUDIES

In the case of Project 1 and Project 3, the dimensional stability of the colloidal dispersions, stored at room temperature and protected from light, was assessed by repeating the PCS analysis 60 days after preparation.

In the case of Project 2, in contrast, the formulations were stored at a temperature of 4 °C for 2 months and then PCS analyses was repeated as previously reported.

In Project 4, on the other hand, a stability study was carried out on TE formulations evaluating both dimensional stability and Z-potential stability, repeating analyses at different time intervals. Specifically, PCS analyses were repeated after 1, 15, 30, 60 and 90 days of storage and Z-potential analyses were repeated after 1, 15, 30 and 60 days. Formulations were stored at 4 °C and protected from light. In addition, the chemical stability of GEN was evaluated repeating disgregation and HPLC analysis after 90 days of storage in the same conditions.

4.6 FRANZ CELLS EXPERIMENTS

To perform in vitro release test (IVRT) and in vitro permeation test (IVPT) were employed Franz vertical diffusion cells (orifice diameter 0.9 cm; PermeGear Inc. Hellertown, PA, USA), assembled with appropriate membranes according to the intended study. Specifically, PTFE and NY membranes were used for IVRT while STRAT-M® membrane was employed for IVPT. The receptor compartment was filled with 5 mL of receiving phase consisting in ethanol/water 50:50 (v/v). The receiving phase was kept under magnetic stirring at 500 rpm and 32 °C of temperature throughout the duration of the experiment. The presence of ethanol and magnetic stirring guarantee the required sink conditions. Before Franz cells assembly, the membranes were rehydrated by immersion in ethanol/water 50:50, v/v for 1 h. The donor compartment was filled with 1 mL of the tested formulation, and then sealed to avoid evaporation.

The experiment is carried out by periodic withdrawals (1 per hour over the period from 0 to 24 h) of 0.5 mL from the receiving compartment, then analysed at HPLC to quantify the amount of drug that passed through the membrane. Each removed sample was replaced with an equal volume of fresh receiving phase.

4.6.1 IN VITRO RELEASE TEST (IVRT)

For data analysis, in the case of Project 1, the amount of released drug (expressed as $\mu g/cm^2$) was graphed as a function of the square root of time and in Project 3, the amount of released drug (expressed as $\mu g/cm^2$) was graphed as a function of time. From the linear portion of the release profile, “R” and “A” values can be obtained. In specific, “R”, the release rate, is obtained by the slope of the curve, while “A” is the amount of drug released at the final sampling point.

Furthermore, to elucidate the mechanism of drug release acted by our nanosystems, data were analysed according to mathematical models such as the zero-order kinetics (cumulative % drug released vs time), first-order kinetics (log cumulative % drug remaining vs. time), Higuchi (cumulative % drug released vs square root of time) and Peppas (log cumulative % drug released vs. log time). The suitability of the model fits was verified using the DDsolver add-in for Excel 2016 (Version 2312 Build 16.0.17126.20126).

4.6.2 IN VITRO PERMEATION TEST (IVPT)

In the case of IVPT, for data analysis, the amount of permeated drug (expressed as μg/ cm^2) was plotted as a function of time. According to Fick's law, under sink conditions, the drug concentration in the receptor compartment is negligible compared with that in the donor compartment, which is equal to the concentration gradient. The linear portion of the curve describes the steady-state permeation through the skin, from which we can calculate a set of descriptive parameters of the process. The steady state flux of drug per unit area "Jss"(μg $cm^{-2}h^{-1}$) is the slope of the curve and can be described by the equation:

$$Jss = P \times Cd \times D/e \quad (3)$$

"P" is the partition coefficient, "Cd" is the drug concentration in the donor compartment, "D" is drug diffusion coefficient, and "e" is the thickness of the membrane. Drug permeability coefficients "Kp" value were calculated from Jss according to the equation:

$$Kp = Jss/Cd \quad (4)$$

Lag time ("Tlag"), which is the time needed to reach steady-state conditions, could be obtained from the intersection of the line with the x-axis and "D" value was calculated from Tlag by the equation:

$$Tlag = e^2/6 \times D \quad (5)$$

At last, P was achieved considering the equation:

$$Kp = D \times P/e \quad (6)$$

4.7 BIOLOGICAL ACTIVITY STUDIES

In order to evaluate the biological activity of the studied formulations, different tests were carried out according to the therapeutic target.

4.7.1 IN VITRO STUDIES (PROJECT 3)

In order to evaluate the biological activity of GOS-containing formulations against melanoma (Project 3), in vitro studies were conducted on A375 melanoma cell line. In vitro experiments were carried out thanks to the collaboration with Prof. Mascia Benedusi from University of Ferrara (Department of Neurosciences and Rehabilitation, University of Ferrara)

MTT assay

A375 melanoma cells were cultured in Dulbecco's modified Eagle's medium High Glucose (DMEM), (Lonza, Milan, Italy), supplemented with 10% FBS (foetal bovine serum), 100 U/mL penicillin, 100 µg/mL streptomycin and 2 mM L-glutamine. Cells were incubated at 37 °C for 24 h in 95% air/5% CO_2 until 80% confluence.

For cell treatments, the different vehicles were at first dissolved in cell culture medium to obtain the stock solutions containing GOS 300 µg/mL, then further diluted to reach different concentrations of GOS (from 0.5 to 50 µg/mL).

Specifically, A375 cells were grown in 96-well plates at a density of 2 × 104 cells/well in 200 µL of media for MTT assay. The day after the cells were treated with different doses of unloaded and GOS-loaded formulations with GOS concentrations ranging from 0.5 µg/mL to 50 µg/mL for 24 and 48 hours. Then, the treatment was completely removed and 50 µL of serum-free media and 50 µL MTT (0.5 mg/mL) were added. After 3h incubation (37 °C, 5% CO_2) the formed insoluble purple formazan crystals were dissolved in 100 µL of dimethyl sulfoxide (DMSO) for 15 min at 37 °C, 5% CO_2. After 5 min shaking, the solution absorbance was read with a spectrophotometer at 590 nm, using 670 nm as reference wavelength. Finally, the values were converted into a percentage of cell viability, compared to control (T0).

Wound healing assay

A375 melanoma cells were grown on 24-well plates at a density of 5 × 104 cells/well in complete DMEM medium to confluent monolayer. The day after the cells were first mechanically scratched with a 200 µL sterile pipette tip and then cellular debris were removed by two washes with 1X PBS (Phosphate Buffer Solution). Based on the MTT assay results, A375 cells were immediately exposed to 0.5 µg/mL of GOS-loaded and unloaded formulations, followed by incubation at 37 °C. Finally, images of the scratches were recorded at different time points (viz. 0, 3, 6, 12, 24 and 48h post- scratch) and the wound healing rate was analyzed by means of ImageJ software (National Institutes of Health, Bethesda, MD, USA) and com-pared to the wound area at T0.

Migration assay

2.2 × 106 A375 melanoma cells were seeded in 10 cm^2 petri dishes and pretreated with 0.5 µg/mL of GOS-loaded and unloaded formulations for 24 h; then, 100,000 cells were re-suspended in 400 µL of serum-free media and seeded in 8 µm pore size transwells (Falcon®

Permeable Support for 12-well Plate with 8.0 μm Transparent PET Membrane, Sterile) coated with 0.15 mg/mL bovine collagen IV. After 30 min, 1100 μL of complete media was added at the bottom of each well, acting as a chemoattractant. After 24 hours the transwell inserts were first fixed with 70% ethanol (for 10 min), then stained with 0.02% of Coomassie Blue (15 min), and rinsed with double-distilled water. The remaining A375 cells that have not migrated from the upper part of the transwell were gently removed with a cotton swab, and pictures of 5 randomly selected fields were acquired (at 20X magnification).

The number of migrated cells present in five fields/well was counted using ImageJ program. Data were reported as percentage of migrated cells, compared to control condition.

4.7.2 EX VIVO STUDIES (PROJECT 1 AND PROJECT 2)

The biological activity of CUR- and PIP-loaded formulations, aimed as protective agents against damage caused by environmental pollutants (Project 1 and Project 2) was evaluated using ex vivo models consisting of human skin explants. The experiments were carried out at the foreign company TEN BIO Technologies, based at the North Carolina Research Campus, in Kannapolis, NC (USA) under the supervision of Prof. Giuseppe Valacchi (NC State University, Plants for Human Health Institute, Animal Science Dept., NC Research Campus).

Human specimens

Human skin explants were obtained from elective abdominoplasties from 3 different donors (Caucasian females) after the approval of the Institutional Biosafety (IBC) Committee at NC State University. Skin biopsies (12 mm) were collected with a punch, and the subcutaneous fat was removed with sterile scissors. The skin biopsies were washed in PBS and then transferred into 6-well plates prefilled with 1 mL of DMEM High Glucose supplemented with 10% Fetal Bovine Serum (FBS), 100 IU/mL penicillin and 100 mg/mL streptomycin (complete medium) using a sterile technique [64]. The samples were incubated at 37 °C in a 5% CO_2/95% air atmosphere for overnight recovery.

Treatment with formulations and DEE exposure

After overnight recovery, the skin biopsy medium was replaced with 1 mL of fresh complete medium, and the samples were treated with the indicated formulations. Briefly, 10 μL (Project 1) or 7.5 μL (Project 2) of each formulation were applied topically on the skin explants and spread using a sterile glass rod. For the combined treatments (ET PIP + ET CUR and SOL PIP + SOL CUR requested in Project 1), 5 μL of each formulation were

applied to the skin and evenly mixed. Some samples were kept untreated as controls. The plates were incubated in a humidified 5% CO_2/95% air atmosphere for 60 min (Project 1) or 30 min (Project 2) before exposure to the diesel engine exhaust (DEE) insult. For all the donors, the experiment was performed in triplicate for each condition. One hour after the first treatment, the skin biopsies were exposed to DEE for 60 min (Project 1) or 30 min (Project 2), as previously described [64], by using a Kubota RTV-X900 diesel engine (KUBOTA Corporation, Gainesville (GA), USA) (3-cylinder, 4-cycle diesel with overhead valves, 1123 cc that has 24.8 HP at 3000 rpm). The untreated control samples (CTRL) were left in the incubator whereas some samples were only exposed to DEE as positive controls (DEE). After DEE exposure, the tissue samples were incubated in a humidified 5% CO_2/95% air atmosphere until the following day. The next day, treatment and exposure were repeated in the same way and samples were collected.

Tissue collection and immunofluorescence assay

The skin explants were fixed in 10% neutral buffered formalin for 48 h at 4 °C, dehydrated and embedded in paraffin. Then, 5 µm-thick sections were deparaffinized in xylene (10 min bath) and then rehydrated through a series of decreasing ratios of alcohols to water (30 sec bath each). The immunohistochemical analysis was performed as previously described [64], selecting antibodies depending on the study. In particular, the tissues were incubated with primary antibodies for 4HNE (dil. 1:400) (AB5605, Millipore Corporation, Burlington, MA, USA), type I collagen (dil. 1:200) (AB138492, Abcam, Cambridge, UK), filaggrin (dil. 1:50) (sc-66192, Santa Cruz Biotechnology, Inc., Dallas, TX, USA) or involucrin (dil. 1:50) (sc-21748, Santa Cruz Biotechnology Inc., USA), in 0.25% BSA in PBS overnight at 4 °C, and with fluorochrome-conjugated secondary antibodies (Alexa Fluor 568, A11004 or Alexa Fluor 488, A11055) diluted 1:1000 in 0.25% BSA in PBS at room temperature for 60 min. Nuclei were stained with DAPI (dil. 1:50,000) (D1306, Invitrogen, Waltham, MA, USA) in PBS. Coverslips were mounted onto glass slides using Fluoromount-G™ Mounting Medium (00-4958-02, ThermoFisher Scientific, Waltham, MA, USA). The tissues were examined using a Zeiss Z1 AxioObserver LSM10 confocal microscope at 40× magnification, and the images were quantified using ImageJ software 1.53a (Java 1.8.0_172, National Institutes of Health, Bethesda, MD, USA).

Statistical analysis

GraphPad Prism 9 (Version 9.4.1 (458), GraphPad Software Inc., La Jolla, CA, USA) was used to perform the statistical analysis. For each of the variables tested, an analysis of

variance (1-way or 2-way ANOVA), followed by Tukey's *post-hoc* test, was assessed. The data are expressed as the mean ± standard deviation of triplicate determinations obtained in three independent experiments, and a p value < 0.05 was considered statistically significant. For all the experiments, the control values were set to 1.0, and the other values were expressed as a fold change.

4.7.3 IN VIVO BIOLOGICAL STUDIES

Patch Test (Project 1 and Project 2)

In order to assess the skin irritation potential, tests on human volunteers were performed thanks to the contribution of the University of Ferrara Cosmetology Center. The study observed the standardized protocols for evaluating the skin compatibility of cosmetic ingredients that might be irritants, as outlined by SCCNFP/0245/99. The protocol was approved by Ethics Committee (study number: 170583). The irritant potential on the skin after single application of the formulations was evaluated. Each test was carried out on 20 healthy and randomly selected male and female volunteers, which have consented in writing to participate. Exclusion of individuals with dermatologic conditions, a history of allergic skin reactions, or those currently undergoing anti-inflammatory treatments was ensured. Each volunteer was administered with 10 mg of formulation containing CUR and PIP, using aluminum Finn chambers (Bracco, Milan, Italy) affixed through adhesive tape to the forearm or back.

Samples were deposit into the chambers using an insulin syringe, and skin contact was maintained for 48 h. Skin reactions, including erythema and/or edema, were assessed after 15 min and again after 24 h, after the removal of the chambers and the cleansing of any residual formulation. Erythema was categorized into three levels: mild, readily apparent and moderate to severe. From the sum of the edema and erythema scores, an average irritation index was calculated. Irritation index values can be interpreted as follows: more than 0.5 means slight irritation, between 2.5 and 5 refers to moderate irritation, between 5 and 8 denotes significant irritation.

Patch Test (Project 4)

In case of Project 4, the patch test was performed at the facilities of COMPLIFE ITALIA S.r.l.(Pavia, Italy). Twenty male and female volunteers with healthy, intact skin were recruited for patch testing in accordance with the principles of the Helsinki Declaration 1964. Thirty percent of volunteers with sensitive skin were included. Subjects with spots or marks in the test area, with dermatological problems, on local or systemic drug therapy, with a

previous clinical history of dermatitis, or with a positive history of atopy were excluded. The tested formulation (TE-GEN-gel and GEN-gel) was applied using the Finn Chamber, an 8 mm diameter aluminum disc. The Finn Chamber was affixed to the skin with a tape that had previously been tested for its safety and ensured the occlusive application of the product. A sufficient amount of product was applied to fill the chamber. The formulations were applied on the back and left in contact with the skin surface for 48 hours. Skin reactions were analyzed at 15 min, 1 hour, and 24 hours after removal of the Finn chamber. A Finn chamber containing an absorbent paper disc soaked in demineralized water was also applied as a negative control. The erythematous reactions were categorized into five groups, according to the degree of erythema: absent, light, clearly visible, moderate, and severe. The edematous reactions were similarly categorized into five groups, according to the degree of edema: absent, light, clearly visible, moderate, and severe. The mean Irritation Index (IIM) was calculated for each experimental time, represented by the sum of the mean erythema value and the mean edema value recorded. This index was used to classify the product under investigation as: non-irritating, slightly irritating, moderately irritating, or highly irritating.

Tape Stripping (Project 4)

The percutaneous absorption of the TE-GEN-gel and GEN-gel formulations was monitored in vivo using the tape stripping method, which is a relatively non-invasive technique that allows *stratum corneum* samples to be taken from the skin [65]. Experiments were carried out thanks to the collaboration with Prof. Stefano Manfredini from University of Ferrara (Department of Life Science and Biotechnology).

Twenty both male and female volunteers with healthy, intact skin were recruited for tape stripping after giving written consent. Subjects with spots or marks in the test area, with dermatological problems, on local or systemic drug therapy, with a previous clinical history of dermatitis or with a positive history of atopy, were excluded. The study was carried out in a partly air-conditioned room at a temperature of 22 ± 2 °C. The anatomical sites chosen were seven areas (10 cm^2) of the inner forearm. Three areas, A, B and C were treated with 200 µL of TE-GEN-gel formulation each, while areas D, E and F were treated with 200 µL GEN-gel formulation each. Area G was the negative control. Tape stripping was conducted at three distinct time points. One hour post-application of the products, tape stripping was performed on areas A, D, and G. Three hours post-application, tape stripping was executed on areas B and E. Six hours post-application, tape stripping was carried out in areas C and F. Rectangular sections of adhesive tape were applied to the skin, adhering precisely to the previously demarcated areas of the forearm (2 cm x 5 cm). The *stratum corneum* of the

treated area was removed through 11 successive tape strippings using '3M' (3M, Minneapolis, MN, USA) invisible adhesive tape. The tape was applied to the test site using forceps, uniformly flattened twice, and removed gently with moderate and even traction. Due to the potential for surface contamination and to eliminate surface lipids, the first (uppermost) tape stripping was discarded. Subsequent tapes were then placed, adhesive side downwards, into a glass container with 15 mL of MeOH (HPLC grade) and subsequently subjected to 30 min of treatment at 99% power in an ultrasonic bath. Solutions were then purified via centrifugation (10 min at 4000 cycles/s) to separate small horny layer particles. The supernatant was than filtered using nylon syringe filters (0.22 μm) and analysed using HPLC.

5. PROJECT 1 – Ethosomes for curcumin and piperine cutaneous delivery for the prevention of pollution-induced skin damage

5.1. INTRODUCTION

Environmental pollution is a worldwide recognized serious concern, affecting human health and the ecosystem. Indeed, many harmful solids, liquids and gases are hugely introduced into the environment due to modern unprecedented urbanization and industrialization, resulting in deleterious effects, involving cardiovascular, respiratory, reproductive and skin damage [66,67,68]. Among pollutants, diesel engine exhaust (DEE) is a complex mixture of gases and particulate matter, responsible for a plethora of systemic pathologies as well as skin conditions spanning from atopic dermatitis, eczema and ageing to melanoma [69,70]. Indeed, since the skin is an outer body organ, it represents, on the one hand, the first barrier against environmental factors and, on the other, the common route by which chemicals can enter the body. Nonetheless, since the skin's defensive potential in some cases can be insufficient to counteract the effect of environmental stressor exposure, a therapeutic and/or protective approach is desirable [71,72].

Many phytocompounds, such as CUR and PIP, possess therapeutic properties due to their pleiotropic potential [73,74]. CUR, besides being employed as a food additive, is recognized for its wide range of pharmacological activities [43,75,76]. In addition, its potential in the treatment of many skin conditions, has also been demonstrated [38].

Notwithstanding CUR's tolerability even at high doses, it is scarcely bioavailable, mainly because of its poor absorption, rapid metabolism and rapid elimination, limiting its therapeutic potential [40]. To increase its absorption, CUR has been investigated in association with PIP, acting as a natural enhancer [48,77,78,79]. The alkaloid PIP, is a natural dietary supplement with a distinct pungent flavour. Besides its therapeutic potential due to its several biological activities [44,74,80] is remarkably studied for its role as a biopotentiator, being able to increase the bioavailability and biological effectiveness of the drugs with which it is associated, inhibiting drug efflux transporters and modulating drug resistance pathways [48,81]. Recently, the synergistic effects of CUR with some phytochemicals, such as PIP, have been found, enabling CUR efficacy to be improved in many pathologies as well as in cancer treatment, suggesting the possibility of administering the two drugs in combination [77].

Regarding skin application, PIP has demonstrated its suitability (i) in the treatment of inflammatory skin diseases such as atopic dermatitis and psoriasis [49] and (ii) in enhancing the skin permeation ability of CUR in the form of a composite double-layer CUR/PIP delivery system [82]. Despite their pharmacological potential, both CUR and PIP are characterized by scarce solubility and chemical instability, restricting their therapeutic use [78]. To overcome these drawbacks, nanotechnology approaches have been undertaken aimed at solubilizing, protecting and delivering the drugs through different routes through nanoencapsulation. For instance, the co-loading of CUR and PIP in human serum albumin nanoparticles was investigated against breast cancer cells [83] while recently, a self-nanoemulsifying drug delivery system demonstrated the therapeutic efficiency of CUR and PIP in an animal model of Alzheimer's disease [84]. Remarkably, the drugs have been individually loaded in monoolein aqueous dispersions, nanoemulsions and polymeric and lipid nanoparticles, as well as in vesicular systems, including liposomes and ET [85-90].

Nevertheless, to the best of our knowledge, the effect of the topical administration of nanoencapsulated CUR in combination with nanoencapsulated PIP has not been investigated yet.

In the present investigation ET were selected as proper drug delivery system. As previously described (chapter 1.3.1), ET can be thought of as transdermal delivery systems, being able to promote the permeability of encapsulated drugs through different skin strata. Moreover, their simple and low-energy-consuming production protocol, together with the biocompatibility of the excipients, make these systems particularly attractive for dermatological applications, as demonstrated by the increasingly growing number of related research articles [12,91,92].

Thus, the aim of the present study is to evaluate the capability of CUR and PIP loaded in ET to prevent skin damage induced by environmental pollution. Particularly, both CUR and PIP were loaded separately in ET prepared by water injection method. The antioxidative effect of the drug-loaded ET, as well as the drug release and permeability, were studied in vitro. Their efficacy against cutaneous oxidative and structural damage was investigated on skin explants pre-treated with ET and exposed to DEE, selected as one of the most toxic air pollutants. At last, a patch test was performed on human volunteers to investigate their possible irritation effect under cutaneous administration.

The present results have been the object of the published paper: "Ethosomes for curcumin and piperine cutaneous delivery to prevent environmental-stressor-induced skin damage".

[Ferrara, F.; Bondi, A.; Pula, W.; Contado, C.; Baldisserotto A.; Manfredini, S.; Boldrini, P.; Sguizzato, M.; Montesi, L.; Benedusi, M.; et al.]. *Antioxidants* 2024, 13, 91. https://doi.org/10.3390/antiox13010091

5.2. RESULTS AND DISCUSSION

5.2.1. PREPARATION OF ETHOSOMES

ET nanovesicles were designed as biocompatible nanocarriers for the dermal and transdermal delivery of drugs. As previously described (chapter 1.3.1), with respect to other nanoparticulate systems, such as liposomes, ET can effectively load large amounts of lipophilic drugs while maintaining their stability. Moreover, their ability to allow drug penetration into the deeper skin layers is due to the presence of ethanol, which acts as a penetration enhancer in synergism with PC [93,94,95]. In the present investigation, water injection method was employed for the preparation. Composition (0.9% w/w PC and 30% v/v ethanol) was selected from previous studies carried out by our research group.

In case of drug-loaded ET, the active compound was previously solubilized in the PC–ethanol solution. The result is a homogeneous milky dispersion, with a characteristic yellow colour in the case of ET–CUR (Figure 10). Remarkable is that the methodology, which is simple and scalable, is conducted entirely at room temperature. This aspect is of particular relevance when working with sensitive drugs such as active molecules of natural origin, which could be degraded by high temperatures. In addition, excessive energy consumption is avoided.

This method enabled us to efficiently load either CUR or PIP in the ET, which composition is reported in Table 2.

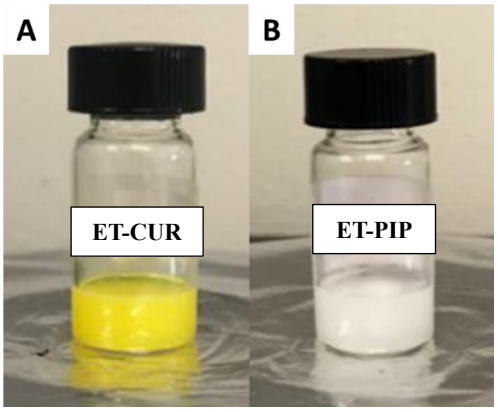

Figure 10. ET-CUR (A) and ET-PIP (B) prepared by water injection method.

Noteworthy, the simultaneous entrapment of the two compounds in a single ET formulation was not achievable, possibly because at the employed concentration (0.25 mg/mL), the drugs in the PC–ethanolic solution exceeded the point of saturation. However, co-administration of the two formulations with PIP e CUR separately encapsulated inside ET could be an advantage in terms of delivery and pharmacological efficacy.

Table 2. Composition of indicated formulations.

Formulation	PC[1] (%, w/w)	Ethanol (%, w/w)	H_2O (%, w/w)	PIP[2] (%, w/w)	CUR[3] (%, w/w)
ET	0.9	29.100	70	-	-
ET-PIP	0.9	29.075	70	0.025	-
ET-CUR	0.9	29.075	70	-	0.025

[1]: soy phosphatidylcholine; [2]: piperine; [3]: curcumin.

5.2.2. SIZE DISTRIBUTION

ET formulations were characterized by size one day after the preparation using PCS method. Results are summarized in the Table 3. No size differences were found between ET-CUR and ET-PIP, whose mean diameter, expressed as Z-Average, was slightly higher with respect to empty ET. The dispersity index was always below 0.2, indicating homogeneous size distributions.

After 2 months of storage at room temperature, a slight Z-Average increase was detected, but the system kept its narrow size distribution (Table 3).

Table 3. Size distribution parameters of ET as determined by PCS.

Formulation	Time (days)	Z-Average (nm) ± s.d.	Dispersity index ± s.d.
ET	1	206.32 ± 33.22	0.144± 0.012
	60	230.36 ± 23.11	0.155± 0.032
ET-PIP	1	213.13 ± 13.18	0.129 ± 0.019
	60	269.8 ± 15.13	0.196 ± 0.069
ET-CUR	1	213.03 ± 8.25	0.127 ± 0.046
	60	242.85 ± 9.97	0.189 ± 0.00

s.d.: standard deviation; data are the mean of 3 independent determinations on different batches.

5.2.3. ENTRAPMENT CAPACITY EVALUATION

The EC was obtained through the ultrafiltration method, which consists in the separation of the vesicular fraction from the aqueous dispersing phase. Subsequently, in order to quantify the amount of drug associated to ET, retentate fraction was diluted in ethanol and subjected to magnetic stirring (chapter 4.4.1) to promote vesicles disaggregation. Similarly, also the total dispersed formulation was diluted in ethanol to quantify the real drug concentration inside the whole formulation. HPLC analysis method was employed for the quantification of the samples. As shown in Table 4, in both cases, most of the drug results associated to the nanovesicles. The EC was higher in the case of ET–CUR (97%) with respect to ET–PIP (79%), probably due to different physiochemical properties. In fact, CUR has higher lipophilicity (log P 3.29) and molecular weight (368.4 g/mol) with respect to PIP (log P 2.78; molecular weight: 285.34 g/mol) suggesting that CUR could possibly be more efficiently retained within the PC double layers of the ET vesicles [96,97].

Table 4. Entrapment capacity of the indicated formulations.

Formulation	EC[1] (%) ± s.d.
ET-PIP	78.95 ± 6.47
ET-CUR	96.87 ± 4.31

1: Entrapment capacity, as defined in Equation (2); data are the mean of 6 independent experiments± s.d.

5.2.4. MORPHOLOGICAL CHARACTERIZATION

The assessment of ET morphology was carried out by TEM. Figure 11 shows TEM micrographs of empty ET (Figure 11a), ET-CUR (Figure 11b), ET-PIP (Figure 11c).

It is possible to appreciate the spherical or ovoidal shape of the nanovesicles and also the characteristic internal multilamellarity. By the way, the presence of the two drugs (both CUR and PIP) did not affect the supramolecular structure of the nanovesicles.

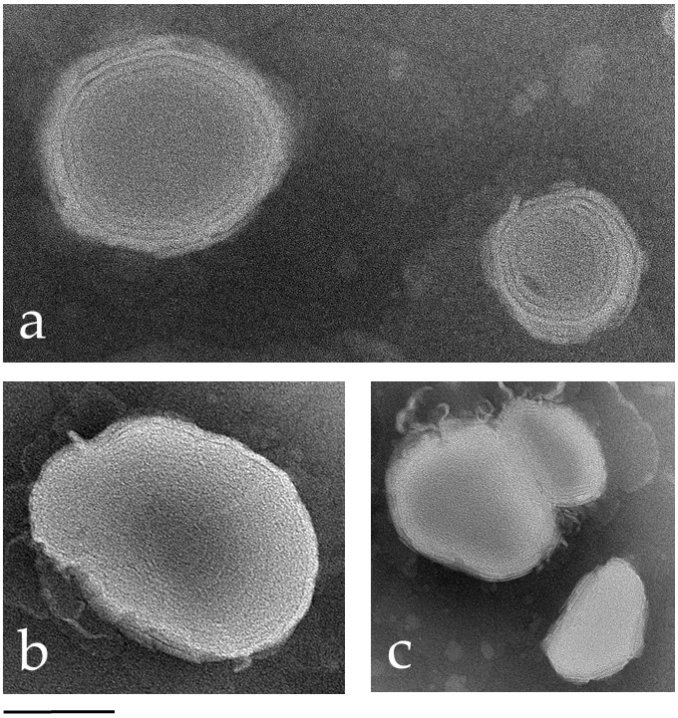

Figure 11. TEM micrographs of ET (a), ET-CUR (b) and ET-PIP (c). The bar corresponds to 150, 100 and 200 nm in panels (a), (b), (c), respectively.

5.2.5. ANTIOXIDANT ACTIVITY EVALUATION

By means of the FRAP test, the in vitro antioxidant activity of the formulations loaded with the two active compounds (ET-CUR and ET-PIP) was evaluated and compared with CUR and PIP solutions (SOL-CUR and SOL-PIP). In addition, empty ET were assayed, as were the combinations of ET–PIP + ET–CUR (PIP: 0.125 mg/mL; CUR: 0.125 mg/mL) and SOL–PIP + SOL–CUR at the same drug concentration. Results are summarized in Table 5.

FRAP test allows to evaluate the ferric ion (Fe^{3+}) reduction potential of the tested sample. The results show that the ET, ET–PIP and SOL–PIP have no antioxidant activity, while the well-known antioxidant activity of CUR was confirmed ($p > 0.6$) [98]. In specific, ET-CUR and SOL-CUR showed very similar values demonstrating that the activity of CUR was not masked or reduced by the encapsulation. Since FRAP is a very fast test, it is assumed that the vesicles are not structurally altered by sample preparation and remain intact during the course of the assay.

Table 5. Antioxidant activity of indicated formulations as resulted from FRAP test.

Formulation	FRAP[1] (µmol TE/g)
ET	n.a.[1]
SOL-PIP	n.a.[1]
ET-PIP	n.a.[1]
SOL-CUR	3042.86 ± 191.73
ET-CUR	3097.27 ± 112.83*
SOL-PIP + SOL-CUR	2996.50 ± 95.54
ET-PIP + ET-CUR	3408.87 ± 68.80*

1: not active ; each value is the mean of at least three different experiments (mean ± SEM). * $p < 0.035$.

From a practical point of view, since in the FRAP assay, SOL–CUR and ET–CUR were diluted in the same solvent, the antioxidant activity of CUR was expected to be the same for the two samples, demonstrating that the drug loaded in the ET did not undergo any chemical degradation. CUR antioxidant or pro-oxidant behaviour depends on its structural form; specifically, the molecule can exist in two tautomeric forms: keto and enol. The CUR antioxidant activity is exerted by the keto form, which is able to donate protons whereas the enol form is more susceptible to degradation [43]. FRAP test is performed in acidic environment which favours the keto form. This occurred equally both for CUR loaded in ET and free in solution. Thus, in both cases, CUR resulted directly available to react with Fe^{3+} complexed with TPTZ and reduce it to Fe^{2+}.

Noteworthy is that the combination of the two drugs in the solution showed the same antioxidant power of CUR detected for ET-CUR and SOL-CUR whereas the combination of the vesicular formulations (ET–PIP + ET–CUR) resulted in a statistically significant ($p< 0.035$) increase in its antioxidant power compared to ET–CUR. This result allows us to state that the combination of ET–PIP and ET–CUR enhances the antioxidant effect of CUR, confirming the evidence published also in other studies [98,99].

5.2.6. IVRT

The IVRT was performed using Franz cells as previously described (chapter 4.6). The membrane chosen to carry out the experiment was a synthetic PTFE membrane. Such a membrane serves only as an inert support to separate the upper compartment from the lower compartment. According to the guidelines [100] the membranes chosen for IVRTs must not interfere in any way with the process of releasing the drug from the vehicle. The aim of the experiment was to compare the release kinetics of CUR and PIP, both loaded within ET and free in ethanol solution. As shown in graph (Figure 12), ET resulted able to control both

CUR and PIP release as compared to the drug solutions. This result is in agreement with expectations and demonstrate their effectiveness as release control systems. Moreover, PIP release was much faster with respect to CUR one, both in ET and solution formulations. As reported in Table 6, the release rate (R) obtained for ET-PIP was 1.75 times higher with respect to ET-CUR. It is likely that, in agreement with the findings for the EC parameter, by virtue of its chemical and physical properties, CUR is more retained by the nanosystem and is released more slowly.

The percentage release profile of the drugs, expressed as a percentage of the drug released, as reported in Figure 12B, confirms the trend obtained by plotting the mass units (μg) per unit area (cm^2) and revealed that the percentage of drug release with respect to the drug loaded in the formulation was 57%, 33%, 24% and 15% in the cases of SOL–PIP, ET–PIP, SOL–CUR and ET–CUR, respectively.

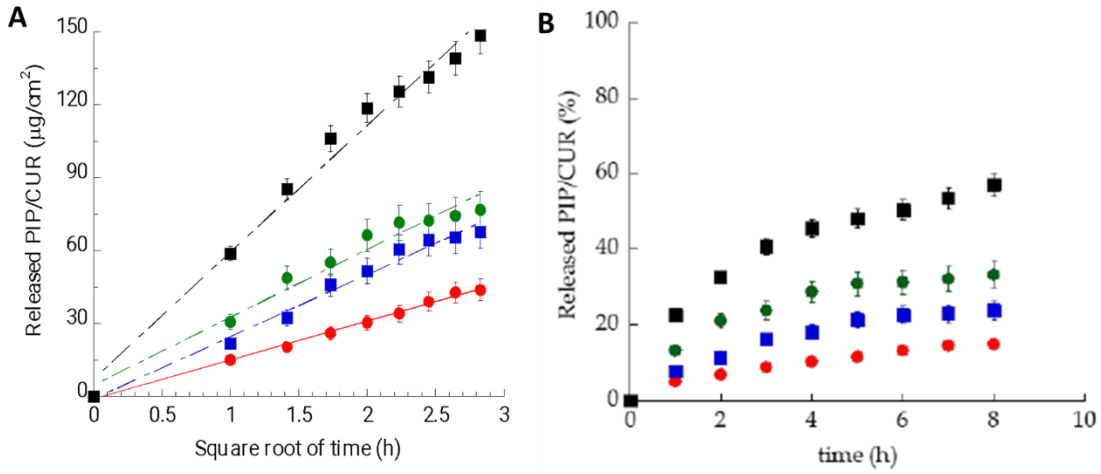

Figure 12. CUR and PIP release kinetics from ET–CUR (red circles), SOL–CUR (blue squares), ET–PIP (green circles) and SOL–PIP (black squares), as determined by Franz cells associated with the PTFE membrane. In panel (A) data are expressed as μg/cm^2 versus the square root of time, while in panel (B) data are expressed as percentage of released drug (referred to the amount of drug loaded in the formulation) versus time. Data are the mean of 6 independent experiments ± s.d.

In order to elucidate the mechanism of drug release from the ET, four different mathematical models were applied to release profiles of selected formulations ET-CUR and ET-PIP, and corresponding solutions, as controls. In specific, zero-order plot, first-order plot, Higuchi plot and Peppas plot were applied [101]. Table 6 reports R^2 values obtained by plotting the release data with the linearization conditions for the different models. It results that CUR and PIP release from ET followed Higuchi kinetics possibly due to the initially controlled drug diffusion through the matrix, as found by other authors [102]. The Peppas equation fitting revealed a Fickian diffusion mechanism with a release exponent (n) of around 0.5 for both ET-CUR and ET-PIP.

Table 6. IVRT parameters and kinetic data of the indicated formulations.

Formulation	R[1] (μg/cm²/h)	A[2] (μg/cm²)	Zero Order Plot (R^2)	First Order Plot (R^2)	Higuchi Plot (R^2)	Peppas Plot (n/R^2)
ET-CUR	15.96 ± 2.52	43.87 ± 8.28	0.935	0.947	0.996	0.54/0.995
SOL-CUR	25.67 ± 5.41	67.75 ± 5.50	0.892	0.912	0.985	0.57/0.977
ET-PIP	27.88 ± 6.04	76.65 ± 7.52	0.805	0.843	0.967	0.43/0.954
SOL-PIP	52.08 ± 4.24	148.49 ± 10.45	0.839	0.917	0.984	0.43/0.982

[1]: release rate; [2]: amount of CUR/PIP released after 8 h; CUR and PIP concentration was 0.25 mg/mL; data are the mean of 6 independent Franz cell experiments ± s.d.

5.2.7. IVPT

The IVPT was conducted using the same Franz cells apparatus and conditions employed for IVRT but selecting STRAT-M® as membrane to separate the donor to the receptor compartments. Since these formulations are intended for topical application, a membrane able to mimic skin hydrophobicity and porosity was chosen. In specific, STRAT-M® is a synthetic membrane made of two polyether sulfone layers overlapped by one polyolefin bottom layer and impregnated with synthetic lipids. Due to this peculiar architecture, is considered as valuable model for *stratum corneum* barrier properties [61,103]. Figure 13 show the CUR (a,b) and PIP (c,d) diffusion profiles through the STRAT-M® membrane and Table 7 reports the diffusion parameters. Drug diffusion across the skin is a complex process that can be summarized in two main steps. The first one is described by the P coefficient, which reflects the preferred distribution of the drug in the skin/membrane or vehicle. The second step, described by the D and Kp coefficients, refers to the diffusion of the drug through the skin (or membrane), depending on its characteristics and vehicle properties [100,104,105].

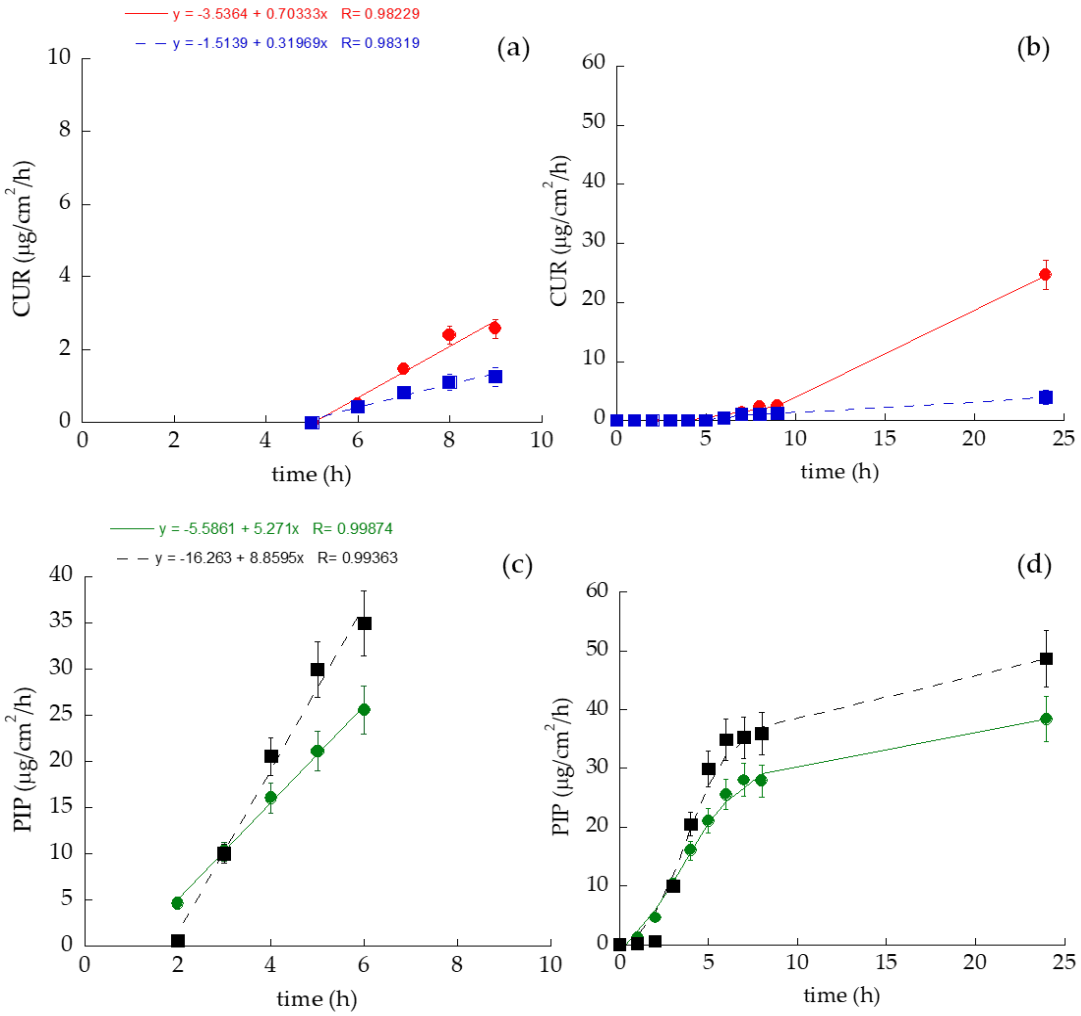

Figure 13. CUR (a,b) and PIP (c,d) permeability kinetics from ET-CUR (red circles), SOL-CUR (blue squares), ET-PIP (green circles) and SOL-PIP (black squares) as determined by Franz cells associated to STRAT-M® membrane. (a,c) show the linear part of the kinetic profile; (b,d) show diffusion profile occurred in 0-24 h. Data are the mean of 6 independent experiments ± s.d.

Table 7. IVPT parameters of the indicated formulations.

IVPT Parameters	ET-CUR	SOL-CUR	ET-PIP	SOL-PIP
Jss[1] (µg/cm²/h)	0.70 ± 0.21	0.32 ± 0.1	5.27 ± 2.2	8.85 ± 3.1
Kp[2] (cm/h) x 10^3	3.12 ± 0.94	1.28 ± 0.40	23.11 ± 9.65	43.81 ± 15.35
Tlag[3] (h)	5.03 ± 0.81	4.74 ± 0.33	1.06 ± 0.052	1.84 ± 0.23
D[4] (cm^2 h^{-1}) x 10^5	3.33 ± 0.54	3.53 ± 0.25	15.80 ± 0.76	9.10 ± 1.14
P[5] membrane/vehicle	2.97 ± 1.37	1.15 ± 0.44	4.64 ± 2.16	15.26 ± 7.25
A[6] (µg/cm^{-2})	24.67 ± 4.1	3.92 ± 0.42	38.40 ± 5.67	48.66 ± 7.44

[1]: Steady-state flux per unit area ; [2]: permeability coefficient ; [3]: lag-time ; [4] diffusion coefficient; [5] partition coefficient ; [6] cumulative amount of drug diffused at 24 h; CUR and PIP concentration was always 0.25 mg/mL; data are the mean of 6 independent Franz cell experiments ± s.d.

As shown in the graph, PIP diffused much faster with respect to CUR both in the case of ET and solution formulations. A lag time was detected in all the diffusion kinetics, which was longer for CUR with respect to PIP, particularly in the case of ET–CUR it was five-fold

higher than ET–PIP, which confirms a stronger association of CUR with the vesicular system. As previously discussed, the higher lipophilicity of CUR with respect to PIP results in a stronger affinity for the drug delivery system and therefore greater retention by nanovesicles and slower diffusion. Comparing the vesicular system with the solution, we can clearly assert that CUR diffusion was much faster from ET with respect to the corresponding solution. Noteworthy, the amount of drug diffused after 24 h (A) was 6.29 times higher in the case of ET-CUR with respect to SOL-CUR. This finding strengthens the hypothesis about the potential of ET as systems capable of promoting the penetration of lipophilic drugs through the skin. In the opposite, in the case of PIP, the drug diffusion was faster in the solution SOL–PIP with respect to ET–PIP, with a slope decline after 9 h. This means that PIP loading in ET did not have a significant impact on its permeability. The Kp values followed the order SOL–PIP > ET–PIP > ET–CUR > SOL–CUR. Particularly in the case of ET–PIP, the Kp value was 7.4-fold higher with respect to ET–CUR. Similarly, the P values suggest in the case of ET–CUR a higher drug partition towards the membrane with respect to the solution, while an opposite behavior was found in the case of PIP. This result suggests that CUR loading in ET could promote a drug interaction towards the STRAT-M® membrane, so the skin. Finally, the highest D value was found in the case of ET–PIP, around five times higher with respect to ET–CUR.

5.2.8. PATCH TEST

In order to evaluate in vivo if ET–CUR and ET–PIP could induce an irritative reaction when applied to the skin, a patch test was performed, on 20 healthy volunteers. The count of irritative reactions noted 15 minutes and 24 hours after the removal of the Finn Chamber was recorded and expressed as irritation indexes. The single application of ET-CUR or ET-PIP resulted in average 0.1 irritation index score, while the combination of the two vesicular formulations led to 0.2 irritation index score. Since we can consider a reaction slightly irritating with an irritation index score above 0.5, we can say that in all cases the reactions were not relevant. For this reason, the formulations can be considered as non-irritating when applied on human skin, either individually or in combination.

5.2.9. BIOLOGICAL ACTIVITY – EX VIVO EXPERIMENT

Once characterised, it was decided to test the biological activity of the formulations via an ex vivo model consisting of human skin biopsies. The objective was to assess the protective action of the two active compounds (CUR and PIP) delivered within the ET formulations, against cutaneous oxidative and structural damage induced by DEE. For this purpose, the

skin explants were pre-treated with the different formulations and exposed to DEE. As a comparison, some of the tissues were pre-treated with the solutions of the drugs (SOL-CUR and SOL-PIP). Moreover, in order to evaluate a potential synergism between CUR and PIP, the combination of the two formulations (both ET and solutions), was also studied. Exposure to environmental pollutants is known to cause oxidative and inflammatory reactions within the human skin that can ultimately result in skin structural damage and premature aging [106]. Thus, in order to evaluate DEE effect on the skin and the activity of the treatments, immunohistochemical analysis was performed, quantifying the expression of three different markers: 4-hydroxy-nonenal (4HNE), filaggrin and collagen type-I.

As shown in Figure 14a, the exposure to DEE induced a significant increase in 4HNE levels in the human skin explants compared to the controls. 4HNE is a reactive aldehyde produced by lipid peroxidative events, which can affect skin proteins' functionality by forming adducts that cause such proteins to lose their activity and be degraded [107]. ROS induced by air pollutants can promote lipid peroxidative events that culminate in the production of secondary mediators, such as 4HNE, that can propagate cutaneous oxidative damage throughout the skin layers [107]. Results show that ET–CUR, ET–PIP and the combination of the drug solutions SOL–PIP + SOL–CUR were found to be the most effective formulations in reducing the levels of 4HNE at basal conditions. In the other hand, SOL-CUR and SOL PIP treatments failed to prevent oxidative damage by DEE, aligning with previous findings on the lack of antioxidant activity of SOL-PIP and the poor permeability of SOL-CUR. Noteworthy is that SOL–CUR cannot properly pass the *stratum corneum*, so it is not available to exert its antioxidant properties. On the contrary, when delivered via ET, CUR can reach the skin layers and be available for the cells, explicating its antioxidant activity. These results are in line with previous work, where ET have been found to be able to reach the deeper layers of the skin, thus allowing the release of a drug within the cutaneous tissues [27].

Of note, CUR has been shown to protect from lipid peroxidative events, behaving as a chain-breaker antioxidant [42]. Indeed, the functional groups present in CUR's structure, such as the ß-diketo group, carbon and phenyl rings, and carbon–carbon double bonds, are able to donate H-atoms, thus protecting biomembranes against peroxidative damage [41,108]. Although PIP was also demonstrated to possess antioxidant properties by quenching ROS, free radicals and reactive metabolic intermediates, its antioxidant activity is strictly related to the dose used [44,80,109]. Thus, we believe that at this concentration, PIP was not able to

exert an evident antioxidant property, whereas CUR prevented the lipid peroxidation cascade occurring within the skin upon DEE exposure.

Moreover, the enhanced permeability of ET-loaded CUR together with its slower release suggests that the skin administration of ET–CUR could promote a prolonged protective effect, while the association with ET–PIP could potentiate CUR action against secondary responses to oxidative stress in the skin. Oxidative stress is typically an immediate response to an insult, but the ensuing cascade can lead to a sustained skin response.

Besides, DEE exposure is associated with reduced levels of filaggrin, a key protein in the skin cornified cell envelope, essential for maintaining structural integrity, hydration and cutaneous barrier properties.

The oxidative and inflammatory events promoted by air pollutants can alter the skin cell differentiation and proliferation processes, affecting skin structural proteins and thus skin integrity and functionality, and rendering the cutaneous tissue more susceptible to being affected by other environmental insults [106,110,111]. The treatment of the skin with natural antioxidant and anti-inflammatory compounds was found to counteract the air pollutants' damage and restore skin homeostasis [64,110,112,113]. In this context, natural antioxidants and anti-inflammatory agents have been shown to counteract pollutants' effects and restore skin equilibrium [114,115].

Thus, the cutaneous structural damage was evaluated by measuring the expression levels of filaggrin. In our study, as expected, the skin explants exposed to DEE showed reduced levels of filaggrin, indicating structural damage promoted by the pollutant. Conversely, the treatment with the different formulations, especially ET–PIP and the combination of ET–PIP + ET–CUR, efficiently counteracted the DEE-induced skin damage (Figure 14b). This result suggests that while CUR alone did not demonstrate protective effects, the presence of PIP may have enhanced CUR's efficacy at the selected dose.

CUR, indeed, is known to exert anti-inflammatory properties by suppressing prostaglandin synthesis, interfering with the signaling mechanisms involved in COX-2 enzyme transcription and inhibiting the LOX pathway [42]. Moreover, CUR has been shown to modulate the activation of the NF-κB by preventing its translocation to the nucleus, which is necessary for the transcription of genes involved in the inflammatory response [42,116,117,118]. Considering the strict link between oxidative and inflammatory responses, CUR has been shown to regulate oxidative stress via both ROS and NF-κB pathways [119]. PIP, as well, has been reported to be a potent inhibitor of NF-κB translocation in melanoma

[120] and to attenuate cigarette-smoke-induced oxidative stress and lung inflammation by upregulating Sirtuin1 (SIRT1) and promoting the inhibition of NF-κB and the activation of the antioxidant response via nuclear factor erythroid 2-related factor 2 (Nrf2) [121]. It should be mentioned that skin structural damage is often a consequence of a combination of oxidative and inflammatory reactions; therefore, it is possible that CUR at the dose applied in this study is not able to exert a protective role, whereas PIP might contribute to the anti-inflammatory response of the skin. Moreover, PIP permeability and diffusion were higher in the case of ET–PIP with respect to ET–CUR, suggesting its capability to counteract structural damage earlier than CUR under our experimental conditions. It is worth recalling that, whereas ROS production is a quick event occurring right after exposure to environmental insults, cutaneous structural damage is the result of a later response of the skin to ox-inflammatory damage. The slower drug diffusion and permeability in the case of ET–CUR could account for its protective effect displayed after a prolonged exposure time. Further experiments are needed to better elucidate the possible protective effect of ET–CUR on chronic exposure.

Finally, type I collagen expression, a protein expressed in the dermis, essential for skin elasticity and strength, which is degraded during ageing, was quantified (Figure 14c). It resulted that all the formulations, besides SOL-CUR, were able to prevent the degradation of collagen-I. Noteworthy, the combination of CUR and PIP, both as SOL–PIP + SOL–CUR and as ET–CUR +ET–PIP, was the most efficient in preventing the damage, suggesting that PIP might act as a biopotentiator of CUR to counteract the skin aging process induced by air pollutants and also their synergistic effect in preserving collagen, suggests their potential in protecting against the skin inflammation process [122]. Nevertheless, although PIP biopotentiator/bioenhancer action is widely studied for the oral route, there is still little knowledge about its effect when co-administered topically. Additional studies will certainly be required to investigate this aspect further.

Indeed, the premature skin aging process induced by exposure to air pollutants is mainly accompanied by a loss of proteins that confer elasticity and mechanical strength to the skin, such as type I collagen. Indeed, the activation of metalloproteinases (MMPs) in the extracellular matrix in response to environmental stressors can promote the degradation of this protein, promoting wrinkle formation and other signs of aging [123]. Notably, CUR can promote type I collagen induction via the inhibition of ROS [124] and modulate MMP activation, as can PIP [120,125]. Taken together, our results show that the combination of

CUR and PIP may be helpful in regulating many inflammatory and oxidative stress pathways, thus broadly protecting the skin from harmful external stimuli.

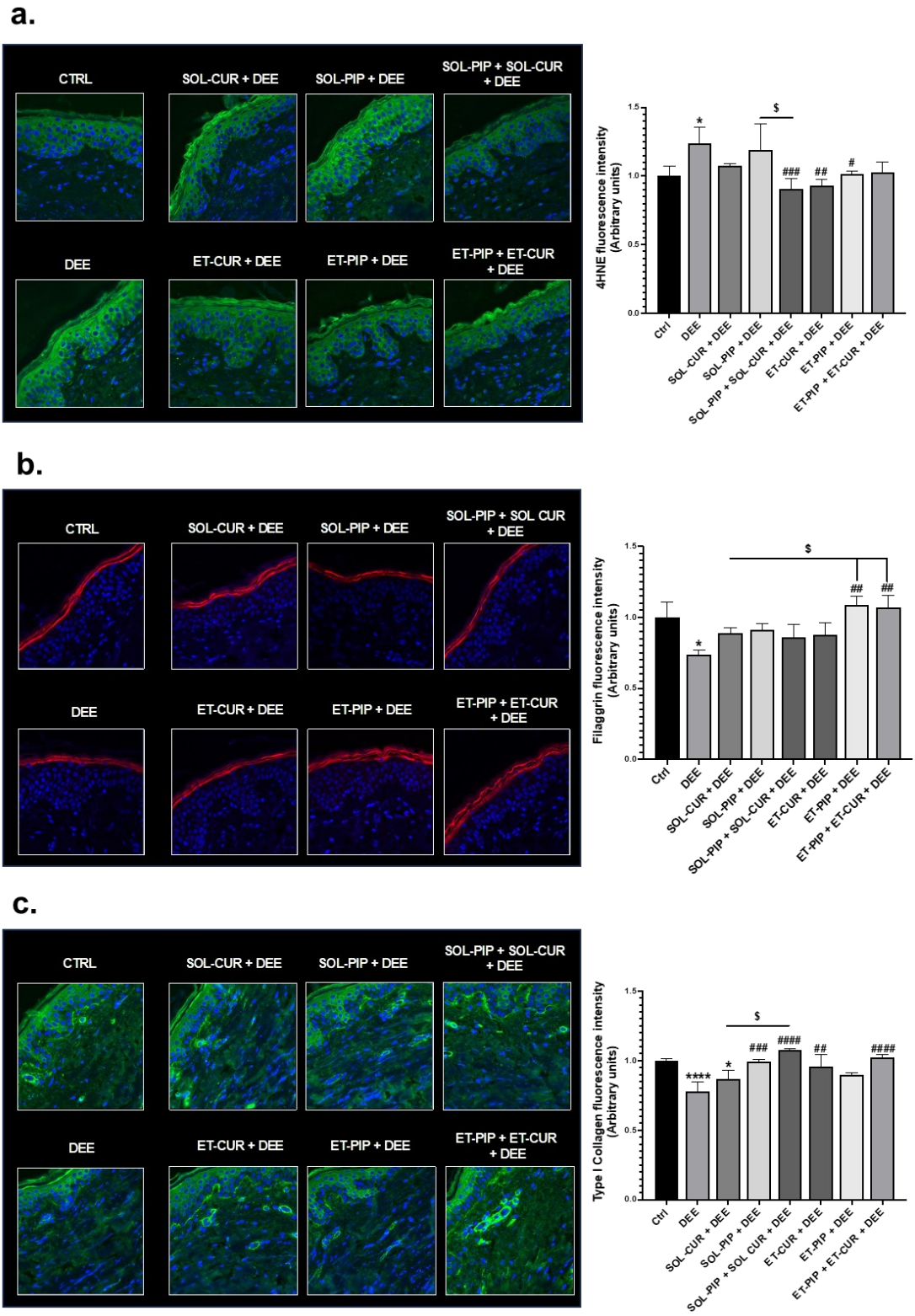

Figure 14. Immunofluorescence staining for 4HNE (a) filaggrin (b) and collagen type I (c) in human skin biopsies treated with the indicated formulations and exposed to DEE. Red or green stainings represent the selected proteins and the blue staining (DAPI) represents nuclei. Images were taken at 40x magnification. The fluorescent signal of the different markers was quantified using the ImageJ software 1.53a (Java 1.8.0_172) and expressed in the graphs. Data are the results of the averages of at least three different experiments, with $^{*,\#,\$}$ $p < 0.05$; $^{**,\#\#,\$\$}$ $p < 0.005$; $^{***,\#\#\#,\$\$\$}$ $p < 0.001$; $^{****,\#\#\#\#,\$\$\$\$}$ $p < 0.0001$ by 2-way ANOVA followed by Tukey's post-hoc comparison test [126]. DEE, SOL–

CUR+DEE, SOL–PIP+DEE, SOL–PIP+SOL–CUR+DEE, ET–CUR, ET–PIP, ET–PIP+ET–CUR+DEE vs. Ctrl (*); CTRL, SOL–CUR+DEE, SOL–PIP+DEE, SOL–PIP+SOL–CUR+DEE, ET–CUR, ET–PIP, ET–PIP+ET–CUR+DEE vs. DEE (#); SOL–PIP+SOL–CUR+DEE vs. SOL–CUR+DEE ($).

6. PROJECT 2 – Co-delivery of curcumin and piperine within spongosomes: a second strategy to prevent pollution-induced skin damage

6.1. INTRODUCTION

The present project is intended as a continuation of the previous one. In particular, the therapeutic objective addressed is still the prevention of skin damage caused by exposure to pollutants. In fact, since the skin is the first defence line between the body and the outside world, prolonged exposure to external insults such as pollutants leads to the formation of ROS and the generation of bioactive molecules that can affect cellular structure and functions [127]. However, endogenous antioxidant defences may not be able to counteract the damaging effects induced by ROS, resulting in cellular impairment and disturbance of skin barrier function. Alterations in *stratum corneum* lipid metabolism as well as the functionality of protein components can promote the development of several skin diseases and disorders [127]. It has been widely recognized that excessive exposure to UV rays, as well as many air pollutants including smoke exposure, factory emissions, automobile exhaust, can be associated with the development of skin conditions [64,128].

As described in the previous chapter, diesel engine emissions are the most common outdoor pollutants worldwide, affecting human health. DEE comprise a complex mixture of solid, condensed, and gaseous fractions, which composition consists in elemental carbon, metals and metal-oxides, toxic inorganic gases, such as carbon dioxide, carbon monoxide, nitric oxide and nitrogen dioxide, as well as a mixture of polyaromatic hydrocarbons, aldehydes and heterocyclic aromatic compounds [129]. Both short- and long-term exposure to such toxicants is associated with oxidative stress and inflammation, which can accelerate the skin aging process, or the onset of diseases such as atopic dermatitis, acne, psoriasis, androgenetic alopecia, and skin cancers [130,131]. In this respect, the administration of molecules able to prevent the skin oxidative insult can represent a strategy to restore the homeostasis skin defence mechanism [132,133]. In particular, phytocompounds such as CUR and PIP possessing anti-oxidant and anti-inflammatory properties, could represent *green* alternatives to synthetic molecules. As mentioned above, however, despite its wide and well-known therapeutic potential, including directed at skin diseases, CUR is characterised by a low bioavailability that hinders its use in therapy [38,39,40,43]. On the other hand, PIP, in addition to being known for its therapeutic potential, presents itself as an interesting way to increase the bioavailability of co-administered molecules [44,45]. Notably, some studies

have demonstrated the efficacy of PIP in increasing CUR topical absorption, suggesting a penetration enhancer role [50,82].

In this regard, already in Project 1 we demonstrated the potential of CUR and PIP, loaded separately in the ET, in preventing skin damage caused by exposure to DEE. Owing to these encouraging results, in the present study, we further explored the possibility of administering both molecules on the skin using a single delivery system. In particular, lipid supramolecular systems based on GMO have been investigated.

GMO is a biodegradable and non-toxic unsaturated monoglyceride which, due to its amphiphilic character, can self-assemble in water leading to different liquid crystalline structures [29]. The dispersion of GMO in water under a high energy input and specific temperature in the presence of surfactants results in the formation of lipid nanostructures with an inner phase consisting of lyotropic liquid crystalline phases. As previously described, (chapter 1.3.2) these lipid supramolecular systems represent attractive nanoplatforms for drug delivery [31], in particular for topical administration of active compounds, due to the structural similarity of GMO dispersions with *stratum corneum* lipid structure [8,32,33].

Preparation modalities and type of surfactants chosen influence the formation of lipid nanostructures with different inner organization, such as cubosomes, hexasomes, or spongosomes (SP). The latest are characterized by an inner "sponge" mesophase organization, a bicontinuous phase less ordered and more fluid compared to cubic phases and classified as "L3" [29,134,135]. The SP architecture presents open structures consisting of a highly convoluted and interconnected three-dimensional network, in which bicontinuous lipid bilayers intersect with nanometer-sized aqueous channels allowing to entrap either hydrophilic or hydrophobic molecules [135].

With respect to liposomes, cubosomes and spongosomes possess a nanochannel network organization enabling a higher drug encapsulation efficacy and sustained release. In addition, cubosome and spongosome advantages with respect to liposomes are related to their larger specific surface area and longer stability, enabling to storage them for long time without phase separation or particle size increase [8,29,31].

As previously reported by other authors, CUR can be efficiently co-loaded in SP; for instance, Rakotoarisoa et al. investigated the neuroprotective potential of these nanostructures as delivery systems of CUR in association with fish oil. Indeed, the SP's large lipid/water interface area enables to solubilize both hydrophilic and lipophilic drugs [135].

In the present study, the possibility of co-loading PIP and CUR in SP was investigated to obtain a single lipid-based dispersion suitable for topical administration. Particularly, the formulation should improve CUR oxinflammatory power [136] and protect the skin against environmental-induced skin damage. After selection of the production method and composition, the GMO dispersions were thoroughly characterized for their physicochemical parameters, as well as their capability to control CUR and PIP diffusion. Afterwards the SP efficacy against cutaneous oxidative and structural damage was investigated on skin explants exposed to DEE, evaluating the skin levels of some proteins such as filaggrin, involucrin, and type I collagen.

The present results have been the object of the published paper: "Spongosome-based co-delivery of curcumin and piperine: a novel strategy for mitigating pollution-induced skin damage" [Bondi, A.; Ferrara, F.; Pula, W.; Mariani, P.; Pepe, A.; Drechsler, M.; Montesi, L.; Manfredini, S.; Valacchi, G.; and Elisabetta Esposito.] *Colloid and Interface Science Communications* 2024, 63, 100811. https://doi.org/10.1016/j.colcom.2024.100811

6.2. RESULTS AND DISCUSSION

6.2.1. PREPARATION AND CHARACTERIZATION OF GMO DISPERSIONS – PREFORMULATORY STUDY

The purpose of the present investigation is to apply GMO-based liquid crystalline structures for the transdermal delivery of CUR and PIP in combination. Joint loading of bioactive compounds in nanoplatforms has been employed to improve their bioavailability and stability. For instance, many studies in the food field have demonstrated the advantages of simultaneously administering phytocompounds such as CUR, PIP, quercetin, genistein, and coenzyme Q10 to improve their bioaccessibility and control their chemical degradation [137].

In particular, SP, new promising platforms for skin delivery, were proposed in the present work as tool for CUR and PIP skin delivery, with the purpose of the prevention of environmentally induced skin damage. As mentioned above, exposure to pollutants can lead to the onset or exacerbation of numerous diseases, from skin aging to cancer [138,139].

In a previous investigation, our research group demonstrated the suitability of GMO dispersions, stabilised by NaChol and NaCas, to load CUR, resulting in different liquid

crystalline structures. The ability to affect cell proliferation by inhibiting the activation of the NFkB/cyclin D1 pathways suggests the possibility of employing GMO dispersions to deliver CUR through the skin [140]. Based on the previous preliminary findings, in the present research study we further explored the GMO dispersion potential as cutaneous delivery system for CUR co-loaded with PIP.

In the first part of the work, we conducted a preformulatory study to obtain GMO dispersions suitable for CUR and PIP solubilization. Table 8 reports the composition of GMO dispersions stabilized by NaChol (GD1), or by a mixture of NaChol and NaCas (GD2). Both dispersions appeared milky, homogeneous, and free from both aggregation and sedimentation.

Table 8. Composition of GMO dispersions.

Formulation	GMO[1] %w/w	NaChol[2] %w/w	NaCas[3] %w/w	H_2O %w/w	Z Average(nm) ± s.d.	DI[4]± s.d.
GD1	4.50	0.15	-	95.350	198.38 ± 23.67	0.20 ± 0.04
GD2	4.50	0.15	0.07	95.325	214.65 ± 11.10	0.21 ± 0.01

[1] Glyceryl monoolein; [2] Na cholate; [3] Na caseinate; [4]Dispersity index.

In the present investigation, we also decided to modify the method previously employed by our research group for the preparation of GMO aqueous dispersions [85,141,142], which was based on lipid phase melting and emulsification, followed by homogenization of the dispersion, resulting for instrumental reason in 50 mL volumes for each batch. Precisely, in order to reduce material waste and costs, we succeeded in developing a procedure based on the hydration of a GMO thin film followed by homogenization, enabling a 10-fold reduction in the preparation volume to 5 mL.

GMO dispersion size distribution parameters, obtained by PCS analysis the day after the preparation, are shown in Table 8. Mean diameters, expressed as Z-Average, are around 200 nm, suitable for promoting drug penetration through the skin [8], only slightly larger in the case of GD2, which is enriched with NaCas in its composition. Dispersity indexes were always around 0.2, demonstrating homogeneous size distribution.

6.2.2. MORPHOLOGY AND SAXS CHARACTERIZATION

In order to investigate the morphology and the inner supramolecular structure of GMO dispersions, Cryo-TEM and SAXS were employed.

The Cryo-TEM micrographs reported in Figure 15 show spheroidal and hexagonal structures with the typical irregular inner organization of sponge phase, both in the case of GD1 (A) and GD2 (B) [29].

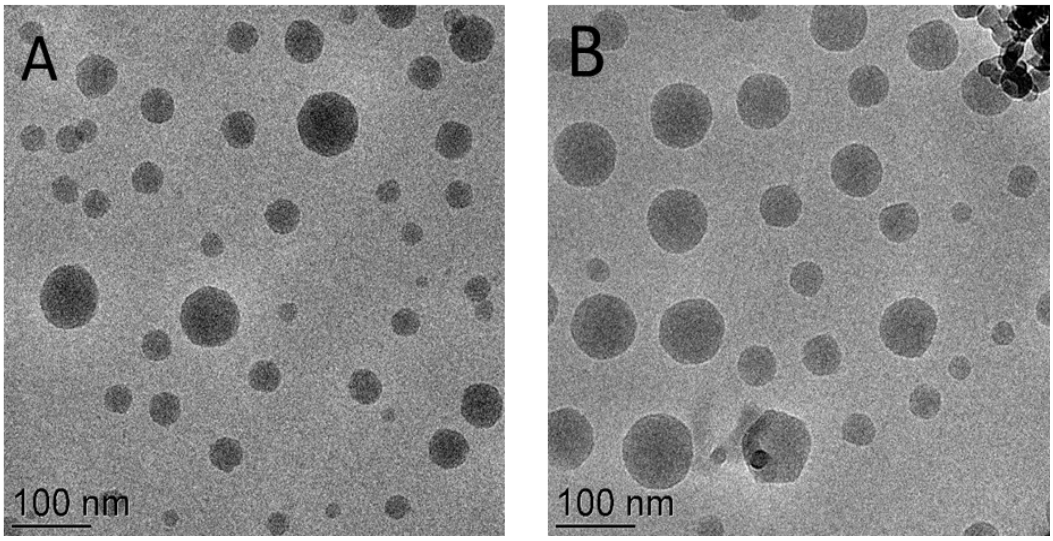

Figure 15. Cryo-TEM micrographs of GD1 (A) and GD2 (B) formulations.

Figure 16 reports the SAXS spectra of GD1 and GD2 measured at 25 °C (Figure 16A) and 37 °C (Figure 16B) in order to mimic the temperature conditions of storage and cutaneous application.

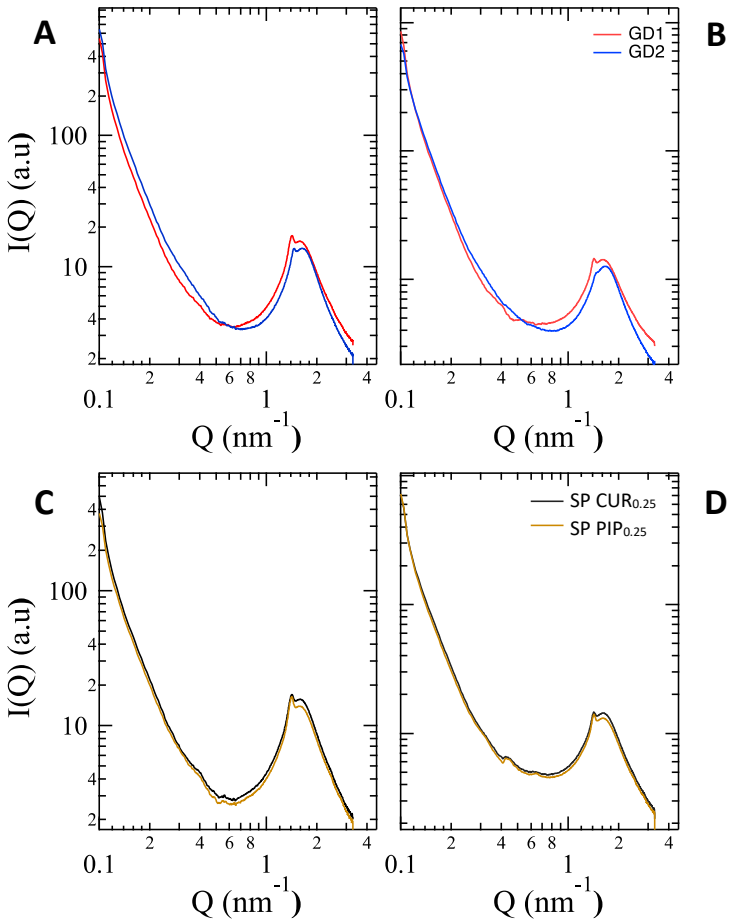

Figure 16. SAXS diffraction spectra of GD1 (red line), GD2 (blue line), SP $CUR_{0.25}$ (black line), and SP $PIP_{0.25}$ (yellow line). Analyses were performed at 25 °C (A, C) or 37 °C (B, D).

For all samples, the SAXS profiles are characterized by a broad correlation peak, centred at $Q_c \approx 1.6$ nm^{-1}, and by a low-intensity narrow peak, centred at $Q_p \approx 1.42$ nm^{-1}. From a qualitative point of view and based on results on dispersed GMO systems [143,144,145], the observed profiles indicate that two coexisting stable lyotropic liquid-crystalline phases occur simultaneously within the GMO dispersions: a sponge L3 phase, indicated by the broad band, and a hexagonal phase, suggested by the presence and position of the narrow peak. The two-phase system is very stable: the SAXS profiles do not change with temperature and composition, indicating that the two phases are in equilibrium with each other [146].

The structural properties of the sponge phase can be derived considering that GMO in water forms at least 3 different inverted, long-range ordered bicontinuous cubic phases [144], whose structure is described in terms of Infinite Periodic Minimal Surfaces, e.g., infinite arrays of connected saddle surfaces (where lipid monolayers are draped) with zero mean curvature at every point on that surface [147]. In some cases, such as after the addition of NaChol [145], the formation of a "molten cubic phase" (the sponge L3-type phase), always characterized by multiconnected saddle-shaped membranes but without long-range order,

has been reported. According to the absence of long-range order, the SAXS profile of the sponge L3 phase shows only one broad peak, just as observed in the present case (Figure 16). This broad peak is related to the cell-cell bilayer correlations: structural parameters can be then obtained by fitting this peak with Equation (7),

$$I(Q) = c / (\xi^{-2} + (Q\text{-}Q_c)^2) \quad (7)$$

where c is a normalization constant, ξ is the correlation length and $L = 2\pi/Q_c$ is a characteristic lipid bilayer correlation distance [143]. Results obtained in the present case are reported in Table 9.

The SAXS profile in Figure 16 also shows the presence of a narrow peak, superposed to the broad band. To assign this peak, two aspects were taken into consideration: first, the value of the hexagonal lattice parameter a, calculated by the peak position Q_p using Equation (8),

$$a = 4\pi / (Q_p \sqrt{3}) \quad (8)$$

(see Table 9), matches well the ones observed for the hexagonal phase occurring in monoolein systems [143,144,148]. Second, an inverted hexagonal phase was reported to form in the phase diagram of a similar monoolein mixture between the cubic and the sponge phase at room temperature and in excess of aqueous medium [143]. Therefore, the presence of an inverted hexagonal phase, which co-exists in equilibrium with the sponge phase within the analysed GMO dispersions, was suggested. It should be noticed that the peak corresponding to the hexagonal phase is narrow but of low intensity, so that a very minimal structuring of the dispersed GMO system should occur in this regard, and considering the pre-eminence of the sponge phase, the nanostructures constituting the spheroidal particles observed in the GMO dispersion can be defined as "spongosomes" [143].

Table 9. Structural parameters for the hexagonal and the sponge L3 phases.

	25 °C				37 °C			
Formulation	**a^1 (nm)**	**L^2 (nm)**	**Q_c^3 (nm^{-1})**	**ξ^4(nm)**	**a^1 (nm)**	**L^2 (nm)**	**Q_c^3 (nm^{-1})**	**ξ^4 (nm)**
GD1	5.11	3.94	1.59	2.34	5.09	3.87	1.63	2.47
GD2	5.00	3.82	1.65	2.35	4.99	3.75	1.68	2.49
SP $CUR_{0.25}$	5.13	3.97	1.58	2.30	5.09	3.89	1.61	2.49
SP $PIP_{0.25}$	5.13	3.99	1.57	2.33	5.09	3.90	1.61	2.48

[1] Inverted hexagonal lattice parameter; [2] L3 sponge cell characteristic distance; [3] Position of the correlation peak of the sponge; [4] Bilayer correlation length.

As already underlined, Figure 16 shows that temperature did not affect the SAXS profiles, indicating the same phase co-existence at 25 °C and 37 °C. Namely, structural parameters change by a small value: on heating, the hexagonal unit cell reduces as well as slightly reduce the bilayers correlation distance in the sponge phase, indicating a shrinking of the bilayer because a higher fluidity of the hydrocarbon chains. By contrast, an increase of the correlation length ξ is observed at 37 °C, suggesting increased thermal fluctuations inside the sponge L3 phase.

Notably, X-ray and cryo-TEM analyses demonstrated that the preparation procedure influences the supramolecular organization of the GMO dispersion. Indeed, the previous method led to unilamellar nanovesicles, cubosomes and hexasomes [85], while the new one resulted in nanodispersions with internal sponge phase organization in both GD1 and GD2. Whereas, by the new developed procedure, different kinds of nanodispersions were obtained, characterized by internal sponge phase organization in both GD1 and GD2. Notably, no previously reported aggregation phenomena were observed, confirming the importance of the applied method in the preparation of lyotropic liquid crystalline nanodispersions.

6.2.3. PREPARATION OF DRUG LOADED SPONGOSOMES

The preliminary formulative study showed similar size distribution, morphology, and inner structure in GD1 and GD2. Thus, GD1 was selected, being based on GMO associated with the single surfactant NaChol, to simplify as much as possible the vehicle composition in view of drug loading. As first approach, CUR and PIP were separately loaded by previous solubilization in ethanol (0.25 or 0.5 mg/mL), resulting in SP dispersions, whose names and compositions are reported in Table 10. The addition of the drugs did not affect macroscopical appearance, except in the case of CUR-loaded formulations whose resulted in the typical yellow colour.

As reported in Table 10, the presence of the drugs led to a slight increase (25-35 nm) in the Z-Average mean diameters with respect to the empty GD1. Dispersity index values slightly increased in the case of the 0.5 mg/mL drug concentration.

Table 10. Composition and size distribution parameters of SP loaded with CUR and/or PIP.

Formulation	GMO[1] %w/w	NaChol[2] %w/w	H_2O %w/w	PIP[3] %w/w	CUR[4] %w/w	Z-Average (nm) ± s.d.	DI[5] ± s.d.
SP $CUR_{0.25}$	4.50	0.15	95.325	-	0.025	223.7 ± 14.4	0.16 ± 0.03
SP $PIP_{0.25}$	4.50	0.15	95.325	0.025	-	228.4 ± 13.6	0.18 ± 0.05
SP $CUR_{0.5}$	4.50	0.15	95.255	-	0.050	241.1 ± 34.5	0.24 ± 0.02
SP $PIP_{0.5}$	4.50	0.15	95.255	0.050	-	232.2 ± 7.6	0.26 ± 0.05
SP $CUR_{0.25}/PIP_{0.25}$	4.50	0.15	95.255	0.025	0.025	243.0 ± 27.2	0.24 ± 0.05
SP $CUR_{0.4}/PIP_{0.1}$	4.50	0.15	95.255	0.010	0.040	264.0 ± 62.2	0.23 ± 0.05

[1] Glyceryl monoolein; [2] Na cholate; [3] piperine; [4] curcumin; [5]Dispersity index. Size distribution parameters refer to the mean values of PCS measurements conducted on 6 different independent batches for each type of SP.

SAXS analyses performed on SP $CUR_{0.25}$ and SP $PIP_{0.25}$ (Figure 16), confirmed the band and the peak typical of unilamellar vesicles and sponge phase L3, found in the case of the empty GD1 dispersion. According to previous results, the key parameters suggest that the presence of the drugs (CUR and PIP) does not alter the characteristics of the dispersed system: in particular, the characteristic distance L related to the correlations between the lipid bilayers in the sponge is quite constant. The value is around 3.95 nm, larger than the GMO bilayer thickness, which is around 3.2 nm; such observation suggests that the hydration level of GMO in the L3 phase remains low, even when the composition of the dispersion is changed (presence of one or two surfactants, presence of the drugs).

As second approach, both CUR and PIP were simultaneously loaded into SP dispersions, following two different associations, namely 1:1 and 1:4 CUR-PIP w/w ratios. Composition of the formulations, as well as size distribution parameters obtained by PCS analysis are summarized in Table 10. Z-Average mean diameters underwent a slight increase (20 nm) in the case of SP $CUR_{0.4}/PIP_{0.1}$, while Dispersity index was still below 0.25, reflecting a homogeneous size distribution.

6.2.4. ENTRAPMENT CAPACITY EVALUATION

To evaluate the amounts of drug associated to SP, the formulations were subjected to ultrafiltration (chapter 4.4.1), to separate the particulate lipidic fraction to the dispersing aqueous phase. Subsequently, disaggregation through ethanolic dilution was performed both on the retentate fraction and on the whole formulation. HPLC analysis allowed the quantification and calculation of EC values summarized in Table 11.

Table 11. Entrapment capacity of indicated formulations.

Formulation	EC[1] % ± s.d.	
	CUR	PIP
SP $CUR_{0.25}$	83.11 ± 13.69	-
SP $PIP_{0.25}$	-	82.68 ± 4.80
SP $CUR_{0.5}$	78.85 ± 17.23	-
SP $PIP_{0.5}$	-	78.23 ± 5.30
SP $CUR_{0.25}/PIP_{0.25}$	76.86 ± 24.90	73.88 ± 23.33
SP $CUR_{0.4}/PIP_{0.1}$	74.34 ± 19.07	71.34 ± 17.27

[1] Entrapment capacity, as defined in Equation (2).

EC values indicated that the drug loaded within the lipid disperse phase ranged between 71 and 83 %, both for CUR and PIP, which means that the most of the drug is associated to the SP nanoplatforms. For sure the composition of SP and their peculiar open structure, consisting of a convoluted and interconnected three-dimensional network, confer a high capability to encapsulate lipophilic molecules [29]. Accordingly, a high encapsulation efficiency was observed for both phytocompounds.

It is noteworthy that the production procedure enabled to simultaneously load both CUR and PIP in two different ratios: SP $CUR_{0.4}/PIP_{0.1}$ and SP $CUR_{0.25}/PIP_{0.25}$.

6.2.5. IVPT

IVPT was employed to predict the in vivo permeation of CUR and PIP separately or jointly loaded in SP $CUR_{0.5}$, SP $PIP_{0.5}$, SP $CUR_{0.25}/PIP_{0.25}$, and SP $CUR_{0.4}/PIP_{0.1}$. Owing to their penetration enhancer potential, both GMO and PIP [33] play a key role in promoting CUR penetration through the *stratum corneum*. Furthermore, liquid crystals are characterized by high bioadhesivity and affinity between their inner structure and the architecture of the *stratum corneum* [8,31].

STRAT-M® membrane was selected because of its ability to mimic the barrier properties of the *stratum corneum*. Drug diffusion profiles are shown in Figure 17, while Table 12 summarizes the calculated diffusion parameters.

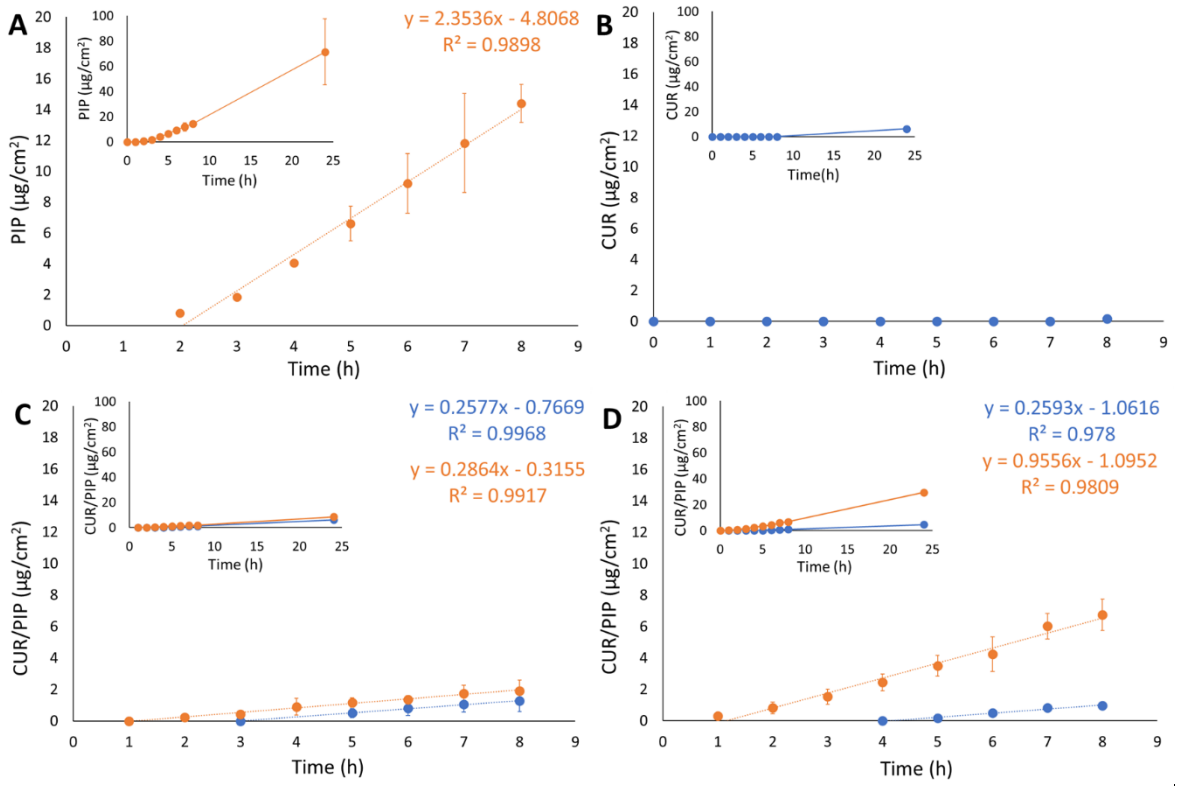

Figure 17. CUR (blu circles) and PIP (orange circles) diffusion profiles from SP $CUR_{0.5}$ (A), SP $PIP_{0.5}$ (B), SP $CUR_{0.4}/PIP_{0.1}$ (C), and SP $CUR_{0.25}/PIP_{0.25}$ (D), as determined by Franz cells associated with the STRAT-M® membrane. The insets in each panel refer to the respective 0-24 h kinetics. Data are the mean of 3 independent experiments ± s.d.

Figure 17 clearly shows that in any case PIP diffused much faster respect to CUR. A lag time was detected in all the diffusion kinetics, longer for CUR with respect to PIP, suggesting that CUR was more strongly retained into the SP ultrastructure, due to the major lipophilic character of the drug (log P 3.29) with respect to PIP (log P 2.78).

Remarkably, in the case of SP $CUR_{0.5}$, CUR was undetectable in the receptor compartment until 8 h, which hampered a detailed evaluation of IVPT parameters, while in case of SP $CUR_{0.25}/PIP_{0.25}$ and SP $CUR_{0.4}/PIP_{0.1}$, where CUR was combined with PIP, a slow CUR diffusion was observed. This phenomenon suggests a possible competition between CUR and PIP within the ultrastructure, which favoured the expulsion of CUR in the presence of PIP. It could be hypothesized that the joint presence of CUR and PIP in SP $CUR_{0.25}/PIP_{0.25}$and SP $CUR_{0.4}/PIP_{0.1}$ can affect the hydrophobic interaction between the drugs and the matrix, with respect to the individually CUR-loaded SP $CUR_{0.5}$, finally improving CUR diffusion [137,149].

Table 12. IVPT parameters of indicated formulations calculated for CUR and PIP respectively.

IVPT Parameters	SP $CUR_{0.5}$	SP $PIP_{0.5}$	SP $CUR_{0.25}/PIP_{0.25}$		SP $CUR_{0.4}/PIP_{0.1}$	
			CUR	PIP	CUR	PIP
Jss[1] (μg/cm^2/h)	-	2.35 ± 0.73	0.26 ± 0.01	0.96 ± 0.12	0.26 ± 0.02	0.29 ± 0.12
Kp[2] (cm/h) × 10^3	-	4.71 ± 1.46	1.04 ± 0.02	3.82 ± 0.25	0.64 ± 0.08	2.86 ± 0.92
Tlag [3] (h)	-	2.04 ± 0.04	4.09 ± 0.21	1.15 ± 0.15	2.98 ± 0.16	1.10 ± 1.18
D[4] (cm^2 h^{-1}) × 10^5	-	8.20 ± 1.03	4.09 ± 1.51	14.61 ± 2.52	5.63 ± 0.13	15.20 ± 3.22
P[5]	-	1.82 ± 0.02	0.80 ± 0.01	0.83 ± 0.05	0.36 ± 0.02	0.60 ± 0.02
A[6] (μg/cm^{-2})	6.35 ± 0.03	71.38 ± 26.22	4.65 ± 0.71	29.45 ± 0.31	6.15 ± 1.08	8.60 ± 1.71

[1]Steady-state flux per unit area; [2]permeability coefficient; [3]lag-time; [4]diffusion coefficient; [5]partition coefficient (membrane/vehicle); [6]cumulative amount of drug diffused at 24 h; data are the mean of 3 independent Franz cell experiments ± s.d.

Notably, Kp values of PIP were roughly 4-fold higher with respect to CUR, both in the case of SP $CUR_{0.25}/PIP_{0.25}$ and SP $CUR_{0.4}/PIP_{0.1}$. Surprisingly, Kp value for CUR was 1.6-fold minor in the case of SP $CUR_{0.4}/PIP_{0.1}$ with respect to SP $CUR_{0.25}/PIP_{0.25,}$ suggesting that the higher the amount of CUR, the stronger its retention in the donor phase. The faster permeation of PIP with respect to CUR in all tested formulations indicates a stronger hydrophobic interaction between CUR and the lipophilic supramolecular structure of the spongiform dispersed phase, whose 3D network architecture involves interconnected internal compartments. Moreover, D values of PIP were 3-fold higher with respect to CUR, both in the case of SP $CUR_{0.25}/PIP_{0.25}$ and SP $CUR_{0.4}/PIP_{0.1}$, indicating that PIP was more promptly available for diffusion and partition to the membrane with respect to CUR. Comparing the co-loaded formulations with SP $PIP_{0.5}$, in the case of PIP, higher P and Kp values were observed, whilst the D values of PIP in the case of SP $CUR_{0.25}/PIP_{0.25}$ and SP $CUR_{0.4}/PIP_{0.1}$ were roughly double with respect to SP $PIP_{0.5}$, suggesting that the association of CUR and PIP can promote the diffusion of both drugs. After 24 h, as expected, the amount of diffused PIP was much higher with respect to CUR, in all tested formulations, while the highest value was obtained for SP $PIP_{0.5}$ formulation, containing a higher drug amount. Furthermore, the combination of these two phytocompounds was effective in promoting both PIP and CUR diffusion across the STRAT-M® membrane.

6.2.6. PATCH TEST

To evaluate the safety of the loaded and unloaded SP applied to the skin, a patch test was conducted on 20 healthy volunteers.

Specifically, formulations GD1, SP $CUR_{0.5}$, SP $PIP_{0.5}$, and SP $CUR_{0.4}/PIP_{0.1}$ were tested to evaluate the number of irritative reactions 15 min and 24 h after the removal of the Finn Chamber. Since the reaction was negligible in all cases, the formulations could be classified as non-irritating to the human skin, so suitable for topical application. These findings are critical for the development of safe and effective dermatological products.

6.2.7. BIOLOGICAL ACTIVITY - EX VIVO EXPERIMENT

To assess the structural damage produced on the skin by DEE and to evaluate the protective activity of the SP formulations, ex vivo test was performed using human skin biopsies as a model.

Specifically, skin biopsies were pre-treated with SP $CUR_{0.5}$, SP $PIP_{0.5}$, SP $CUR_{0.25}/PIP_{0.25}$ and SP $CUR_{0.4}/PIP_{0.1}$ formulations and then exposed to DEE; CTRL biopsies remained untreated and unexposed while DEE biopsies were exposed to the pollutant but without treatment. Then, immunofluorescence assays were carried out on skin tissue to evaluate the expression of key protein involved in the processes of differentiation of the epidermis (involucrin), in the formation of the skin barrier (filaggrin), and in conferring support to the skin (type I collagen), in response to DEE exposure. The altered expression of these proteins is in fact an indication of a structural damage of the skin tissue. Specifically, filaggrin is a late differentiation marker, located in *stratum corneum* in which binds to keratin intermediate filaments, causing their aggregation into macrofibrils. This process contributes to cellular compaction and permits the extensive crosslinking of keratin intermediate filaments to form a highly insoluble keratin matrix [150]. Involucrin is a cytoplasmic protein that is synthesized in human squamous epithelial cells. This protein is present in the maturing cells of the upper *stratum spinosum* and *stratum granulosum* and is a marker of keratinocytes maturation that immediately precedes the final events of terminal differentiation [151]. Type I collagen, is one of the main types of collagens present in the skin, known to give elasticity and mechanical resistance to the cutaneous tissue, as well as to be involved in the regenerative processes of the skin [152]. A reduction in type 1 collagen, as previously reported, is often associated with the skin aging process, of which exposure to atmospheric agents is now one of the main causes (premature skin aging) [106].

As expected, DEE exposure caused a depletion in all three markers expression levels, confirming the harmful action of the pollutant, even after a short exposure. However, pre-treatment with SP $PIP_{0.5}$ could prevent the loss in filaggrin expression levels compared to DEE samples (Figure 18A), suggesting that this formulation is able to counteract the

cutaneous barrier damage induced by the environmental pollutant exposure. On the other hand, SP $CUR_{0.5}$ was unable to prevent stress-induced filaggrin loss promoted by DEE exposure. Interestingly, in the case of the filaggrin marker, CUR alone had no effect, while the association with the smaller amount of PIP and higher CUR was even found to be the most effective, suggesting a possible enhanced diffusion of the two phytocompounds, as recently found in the case of ET (Project 1). An opposite trend could be observed in the case of involucrin (Figure 18B), in which topical application of SP $CUR_{0.5}$ significantly prevent the decrease in involucrin expression levels in comparison with untreated biopsies exposed to the pollutant (DEE); whilst SP $PIP_{0.5}$ showed almost no protective effect against involucrin loss. In both cases, SP $CUR_{0.4}/PIP_{0.1}$ showed a higher protective effect with respect to SP $CUR_{0.25}/PIP_{0.25}$, indicating that the 1:4 w/w CUR-PIP association seems more efficient with respect to the 1:1 w/w association, maybe due to the higher CUR amount.

Regarding type I collagen expression, on the contrary, no significant difference between treated and untreated tissues was detected by 2-way ANOVA analysis (Figure 18C). However, it is still possible to recognize a trend from the graph, which suggest a slightly protective effect exerted especially by SP $CUR_{0.4}/PIP_{0.1}$. This result may propose a protective action of the formulations after prolonged treatment. In fact, considering that the process of skin aging is due to a continuous and prolonged exposure to environmental pollutants, 48 h of exposure to DEE may not yet be sufficient to appreciate a significant protective effect of the formulations. Moreover, it is likely that, over the duration of the experiment, CUR and PIP were not able to penetrate deep enough to carry out their protective action on the dermis. In contrast, the action of the formulation was more effective on the superficial layers of the epidermis, as evidenced by the levels of the markers filaggrin and involucrin. A possible long-term efficacy of the SP formulation could then be proposed.

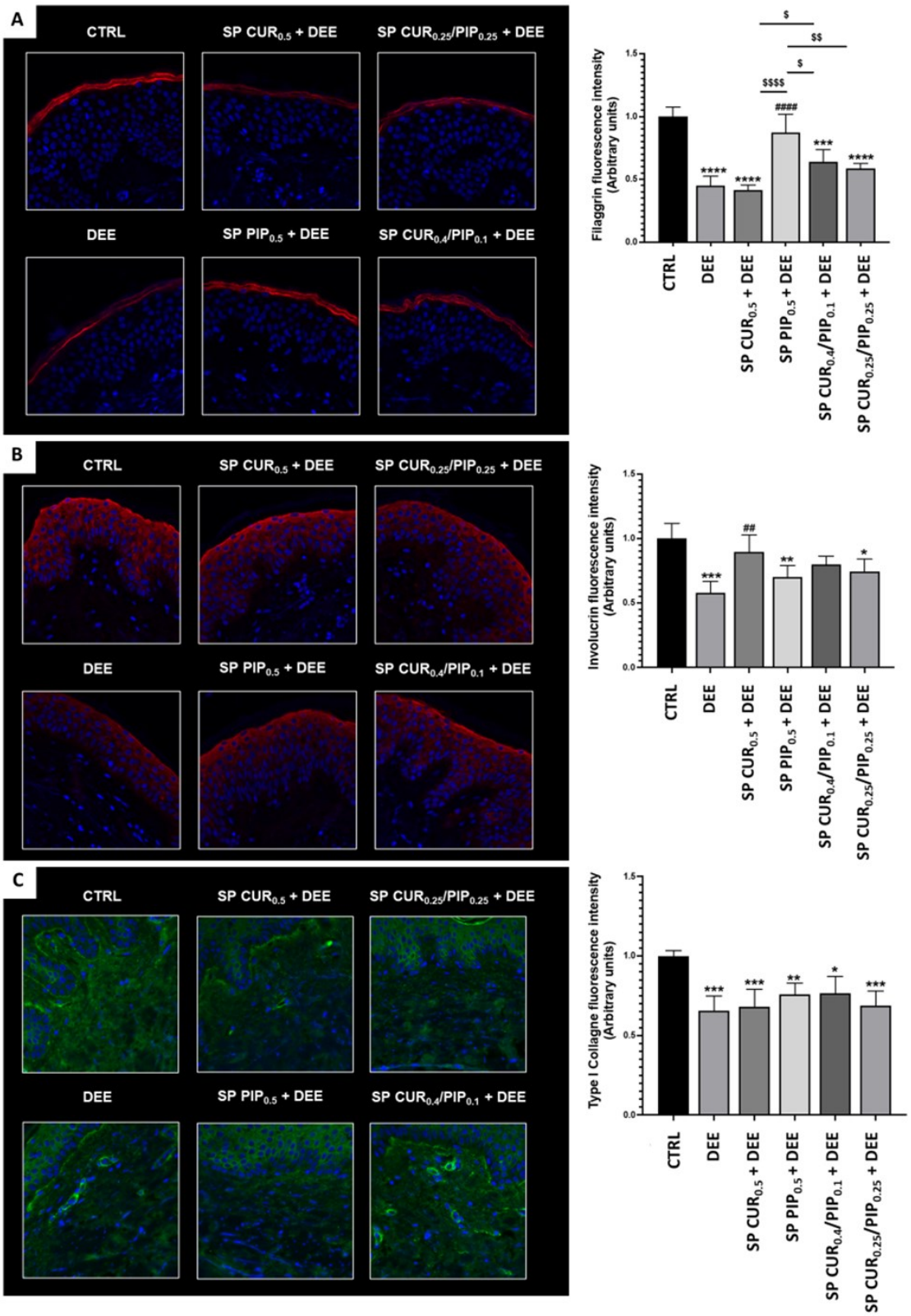

Figure 18. Immunofluorescence staining for filaggrin (A), involucrin (B), and type I collagen (C) in human skin biopsies treated with the indicated formulations and exposed or not to DEE. Red or green staining represents the indicated proteins, and the blue staining (DAPI) represents nuclei. Images were taken at 40× magnification. The fluorescent signal of the different markers was quantified using ImageJ software 1.53a (Java 1.8.0_172) and expressed in the graphs. Data are the results of the averages of at least three different experiments, with:*,$, $p < 0.05$;**, $$,##, $p < 0.005$; ***, $p = 0.0001$; and ****,####,$$$$, $p < 0.0001$, by 2-way ANOVA followed by Tukey's post-hoc comparison test [126]. DEE, SP $CUR_{0.5}$, SP $PIP_{0.5}$, SP $CUR_{0.25}/PIP_{0.25}$, SP $CUR_{0.4}/PIP_{0.1}$, vs. CTRL (*); CTRL, SP $CUR_{0.5}$, SP $PIP_{0.5}$, SP $CUR_{0.25}/PIP_{0.25}$, SP $CUR_{0.4}/PIP_{0.1}$ vs. DEE (#); SP $CUR_{0.5}$, SP $CUR_{0.25}/PIP_{0.25}$, SP $CUR_{0.4}/PIP_{0.1}$ vs. SP $PIP_{0.5}$ and SP $CUR_{0.5}$ vs SP $CUR_{0.4}/PIP_{0.1}$ ($).

7. PROJECT 3 – Gossypin-loaded ethosomal gel for the topical treatment of cutaneous melanoma: a preliminary study

7.1. INTRODUCTION

Cutaneous melanoma (hereafter, melanoma) is the most aggressive form of skin cancer. Based on epidemiological data, in 2020 more than 300 000 new melanoma cases and about 60 000 deaths occurred [153]. Moreover, a 50% increase in new cases and deaths over the next two decades has also been estimated. The incidence of this human cancer varies greatly between countries, not only due to differences in skin phenotype and sun exposure, but also due to easier or lesser access to early diagnosis and treatments [154,155,156]. Notwithstanding recent significant advancements in the clinical management of advanced melanoma through targeted therapies and immunotherapy, treatment failures, severe adverse effects, and resistance to current therapies still persist [157]. These challenges emphasize the need for alternative treatment options. One possible solution can be found in active compounds of natural origin. Indeed, nature represents a very rich resource of bioactives, particularly derived from plants, with promising therapeutical properties as anti-cancer drugs, or as adjuvants [158,159]. Nevertheless, their use in cancer treatment is still limited by their low stability, scarce solubility and bioavailability. At this regard, the development of nanotechnological delivery systems could represent a smart approach to overcome these drawbacks.

GOS, as previously reported (chapter 1.4.3) is a flavanol glucoside which can be found in roots and flowers of several hibiscus species, belonging to the *Malvaceae* family. GOS possesses a wide range of activities of therapeutic interest, but those that most caught our attention in the present research are the antioxidant and antitumor activities [51,52]. Specifically, it can arrest the cell cycle and inhibit proliferation, these effects are achieved through the modulation of various cellular pathways. One key mechanism involves the inhibition of NF-κB, a protein complex that plays a crucial role in inflammation and cell survival. By inhibiting NF-κB, GOS can reduce inflammation and promote tumor cell death. In addition, GOS inhibits the TNF-induced MMP9 expression: TNF can stimulate the production of MMP9, an enzyme that degrades the extracellular matrix and facilitates tumor invasion and metastasis. By inhibiting TNF-induced MMP9 expression, GOS can hinder tumor spread [52].

In this context, GOS has been proposed for the treatment of melanoma [53,54]. Rajkumar and colleagues have pioneered research into the potential transdermal application of GOS by means of vesicular gel formulations, namely proniosomal gels [54]. Therefore, the present study takes part of this area of research, aimed at identifying alternative therapeutic strategies for the treatment of cutaneous melanoma, which would be minimally invasive, exploiting the advantages of the topical route of administration [2].

For this purpose, GOS delivery though ET has been proposed, due to their promising potential as transdermal delivery systems. As previously described (chapter 1.3.1), high ethanol content is a key aspect allow nanovesicles to penetrate to the deeper layers of the skin. Due to its well-known penetration-enhancer behaviour, ethanol is able to transiently disorganize the *stratum corneum* barrier, allowing transdermal penetration by nanovesicles, made more malleable by ethanol itself [6,12,18]. Noteworthy, in a recent study by our research group [27], TEM images confirmed the ability of ET to reach the deeper skin layers intact. For this reason, ET emerge as an effective delivery system for the treatment of diseases involving deep skin layers such as melanoma.

This study aimed to develop and characterize ET for the topical delivery of GOS to treat cutaneous melanoma. Two different methodologies were employed to produce ET, which were then compared to identify the optimal method for GOS loading. The resulting colloidal dispersions were thoroughly characterized, evaluating particle size and morphology, GOS entrapment capacity, as well as in vitro release and permeation. To enhance the applicability and residence time of the formulations on the skin, the ET dispersions were thickened using X-Gum. The ethosomal gels thus produced were then characterized by leakage and spreadability tests and their antioxidant activity was also evaluated in vitro. The internal structural organization was studied using SAXS and WAXS techniques. Finally, the biological activity of the formulations was tested by in vitro tests on A375 melanoma cell line.

7.2. RESULTS AND DISCUSSION

7.2.1. PREPARATION OF ETHOSOMES

In order to enhance GOS penetration through the skin, ET were selected as a proper vehicle. Furthermore, in the present investigation, two different methods of producing ET were compared. The first method, “water injection”, has already been employed by our research

group [25,60,61] being able to obtain stable vesicles with an average diameter of around 200 nm and homogeneous size distribution. As described in previous section (chapter 4.1.1), this method is based on the gradual and continuous addition of water to a PC ethanol solution kept under magnetic stirring. The second method here proposed involves an inversion in the way the two phases are mixed. It is defined as "ethanol injection" method precisely because in this case the PC ethanol solution that is gradually added to water, under magnetic stirring.

In Table 13 it is possible to find the composition of the ET dispersions, prepared using water injection (ET_{WI}) or ethanol injection (ET_{EI}) method.

Table 13. Composition of indicated formulations.

Formulation	PC[1] (%, w/w)	Ethanol (%, w/w)	H_2O (%, w/w)	GOS[2] (%, w/w)
$ET_{WI/EI}$	0.9	29.1	70	-
ET-$GOS_{WI/EI}$	0.9	28.8	70	0.03

[1]: soy phosphatidylcholine; [2]: gossypin.

Both methods resulted in homogeneous formulations with an opaque and stable appearance over time. For this reason, both of the techniques were then used to produce GOS-loaded ET (ET-GOS), by the pre-solubilization of GOS in PC-ethanol solution. Loaded formulations' composition is reported in Table 13. Both of the methodologies allowed the loading of 0.3 mg/mL of GOS and resulted to be free of sedimentation phenomena. Noteworthy is that ET_{EI} appear much transparent with respect to the one prepared with water injection method and this difference in terms of opacity occurred also in ET-GOS, which showed also a yellowish color due to GOS presence (Figure 19).

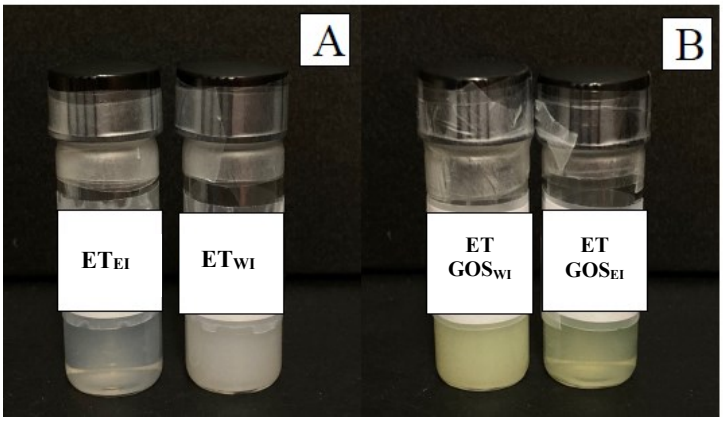

Figure 19. (A) Empty ET prepared by water injection and ethanol injection methods. (B) GOS-loaded ET prepared with water injection and ethanol injection methods.

7.2.2. SIZE DISTRIBUTION AND STABILITY

Size characterization was evaluated by PCS one day after ET preparation. The results reported in the Table 14 suggested that the preparation method affected ET size. Precisely, as the formulations are identical in composition, dimensional variations must be attributed to the preparation method alone. It can therefore be deduced that simply reversing the way the two phases are mixed is capable of bringing about significant changes in terms of size.

In particular, vesicle mean diameter (Z-Average) of ET_{EI}, was 50-60 nm smaller with respect to ET_{WI}, while with both methods, homogeneous size distributions were obtained, as evidenced by the Dispersity index minor than 0.2.

To justify the size difference some aspects can be considered. It is known that vesicles form spontaneously by self-assembly of PC units at the ethanol-water interface, a process promoted by mixing. Specifically, a mutual diffusion between the ethanol and water solvents at the interface occurs, forcing the PC units to associate in bilayered structures, which then fold to form vesicles. It can be assumed that in the case of the ethanol injection method, in which the organic solution is gradually added in an excess of water, a rapid depletion of the organic solvent takes place, resulting in a thinning of the diffusion length. As previously observed in microfluidic systems [160], a rapid depletion of the organic solvent leads to an acceleration of the bilayer closure and thus to smaller vesicles. In contrast, with the water injection method, where water is added in an excess of PC-ethanol solution, the length of the diffusion layer tends to be increased and vesiculation occurs more gradually, favoring larger structures.

In case of GOS-loaded formulations, it was found that the presence of the drug did not affect the size of the nanovesicles, and it was observed the same size reduction between ET-GOS_{EI}

and ET-GOS$_{WI}$. Dispersity index was always below 0.2, meaning homogeneous size distribution also in loaded formulations.

Table 14. Size distribution parameters and Entrapment capacity of indicated formulations.

Formulation	Time (days)	Z-Average (nm) ± s.d.	Dispersity index ± s.d.	EC[1] (%)± s.d.
ET$_{WI}$	1	213.73 ± 9.72	0.15 ± 0.01	-
	60	243.20 ± 0.00	0.26 ± 0.00	-
ET$_{EI}$	1	146.78 ± 4.10	0.19 ± 0.02	-
	60	155.33 ± 6.14	0.20 ± 0.00	-
ET-GOS$_{WI}$	1	197.13± 11.43	0.15 ± 0.03	89.9 ± 7.5
	60	202.67 ± 5.45	0.16 ± 0.06	-
ET-GOS$_{EI}$	1	148.70 ± 7.75	0.17 ± 0.02	94.3 ± 4.5
	60	165.25 ± 4.74	0.19 ± 0.02	-

[1] Entrapment capacity calculated following Equation (2). data are the mean of 4 independent determinations on different batches.

The size stability of the formulations was also assessed by repeating the analysis by PCS after 60 days of storage at room temperature and protected from light. As shown in Table 14, a slight increase in the average diameter over time was observed while size distribution remained homogeneous, with a Dispersity index increase after 2 months in the case of ET$_{WI}$.

7.2.3. MORPHOLOGICAL CHARCTERIZATION

The morphology of the nanovesicles produced by the two different methods: ET$_{EI}$ and ET$_{WI}$ was assessed using Cryo-TEM. The images obtained for the two formulations are shown in Figure 20.

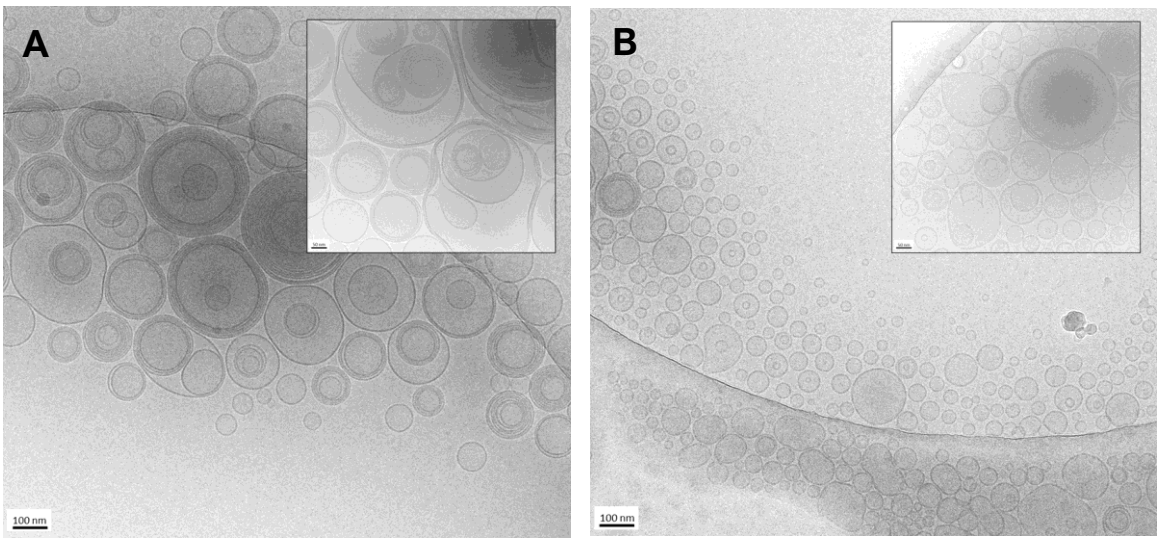

Figure 20. Cryo-transmission electron microscopy (Cryo-TEM) images of ET_{WI} (A) and ET_{EI} (B). Bar correspond to 100 nm in panel (A) and (B) and 50 nm in the inset of panel (A) and (B).

In both cases the formation of mostly spherical or ovoidal vesicles was observed, the size of which corresponds to that obtained through PCS analysis. In the case of ET_{WI} (panel A and inset), a prevalence of multilamellar and oligolamellar vesicles is observable. In contrast, in case of ET_{EI} (panel B and inset), a majority of unilamellar and oligolamellar vesicles is evident, suggesting the different preparation method influence on vesicle morphology. It is possible to assume that the rapid depletion of the organic solvent in the ethanol injection method leads to quicker vesiculation, thereby hindering the formation of multilamellar structures. On the contrary, the addition of water to the excess PC-ethanol solution not only promotes more gradual vesiculation, leading to the formation of larger structures, but also the assembly of multiple bilayers, resulting in a predominance of oligolamellar and multilamellar vesicles.

7.2.4. ENTRAPMENT CAPACITY EVALUATION

Entrapment capacity was evaluated through the ultrafiltration method which allows us to separate the vesicular fraction from the aqueous dispersing phase. Retentate fraction and whole formulations were disaggregated by dilution in ethanol and HPLC analysis allowed to quantify GOS concentration: Results, reported in Table 14, show, as expected, that the most of the drug is associated to nanovesicles. Moreover, a higher entrapment capacity was found for ET-GOS_{EI} with respect to ET-GOS_{WI}, evidencing the higher potential of ethanol injection method for GOS loading. This aspect certainly represents an advantage in order to exploit the properties of the nanocarrier for drug delivery.

7.2.5. IVRT

Franz cell apparatus was employed to perform IVRT with the objective to evaluate the ET capability to control GOS release. Synthetic nylon membrane was selected as an inert support to separate the upper and lower compartments. In the study, the release of GOS from ET-GOS_{WI} and ET-GOS_{EI} was compared to a 30:70 ethanol/water GOS solution (SOL-GOS) containing GOS 0.3 mg/mL. As expected, the ET achieved control of GOS release with respect to SOL-GOS. Indeed, as shown in Figure 21, GOS release from SOL-GOS was much faster respect to the ET formulations. No particular differences were observed between the release profiles obtained in the case of ET-GOS_{WI} and ET-GOS_{EI}.

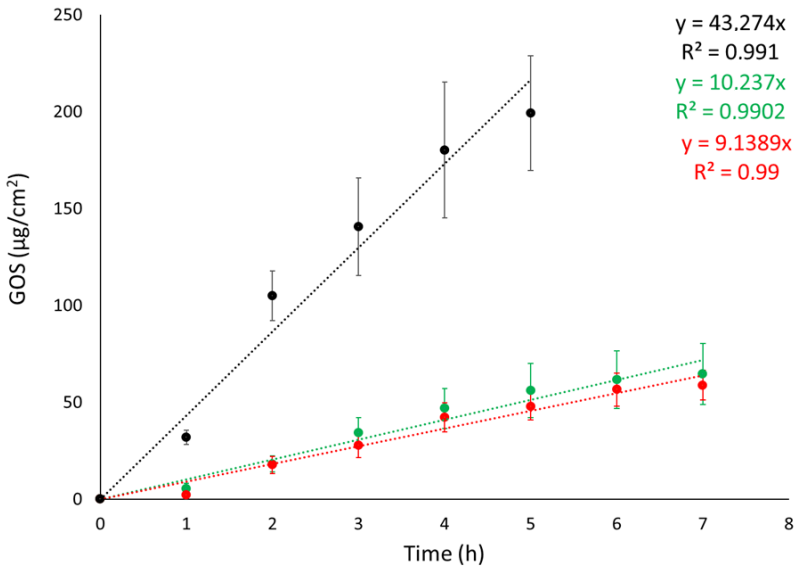

Figure 21. GOS release kinetic from ET-GOS_{WI} (green circles), ET-GOS_{EI} (red circles), SOL–GOS (black circles), as determined by Franz cells associated with the nylon membrane. Data are the mean of 4 independent experiments ± s.d.

Zero-order plot, first-order plot, Higuchi plot and Peppas plot were applied in order to clarify the mechanism of drug release from the ET. Table 15 shows the R^2 values obtained by plotting the release profile of the formulations according to the different mathematical models. It can be observed that for both ET-GOS_{WI} and ET-GOS_{EI} the profile can be better described by First order kinetic model, while the n values obtained from the Peppas plot, reveal a non-Fickian diffusion mechanism.

Table 15. IVRT parameters and kinetic data of the indicated formulations.

Formulation	R[1] (μg/cm²/h)	A[2] (μg/cm²)	Zero Order Plot (R^2)	First Order Plot (R^2)	Higuchi Plot (R^2)	Peppas Plot (n/R^2)
ET-GOS$_{WI}$	10.77 ± 2.57	146.15 ± 5.15	0.968	0.973	0.909	1.46/0.950
ET-GOS$_{EI}$	9.27 ± 1.70	147.60 ± 9.12	0.970	0.975	0.896	1.66/0.936
SOL-GOS	43.27 ± 7.14	199.14 ± 29.69	0.972	0.989	0.924	1.93/0.729

[1]: Release rate; [2]: amount of GOS released after 24 h (ET-GOS$_{WI}$ and ET-GOS$_{WI}$) and 5 h (SOL-GOS); GOS concentration was 0.3 mg/mL; data are the mean of 4 independent Franz cell experiments ± s.d.

7.2.6. IVPT

IVPT was performed using Franz Cells apparatus associated with STRAT-M® membrane, selected because of its capability to mimic the barrier properties of the *stratum corneum*. The aim of the test is to evaluate the ability of ET to enhance GOS diffusion in vitro, comparing ET-GOS prepared with ethanol injection and water injection methods, with respect to GOS free in solution. The diffusion profiles (0-24h) are shown in the Figure 22 and calculated diffusion parameters are reported in Table 16.

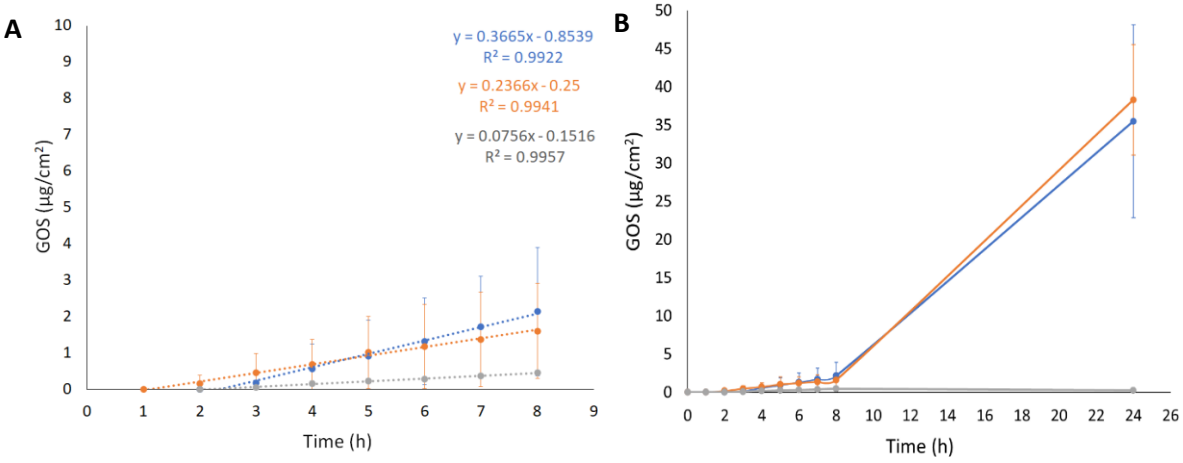

Figure 22. GOS diffusion profiles from ET GOS$_{EI}$ (blue circles), ET GOS$_{WI}$ (orange circles) and SOL GOS (grey circles), as determined by Franz cells associated with the STRAT-M® membrane. (A) shows 0-8 h linearized profile and (B) 0-24 h diffusion. Data are the mean of 6 independent experiments ± s.d.

As shown in Figure 22, the diffusion of GOS from SOL-GOS was much slower with respect to the ET formulations, confirming the potential of the vesicular systems in increasing diffusion of GOS drug through the skin. A certain lag-time was found in all cases, following the order: ET-GOS$_{EI}$ > SOL-GOS > ET-GOS$_{WI}$. In particular, Kp values of ET-GOS$_{WI}$ and ET-GOS$_{EI}$ were respectively 3 and 4.5-fold higher with respect to SOL-GOS. Interestingly, the P value obtained in the case of the ET-GOS$_{EI}$ was 3.35-fold higher with respect to ET-

GOS_{WI}, suggesting a greater GOS partitioning towards the membrane. The amount of drug permeated after 24 h (A value in Table 16) was only 0.26 μg/cm^2, thus roughly 140-fold lower with respect to the amount permeated in the case of ET-GOS_{WI} and ET-GOS_{EI}.

Table 16. IVPT parameters of the indicated formulations.

IVPT Parameters	ET-GOS_{WI}	ET-GOS_{EI}	SOL-GOS
Jss[1] (μg/cm^2/h)	0.241 ± 0.192	0.387 ± 0.267	0.077 ± 0.020
Kp[2] (cm/h) x 10^3	0.737 ± 0.547	1.115 ± 0.600	0.248 ± 0.063
Tlag[3] (h)	1.498 ± 0.858	2.846 ± 0.667	1.894 ± 1.554
D[4] (cm^2 h^{-1}) x 10^5	13.377 ± 7.662	6.141 ± 1.646	5.590 ± 10.936
P[5] membrane/vehicle	0.164 ± 0.035	0.550 ± 0.145	0.098 ± 0.096
A[6] (μg/cm^2)	38.306 ± 4.057	35.452 ± 12.640	0.260 ± 0.000

[1]: Steady-state flux per unit area ; [2]: permeability coefficient ; [3]: lag-time ; [4] diffusion coefficient; [5] partition coefficient ; [6] cumulative amount of GOS diffused at 24 h; GOS concentration was always 0.3 mg/mL; data are the mean of 6 independent Franz cell experiments ± s.d.

7.2.7. ETHOSOMAL GEL PREPARATION AND CHARACTERIZATION

In order to facilitate topical application of the formulations, ET were thickened by X-Gum, a natural biocompatible polysaccharide widely used in various fields including food, pharmaceuticals and cosmetics [161]. ET gels were prepared by direct addition of X-Gum to ethosomal dispersion (both ET_{WI} and ET_{EI}) kept under magnetic stirring until the complete gum dispersion.

In order to identify the best characteristics of the gel, 3 different X-Gum concentration were evaluated (i.e. 0.5, 0.75 and 1 % w/w). Homogeneous gels were obtained in all three cases. No macroscopical differences were detected between ET_{WI} gel and ET_{EI} gel, showing an increase of thickening and opacity, as a function of the X-Gum amount.

The best composition was selected based on spreadability and leakage assays, the results of which are summarized in Table 17. It is observed that an increased percentage of X-Gum leads to lower leakage and spreadability values. No differences between ET_{WI} gel and ET_{EI} gel were detected.

Table 17. Spreadability and leakage test results of reported formulations.

Formulation	X-Gum % (w/w)	Spreadability[1] (g cm/s)	Leakage[2] (cm)
ET_{WI} gel	0.5 %	23.33 ± 1.52	1.96 ± 0.15
	0.75 %	18.67 ± 0.58	0.87 ± 0.20
	1 %	17.67 ± 0.58	0.50 ± 0.10
ET_{EI} gel	0.5 %	24.00 ± 3.60	1.73 ± 0.06
	0.75 %	20.00 ± 1.00	0.87 ± 0.06
	1 %	18.00 ± 1.00	0.63 ± 0.15

[1]:calculated as reported in Equation (1); [2]: running distance along the slide; data are the mean of 3 independent measurements ± s.d.

In the light of these results, 0.5% X-Gum was selected as corresponding to a higher spreadability. Spreadability parameter is particularly relevant to ensure smooth and comfortable application of the product on the skin and easy extrusion from the container. The leakage parameter, on the other hand, although lower, is still acceptable for application on the skin.

7.2.8. X-RAY SCATTERING ANALYSES

SAXS allowed to investigate the structure of ET prepared by ethanol injection and water injection methods, as well as their semi-solid forms, considering also the effect of temperature. The characteristic SAXS profile of these vesicular nanosystems measured at 25°C is illustrated in Figure 23A where the broad band between 0.6 and 1.3 nm^{-1} indicates the presence of the lipid bilayer of ET. The main difference regards a small Bragg-peak observed at Q = 0.87 nm^{-1} for the formulation ET_{WI} (see the black vertical line). This result should reflect the multilamellar vesicle that characterized this sample, confirming the results obtained by Cryo-TEM, and providing an interlamellar distance of 7.22 nm, in agreement with previous results on similar drug-delivery systems [162]. Moreover, the peak remains stable also in the presence of X-Gum (ET_{WI} 0.5% gel) and GOS (ET-GOS_{WI} 0.5% gel) (Figure 23C), indicating that the lamellar organization is maintained. Concerning the formulation ET_{EI}, Figure 23B shows the absence of changes when X-Gum and GOS are present in the system. The SAXS data obtained in the presence of X-Gum (green and grey curves) illustrate a profile that masks the band of the lipid bilayer because of the high signal of the polymer in this component. However, the presence of the lamellar bilayer in ET_{WI} sample is still visible in Figure 23C, as indicated by the Bragg-peak highlighted by the vertical line.

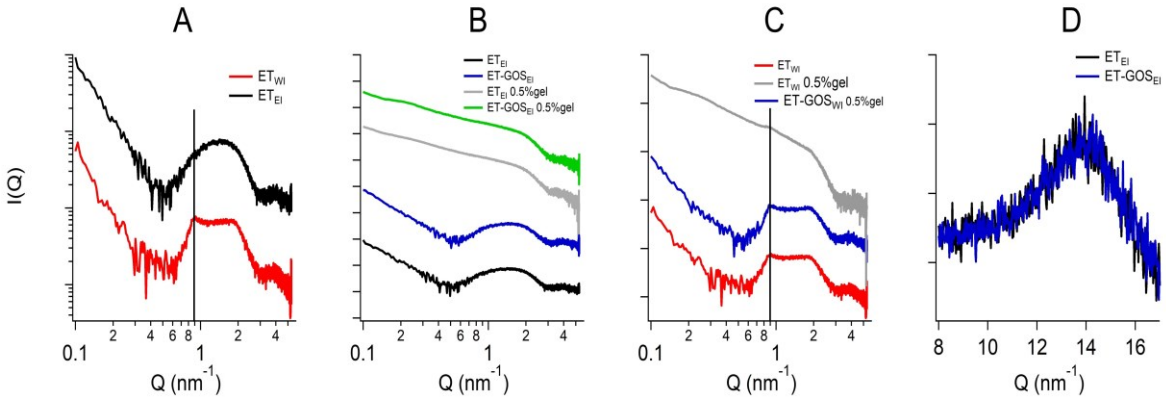

Figure 23. Comparison among the SAXS profiles of ET_{EI} and ET_{WI} (A), ET_{EI}, ET-GOS_{EI}, ET-GOS_{EI} 0.5% gel (B), and ET-GOS_{WI} 0.5% gel (C). The black vertical line in panel C indicates a peak in the Q position of 0.87 nm^{-1} visible in each profile. Comparison between WAXS profiles of ET_{EI} and ET-GOS_{EI} (D).

Regarding the WAXS measurements, a few results are indicated in Figure 23D, being very similar for each analysed sample. WAXS data related to samples ET_{EI} and ET-GOS_{EI} show the same scattering profile, suggesting the absence of differences in the single lipid composition of the vesicle bilayer. Both SAXS and WAXS profiles of ET_{EI} and ET-GOS_{EI} samples are similar to plurethosome profiles, previously investigated by our research group [162].

SAXS measurements were performed also at 37 °C, as shown in Figure 24. A comparison between the situation occurring at 25 °C and 37 °C is highlighted, indicating the stability of ET formulation also at body temperature. A slight difference is observed for the formulation ET_{WI} where SAXS data illustrates a lower intensity of the peak in the position Q=0.87nm^{-1}.

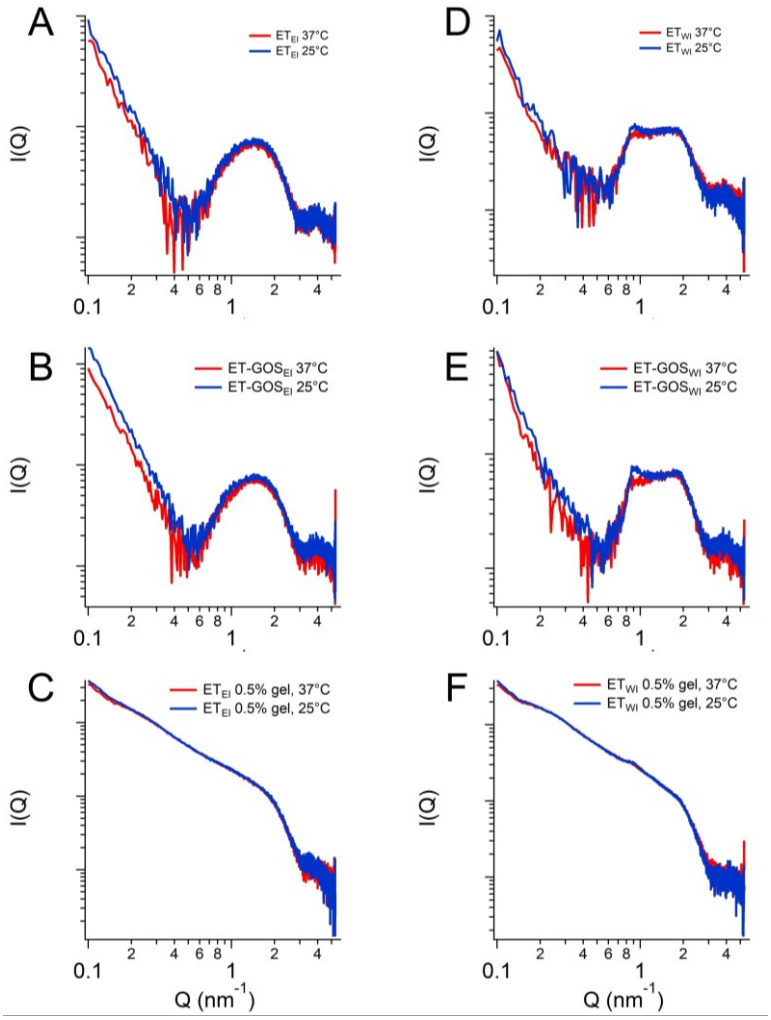

Figure 24. SAXS profiles of ET_{EI} (A), ET-GOS_{EI} (B), ET_{EI} 0.5% gel (C), ET_{WI} (D), ET-GOS_{WI} (E), ET_{WI} 0.5% gel (F) at 25°C and 37°C.

Based on this result, a temperature scan from 15 to 60 °C was performed for both ET_{WI} and ET-GOS_{WI} samples, to study a possible alteration of the vesicle structure due to the storage of these formulations. The results obtained from the temperature scan are reported in Figure 25, considering both sample ET_{WI} (Figure 25A) and ET-GOS_{WI} (Figure 25B).

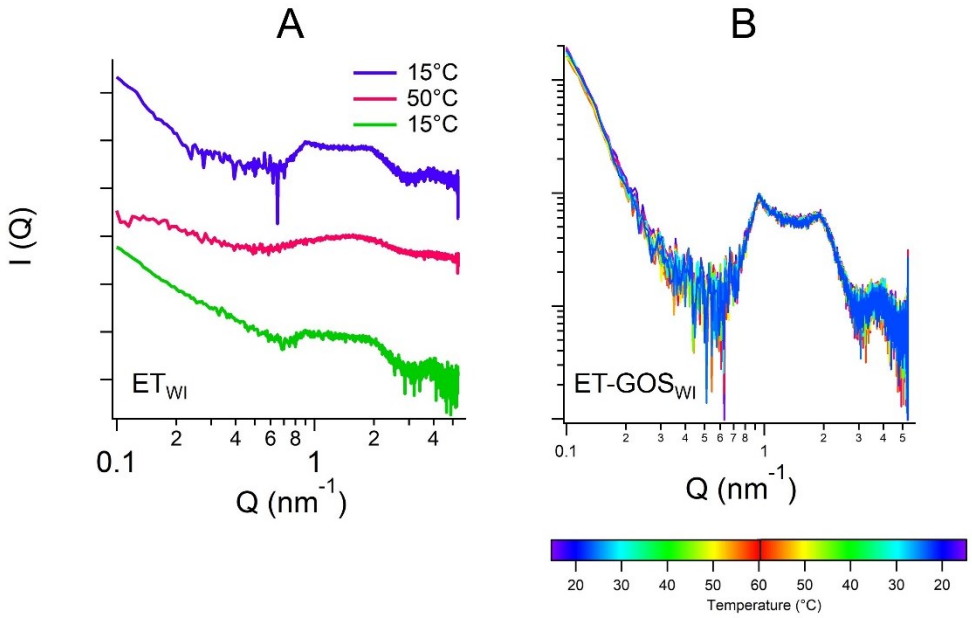

Figure 25. SAXS profile of ET$_{WI}$ (A) and ET-GOS$_{WI}$ (B) obtained through a temperature scan between 15°C and 60°C both in heating and cooling.

The result shown in Figure 25A regards only three curves to provide a clearer understanding and here two situations can be emphasized. On one side, the characteristical Bragg-peak has a lower intensity by increasing temperature, indicating that a possible alteration of some lipid lamellar of these vesicular nanosystems occurs, without destroying the ET structure. This aspect is also confirmed by the reversible nature of ET$_{WI}$ sample. Indeed, when the temperature returns to 15 °C by cooling down the sample, the peak shows the same starting position. Conversely, in the case of ET-GOS$_{WI}$ the SAXS profiles as a function of temperature are not altered, indicating that this formulation remains stable also at high temperature (Figure 25B).

Based on the obtained results, the ethanol injection method was selected for subsequent tests. ET-GOS$_{EI}$ were in fact characterized by (a) smaller vesicles with respect to ET-GOS$_{WI}$, possibly improving penetration through the skin and cell uptake, (b) higher GOS EC values, and (c) higher stability as a function of temperature, as suggested by SAXS results.

7.2.9. ANTIOXIDANT ACTIVITY EVALUATION

In order to assess the antioxidant activity of GOS loaded in ET, a DPPH test was performed. The antioxidant activity of free GOS in solution (SOL-GOS) was compared with that of the active compound loaded in ET (ET-GOS$_{EI}$) and in the thickened formulation ET-GOS$_{EI}$-0.5%gel. IC$_{50}$ values are shown in Table 18.

Table 18. Antioxidant activity of indicated formulations as resulted from DPPH test.

Formulation	DPPH IC_{50} (µg/mL)
ET-GOS_{EI}	6.77 ± 0.283 *
ET-GOS_{EI}-0.5%gel	10.625 ± 0.163 *
SOL-GOS	7.435 ± 0.403

Each value is the mean of at least 3 different experiments (mean ± SEM). * $p < 0.005$

By comparing the IC_{50} values, it is evident that the antioxidant activity of GOS is maintained even when loaded within ET. Conversely, the IC_{50} values obtained for ET-GOS_{EI} are significantly lower with respect to ET-GOS_{EI}-0.5%gel ($p < 0.005$). This result can be attributed to the 3D structure of the gel, which slows GOS release from the vesicles, possibly resulting in a prolonged effect of the drug.

On the other hand, empty formulations (i.e. ET_{EI} and ET_{EI}-0.5%gel) tested as controls, did not show any antioxidant activity (data not shown), confirming that the activity detected for drug loaded formulations is attributable to the contribution of GOS.

7.2.10. BIOLOGICAL ACTIVITY – IN VITRO EXPERIMENTS

Wound healing and migration assays were conducted on A375 melanoma cells to investigate the potential of GOS loaded in ET and in ET gel in the treatment of melanoma. Indeed, some studies indicate the anticancer effects of GOS and its role in melanoma progression [53]. Particularly, the formulations: ET-GOS_{EI}, ET-GOS_{EI}-0.5%gel, SOL-GOS, were tested and compared with unloaded formulations: ET_{EI}, ET-0.5%gel and vehicle (EtOH/H_2O 30:70 v/v).

Mtt assay

First, cytotoxicity of formulations was determined by MTT assay on A375 melanoma cell line. Specifically, cells were treated with different amounts formulations (i.e. 0.5, 1, 2.5, 5, 10, 20 and 50 µg/mL) and viability was evaluated after 24 h and 48 h from the treatments.

As depicted in Figure 26, while after 24 h cell viability decreased only for doses higher than 2.5 µg/mL (panel a) after 48 h a decrease (viability under 80% threshold), in cell viability was detected just at lower dosages of GOS compared to untreated cells (panel b). Therefore, we selected 0.5 µg/mL dose of GOS-loaded and unloaded formulations for the next experiments, as the non-toxic concentration that did not induce a reduction in cell viability higher than 25%.

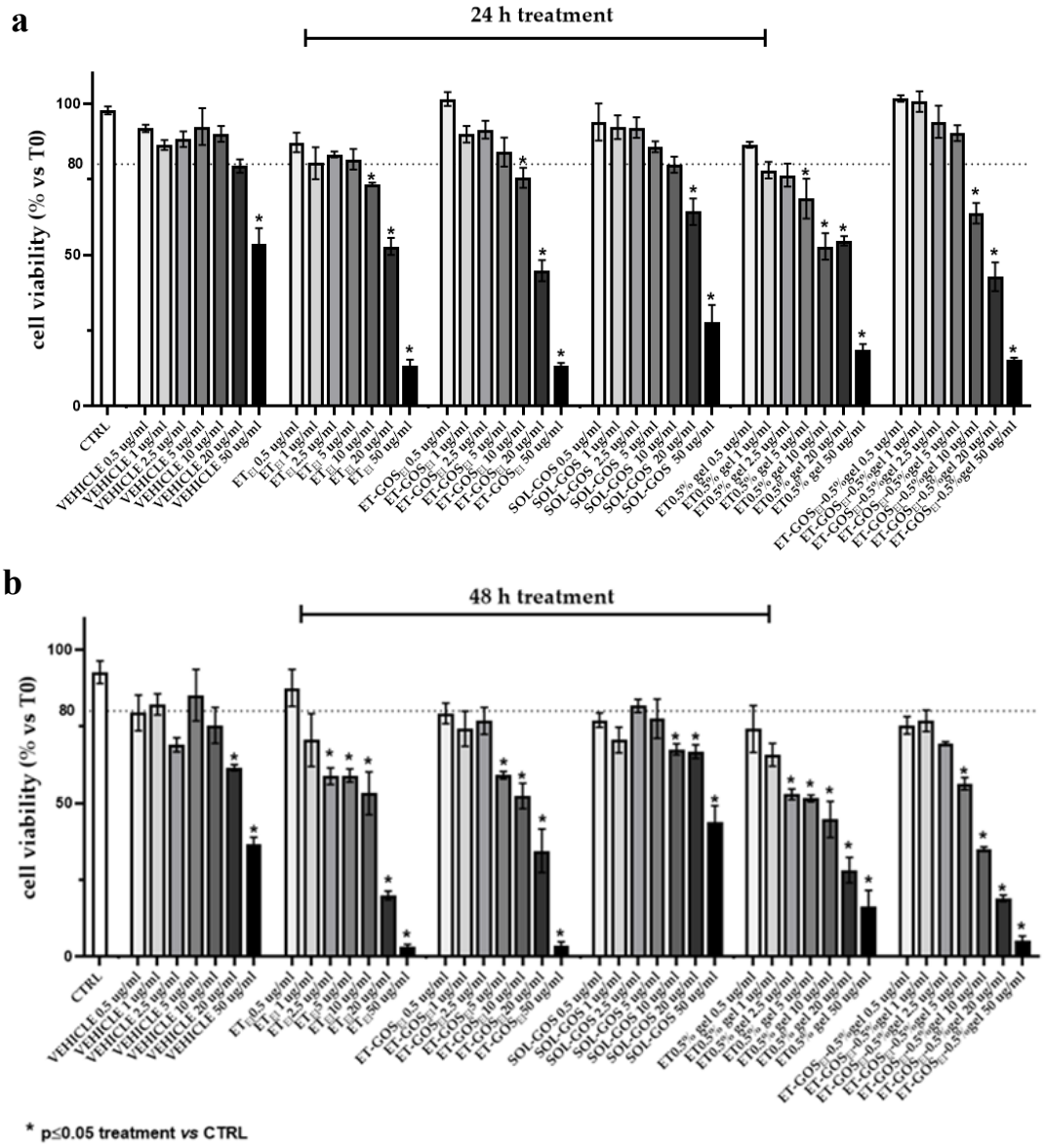

Figure 26. A375 melanoma cells viability evaluated by MTT test after 24 h (a) or 48 h (b) of treatment with GOS-loaded or unloaded formulations. Data are the results of three independent experiments performed in triplicate. Data appear as the mean ± SE. * $p < 0.05$ by two-way ANOVA (Post-hoc test: Tukey Test) Ctrl vs treated cells.

Wound healing assay

To evaluate the possible effect of GOS-loaded and unloaded formulations on melanoma cell migration, the wound healing assay was performed on A375 cell line. As depicted in Figure 27, cells treated with ET-GOS$_{EI}$, ET-GOS$_{EI}$-0.5%gel and SOL-GOS showed a delayed wound closure compared to the control cells. In addition, when GOS was loaded inside ET-GOS$_{EI}$ the wound closure rate was slightly slower than in case of the solution, confirming the controlled-release potential of the nanocarrier. Furthermore, when the cells were treated with the gelified formulation (ET-GOS$_{EI}$-0.5%gel), wound closure was even more delayed, with 75% still open after 48h. This result is not only statistically significant compared to the

control, but also significantly different from those obtained upon A375 cells treatment with the other two formulations containing GOS. Taken together the wound healing data, firstly confirm the potential antitumoral effect of GOS, then strengthens the hypothesis concerning the ability of the viscous formulation to prolong and further control the release of the encapsulated drug.

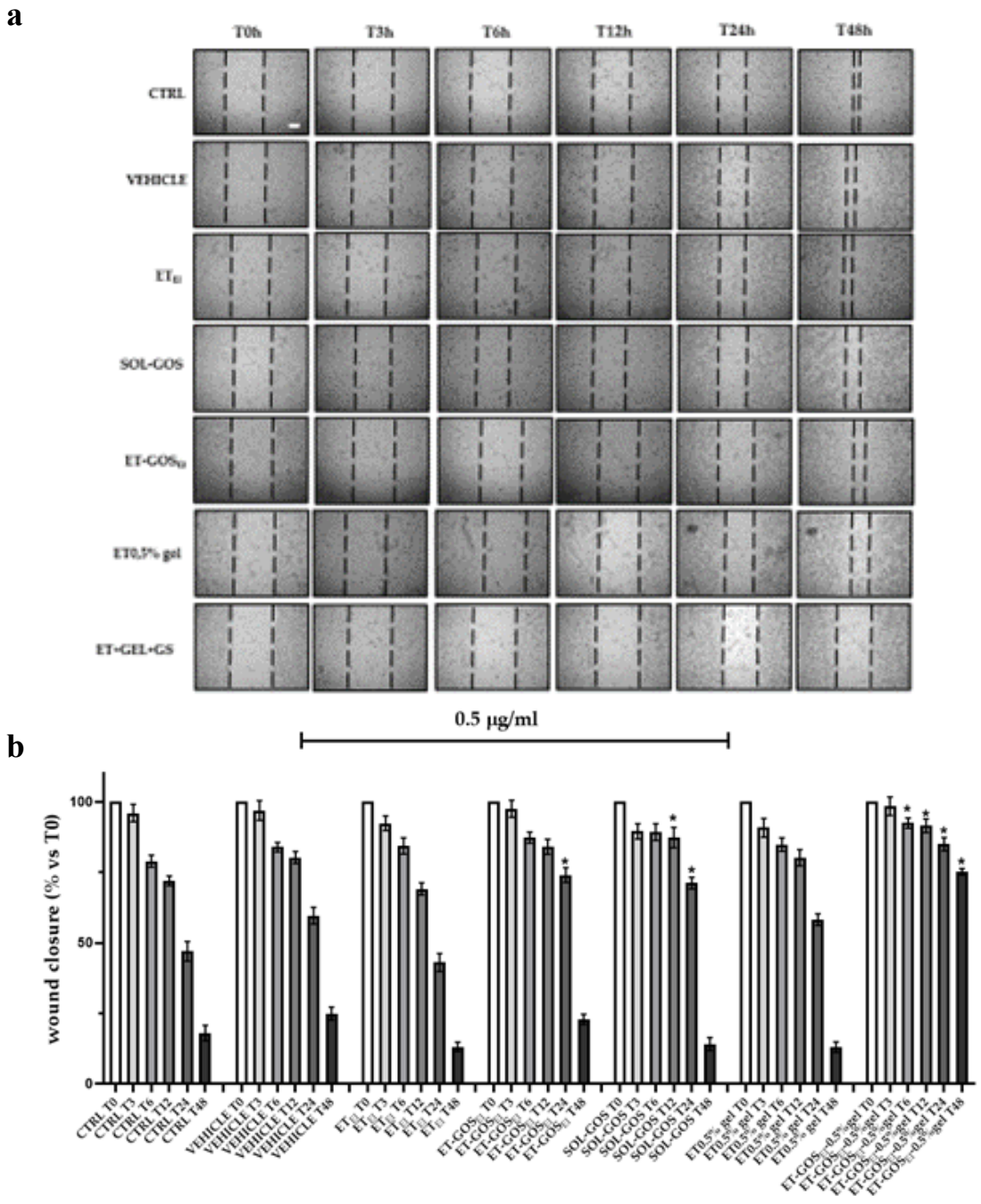

Figure 27. Effect of treatment with 0.5 µg/mL of GOS-loaded or unloaded formulations on the wound closure in A375 melanoma cells. (a) Scratch was performed on confluent monolayer of A375 cells, and different images were taken to measure wound area at different time points (0, 3, 6, 12, 24 and 48 h; scale bar 200 µm). (b) Quantification of the wound area at each time point via ImageJ. Data are shown as percent of 0 h. Data are the results of 3 independent experiments performed in triplicate. a: $p < 0.05$ vs. Ctrl by one-way ANOVA**.**

Transwell migration assay

Since the in vitro scratch assay cannot distinguish the effects of proliferation from migration, the transwell migration assay was conducted to better understand the possible role of GOS-loaded or unloaded formulations on melanoma cells migration. As shown in Figure 28, after 24 h of pretreatment of A375 melanoma cells with vehicle, or with GOS-unloaded formulations no migratory effect was observed, excluding, any potential migratory effect due to the empty vehicle. Conversely, upon SOL-GOS, ET-GOS$_{EI}$ and ET-GOS$_{EI}$-0.5%gel a significant reduction of cellular migration was noticed. This effect was particularly significant in the case of ET-GOS$_{EI}$-0,5%gel; indeed, in this case, the migratory ability was not only reduced when compared to control condition, but also when compared to SOL-GOS and ET-GOS$_{EI}$ confirming the delayed wound closure results above reported (Figure 27).

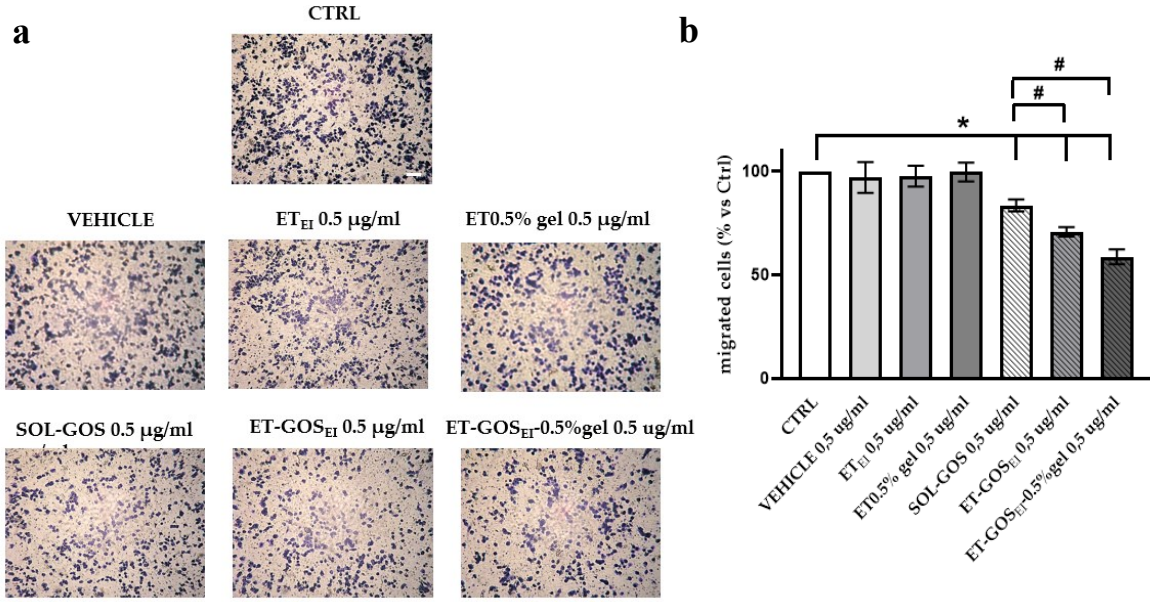

Figure 28. A375 melanoma cells migration after treatment with with 0.5 µg/mL of GOS-loaded or unloaded formulations. (**a**): representative images of A375 transwell migration after 24 h incubation with the different formulations (scale bar 200 µm). (**b**): ImageJ quantification of the migrated cells. Data are shown as average of 5 picture fields (20× magnification). * $p < 0.05$ treatment vs. CTRL; # $p < 0.05$ GOS-loaded vs. SOL-GOS by two-way ANOVA.

8. PROJECT 4 – Genistein-loaded transethosomal gel for the prevention of non-melanoma skin cancers: a preliminary study on human volunteers

8.1 INTRODUCTION

It is well known that chronic exposure to UV radiation is associated with the onset of several skin disorders, that can go from skin ageing to cancer [127,163,164]. In particular, it is estimated that around 90% of non-melanoma skin cancers (NMSC) and 65% of melanomas can be attributed to UV radiation [165]. The interest of the present study is focused on NMSC, which represent the most common human cancers and whose incidence is still increasing [166,167,168]. The term "NMSC" (or keratinocyte carcinomas) encompasses different cutaneous neoplasms, but is mainly used to define basal-cell carcinomas and squamous-cell carcinomas which are the most recurrent [166,167,168].

The main mechanism by which UV radiation (particularly UVA and UVB) causes damage to epidermal cells is through the production of reactive oxygen species (ROS). Despite the activity in our skin of endogenous antioxidant systems, both of enzymatic and non-enzymatic in nature, their capacity may be exceeded by excessive ROS accumulation, leading to oxidative stress [127,133]. Added to this is the direct action of UV radiation on macromolecules, in particular DNA, which is subject to mutations that can lead to carcinogenic transformations. Moreover, UV radiations possess also immunosuppressive effect, which may be crucial for the development of skin cancers [127,169].

With a perspective of identifying new photo- and chemo-preventive treatments, interest in active molecules of natural origin, in particular polyphenols, has recently grown [163]. In particular, in the present investigation, we pointed our attention on GEN. GEN, as previously reported (chapter 1.4.4), is an isoflavone, characterized by a wide range of biological activities, not only associated to its estrogen-like action but also antioxidant [57,58], anti-inflammatory, antimicrobial effect, and it has been widely studied for its chemopreventive and anti-cancer action against several types of tumors [55]. Moreover, it has been the subject of several studies for its potential in preventing skin damage, particularly UV-induced photodamage and as a chemopreventive agent [56,59,170,171].

In particular, Wei et.al [59] demonstrated that GEN administration was effective in preventing UVB-induced skin carcinogenesis in mouse models, resulting even more efficacious when applied topically than when administered orally. Moreover, topical

application of GEN efficaciously protected against UVB-induced skin photodamage on human skin in clinical trial and PUVA-induced photodamage in hairless mouse skin [59].

However, GEN low solubility and metabolic susceptibility represents a hindrance to its therapeutic application. Thus, in the present study, in order to overcome GEN limitations, its delivery though vesicular nanosystems such as ET and TE have been proposed, by virtue of their promising potential for topical drug delivery. As mentioned above (chapter 1.3.1), TE differs from ET for the presence of an edge activator in their composition, which further enhances the flexibility of the nanovesicles [6,24].

GEN has already been investigated for its incorporation into nano-based delivery systems for dermatological purposes [56], but to the best of our knowledge, its delivery via ET and TE has not been considered yet.

Accordingly, the first part of the work consisted in a preformulatory study with the purpose to select the best vehicle for GEN delivery. ET and TE have been prepared by the two methodologies: water injection and ethanol injection. The selected colloidal dispersions were then characterised in terms of size, pH, Zeta potential and morphology. Entrapment capacity as well as in vitro permeation of GEN was evaluated. Then, in order to simplify the application of the dispersion to the skin surface and increase its permanence in situ, colloidal dispersions were gelified with X-Gum. The amount of X-Gum was selected by means of leakage and spreadability tests and then formulations were characterized by rheology and SAXS. Antioxidant activity was also evaluated in vitro by PCL test. Finally, in vivo evaluations on healthy human volunteers were performed to prove the safety of the formulations and the potentiality of the vesicular vehicle for the skin delivery of GEN.

8.2. RESULTS AND DISCUSSION

8.2.1. PREPARATION OF ETHOSOMES AND TRANSETHOSOMES – PREFORMULATORY STUDY

Lipid nanovesicular systems such as ET and TE were chosen in order to deliver GEN through the skin. As previously reported (chapter 1.3.1), such nanovesicular systems are designed to improve transdermal delivery of drugs, given the presence of ethanol in their composition. TE can be seen as a second generation of ET, firstly produced by Song et al. in 2012 [24] to further increase the permeability of nanovesicles thanks to the addition of an edge activator

in the composition. Specifically, the composition of ET and TE formulations produced in the present project, which is itself based on previous studies conducted by our research group [25,26,61] is shown in Table 19. It is worth noting that the content of PC, EtOH and water is almost unchanged between ET and TE, what changes is the presence of Tween 80 (TW80), a non-ionic surfactant, selected as edge activator in the case of TE.

ET and TE were produced using the two different methods: the water injection method (WI) already standardised by our research group, and the ethanol injection (EI) one, which was introduced for the first time in Project 3, for GOS delivery.

The aim of this first part of the work, thus, is to identify the most appropriate nanosystem (and method) for the delivery of GEN.

Table 19. Composition and size distribution parameters of indicated formulations.

Formulation	PC[1] (%, w/w)	Ethanol (%, w/w)	TW80[2] (% w/w)	H_2O (%, w/w)	Z-Average (nm) ± s.d.	Dispersity index ± s.d.
ET_{WI}	0.9	29.1		70	203.88 ± 9.53	0.18 ± 0.05
ET_{EI}	0.9	29.1		70	145.40 ± 5.95	0.21 ± 0.02
TE_{WI}	0.9	28.8	0.3	70	136.15 ± 10.99	0.14 ± 0.01
TE_{EI}	0.9	28.8	0.3	70	107.78 ± 3.48	0.13 ± 0.01

[1]: soy phosphatidylcholine; [2]: tween 80; s.d.: standard deviation; data are the mean of 4 independent determinations on different batches.

All formulations appear macroscopically homogeneous and free of separation phenomena (Figure 29). The colour is opaque white in the case of ET_{WI}, more transparent in the case of ET_{EI}. TE result more transparent than ET and no differences in their appearance are noticeable between TE_{WI} and TE_{EI}.

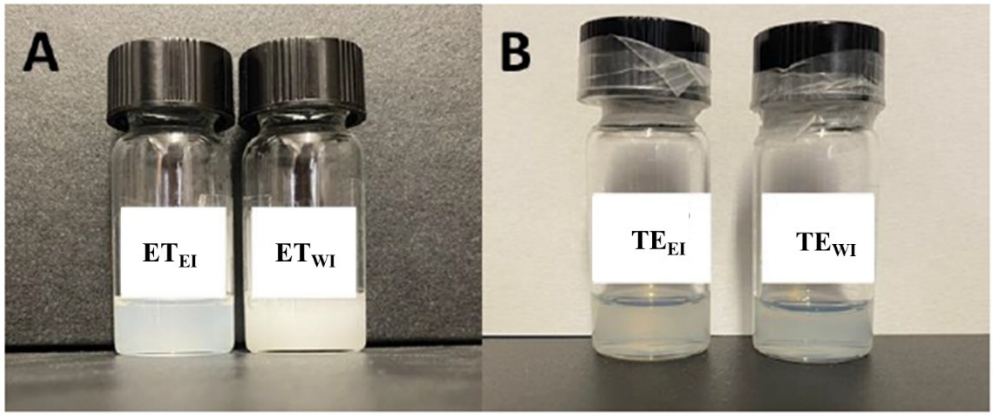

Figure 29. ET (A) and TE (B) prepared by water injection (WI) and ethanol injection (EI) methods.

Table 19 also shows size distribution results, again obtained by PCS analysis on the day after preparation. All formulations show a homogeneous size distribution, confirmed by the Dispersity indexes values, always around or less than 0.2. Regarding the Z-Average results, in order from largest to smallest there are: $ET_{WI} > ET_{EI} > TE_{WI} > TE_{EI}$. Previous studies had already pointed out that the presence of TW80 in TE led to a reduction in nanovesicle size when compared to ET prepared with the same PC content. It is likely that the surfactant intercalates in the bilayer, altering the lipid packing and leading to a size decrease. Furthermore, the result obtained in the previous study (Project 3) is confirmed, as the switch from water injection to ethanol injection led to a reduction in the average diameter of the nanovesicles. This change is more significant in the case of ET, but it is also visible in TE, where there is a size decrease of about 20 nm.

In light of these results, both ET and TE prepared with the two different methodologies appear promising for the delivery of GEN. Therefore, the next phase of the preformulatory study saw the loading of the drug into the nanosystems. In particular, both ET and TE were produced at different concentrations of GEN (in range between 0.5-0.2 mg/mL) using both methods (ethanol injection and water injection) in order to identify which vehicle could be used to load the maximum content of active principle. As described in chapter 4.1.1, in order to load GEN, the active compound was solubilised in the ethanol solution prior to mixing the two phases.

It was found that ET loaded with GEN at all concentrations greater than or equal to 0.2 mg/mL showed phase separation. In contrast, it was possible to load TE up to 0.25 mg/mL of GEN. No differences were observed between the two preparation methods. This result is probably a consequence of the interaction of GEN with the vesicles and its arrangement within the phospholipid bilayer. In the case of ET, excessively high concentrations of GEN led to an alteration of the phospholipid packing resulting in vesicle rupture and phase separation. In the case of TE, however, the presence of TW80 led to a stabilisation of the system.

Thus, TE prepared by both water injection and ethanol injection methods were selected for subsequent characterization steps. Table 20 shows the composition of TE-loaded formulations ($TE_{WI/EI}$ GEN).

Table 20. Composition of indicated formulations.

Formulation	PC[1] (%, w/w)	Ethanol (%, w/w)	TW80[2] (% w/w)	H_2O (%, w/w)	GEN[3] (% w/w)
$TE_{WI/EI}$	0.9	28.800	0.3	70	-
$TE_{WI/EI}$ GEN	0.9	28.775	0.3	70	0.025

[1]: soy phosphatidylcholine; [2]: tween 80; [3]: genistein.

8.2.2. NANOVESICLES CHARACTERIZATION

The day after preparation, the selected formulations ($TE_{WI/EI}$ loaded and unloaded with GEN) were characterized in terms of size, Z-potential and pH. The results of the various analyses are shown in Table 21.

Table 21. Z-Average, Dispersity index, pH and Z-potential of indicated formulations.

Formulation	Z-Average (nm) ± s.d.	Dispersity index ± s.d.	pH ± s.d.	Z-potential ± s.d.
TE_{WI}	136.15 ± 10.99	0.14 ± 0.01	5.35 ± 0.07	-21.86 ± 2.80
TE_{EI}	107.78 ± 3.48	0.13 ± 0.01	5.28 ± 0.18	-23.80 ± 6.34
$TE\text{-}GEN_{WI}$	144.65 ± 9.26	0.20 ± 0.08	5.34 ± 0.06	-24.62 ± 5.36
$TE\text{-}GEN_{EI}$	111.99 ± 2.61	0.14± 0.01	5.65 ± 0.32	-19.59 ± 5.01

s.d.: standard deviation; data are the mean of 4 independent determinations on different batches.

The results of the PCS analyses revealed a homogeneous size distribution of all samples, evidenced by the Dispersity index value never higher than 0.2. Similar to what has already been observed in the case of ET (Project 3), a discrete difference in the average diameter of the vesicles prepared with the two different methods is also evident in the case of TE. In particular, the use of the ethanol injection method leads to smaller nanovesicles, both in the case of formulations with and without the active compound. As previously discussed, (Project 3), we can suppose that the rapid depletion of the organic solvent that occurs in ethanol injection method leads to a faster closure of the bilayer, thus to smaller nanovesicles.

The presence of GEN seems to bring a slight increase in the size of vesicles prepared by both methodologies, but it is not particularly significant.

In each case, the pH value is weakly acidic and not affected by the presence or absence of GEN and the method of preparation. As the skin is weakly acidic (*stratum corneum* physiological pH is in the range 4.1-5.8 [172]), the pH of the formulations can be considered as suitable for a topical application.

The Z-potential assumes, as expected, a negative value due to the presence of PC and ethanol in the composition of the nanovesicles. Furthermore, it is noted that in each case it is around -20 mV, which is in support of a stabilisation of the system realised as a result of an electrostatic repulsion of the nanovesicles that hinders their aggregation over time.

The assessment of entrapment capacity was evaluated the day after preparation using the ultrafiltration method. As expected, since GEN is a lipophilic molecule, complete association with the nanovesicles was observed (EC = 100%). No differences were detected between ethanol injection and water injection methods.

8.2.3. MORPHOLOGICAL CHARACTERIZATION

To gain insights into the morphology of the produced TE, visualization was carried out using Cryo-TEM. Specifically, the images obtained for TE_{WI} and TE_{EI} are shown in Figure 30.

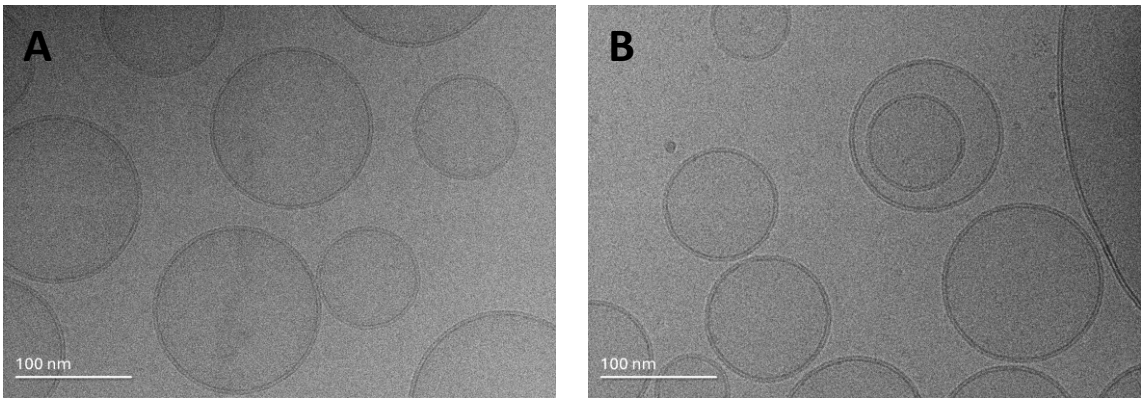

Figure 30. Cryo-transmission electron microscopy (Cryo-TEM) images of TE_{WI} (A) and TE_{EI} (B). Bar corresponds to 100 nm.

In both cases, spherical, unilamellar vesicles were found, the size of which is consistent with the data obtained from the PCS analysis. Unlike what was observed in the case of ET (Project 3), there are no morphological differences in TE produced by the two different methods. The final morphology of the vesicles is therefore predominantly dependent upon the presence of TW80. The surfactant, in fact, arranges itself by intercalating into the phospholipid bilayer and exposing its polar head outward, creating steric hindrance that prevents the assembly of multiple bilayers, thus promoting a unilamellar structure. The result aligns with previous findings from our research group [26,27], where TE produced with the same composition (using water injection method) showed a unilamellar structure.

No differences were detected between loaded and unloaded formulations (data not shown), meaning that GEN do not affect supramolecular organization of the nanovesicles.

Considering the obtained results, and seeing substantial similarities between the TE produced by the two different methods, the ethanol injection method was chosen for further evaluations, based on a possible advantage offered by size reduction.

8.2.4. IVPT

In order to predict the in vivo behaviour of TE-GEN$_{EI}$, an IVPT was conducted using Franz cells apparatus assembled with STRAT-M® membrane, selected as in previous projects due to its capability to mimic *stratum corneum* characteristics. Therefore, the aim of the test is to assess the diffusion of GEN through the skin when delivered within TE. In addition, a comparison was performed with GEN dispersed in EtOH/H_2O 30:70 (SOSP-GEN), at the same concentration as the TE-GEN$_{EI}$. SOSP-GEN is in fact a suspension of active compound, as GEN is not soluble in EtOH/H_2O 30:70. This confirms the ability of the vesicular system, like TE, to favour the solubilisation of lipophilic drugs. It was decided to maintain the same EtOH and GEN content as in TE-GEN$_{EI}$ in order to make the comparison between the two systems more effective, being the difference exclusively attributable to the presence of vesicular nanosystem.

GEN diffusion profiles are shown in Figure 31, while Table 22 shows IVPT parameters.

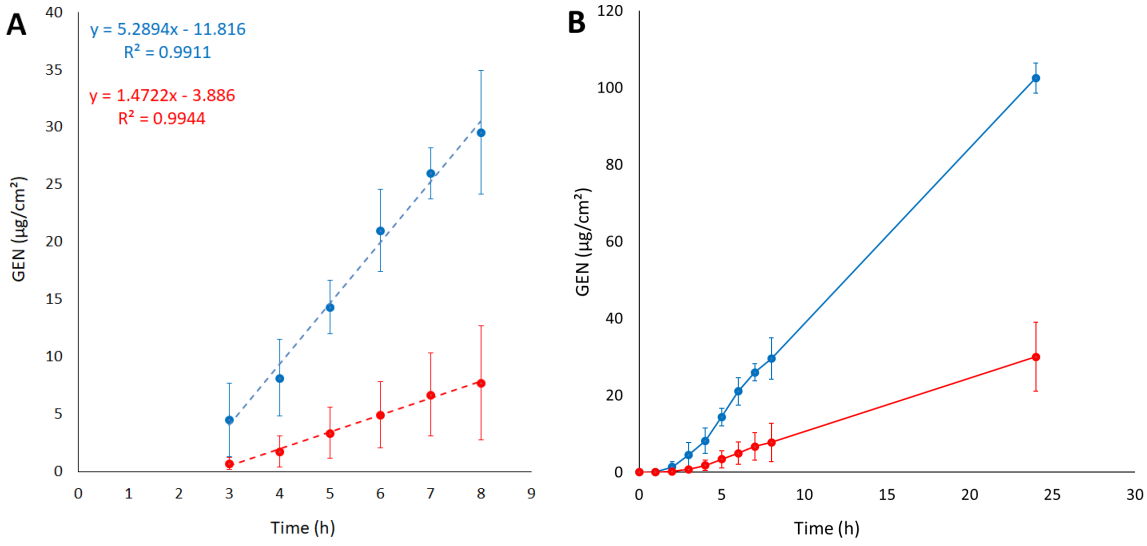

Figure 31. GEN permeability kinetics from TE-GEN$_{EI}$ (blue circles), SOSP-GEN (red circles) as determined by Franz cells associated with the STRAT-M® membrane. Panel (A) show the linear part of the kinetic profiles, while panel (B) show diffusion profile over 0–24 h. Data are the mean of 4 independent experiments ± s.d.

As can be seen from the graphs (Figure 31), GEN diffuses much faster through the membrane when delivered into the TE than in SOSP-GEN. This confirms the potential of vesicular systems in promoting the penetration of active compounds through the skin. Precisely, the

amount of GEN permeated after 24 h (A value in Table 22) was around 30 μg/cm^2 for SOSP-GEN and 102 μg/cm^2 for TE-GEN$_{EI}$.

Table 22. IVPT parameters of the indicated formulations.

IVPT Parameters	TE-GEN$_{EI}$	SOSP-GEN
Jss [1] (μg/cm^2/h)	5.34 ± 1.05	1.62 ± 0.68
Kp [2] (cm/h) × 10^3	21.08 ± 3.64	6.49 ± 2.74
Tlag [3] (h)	2.14 ± 0.72	3.05 ± 0.56
D [4] (cm^2 h^{-1}) × 10^5	8.38 ± 2.54	5.62 ± 0.99
P [5] membrane/vehicle	8.79 ± 4.37	3.54 ± 0.93
A [6] (μg/cm^2)	102.50 ± 3.96	30.02 ± 8.97

[1]: steady-state flux per unit area; [2]: permeability coefficient; [3]: lag time; [4]: diffusion coefficient; [5]: partition coefficient; [6]: cumulative amount of GEN diffused at 24 h; GEN concentration was always 0.25 mg/mL. Data are the mean of 4 independent Franz cell experiments ± s.d.

As shown in Table 22, a certain lag-time is observed in both cases, which is longer in the case of the SOSP-GEN than in the vesicular formulation. Furthermore, the greater diffusion of the drug in the case of TE is confirmed. The Kp value is much higher, demonstrating an increase in GEN permeation through the membrane. The D and P values are also higher than in the case of the suspension, demonstrating that TE are able to facilitate the diffusion and partition of the active compound across the membrane/skin.

8.2.5. STABILITY STUDIES

In order to evaluate the stability of the vesicular formulations (TE$_{EI}$ and TE-GEN$_{EI}$), PCS analyses and Z-potential evaluations were repeated at different time intervals (1-15-30-60-90 days). In addition, the ability of the formulation to control GEN degradation was also assessed by quantifying the drug concentration over time and comparing it with that of day one. All formulations were stored at 4 °C and protected from light.

Size stability

Both the empty formulation (TE$_{EI}$) and the GEN-loaded formulation (TE-GEN$_{EI}$) resulted dimensionally stable over time. In particular, a slight increase in mean diameter (Figure 32A) was observed, possibly the result of modest vesicle aggregation or fusion. The Dispersity index (Figure 32B), on the other hand, remained always below 0.2, confirming a homogeneous size distribution even three months after preparation.

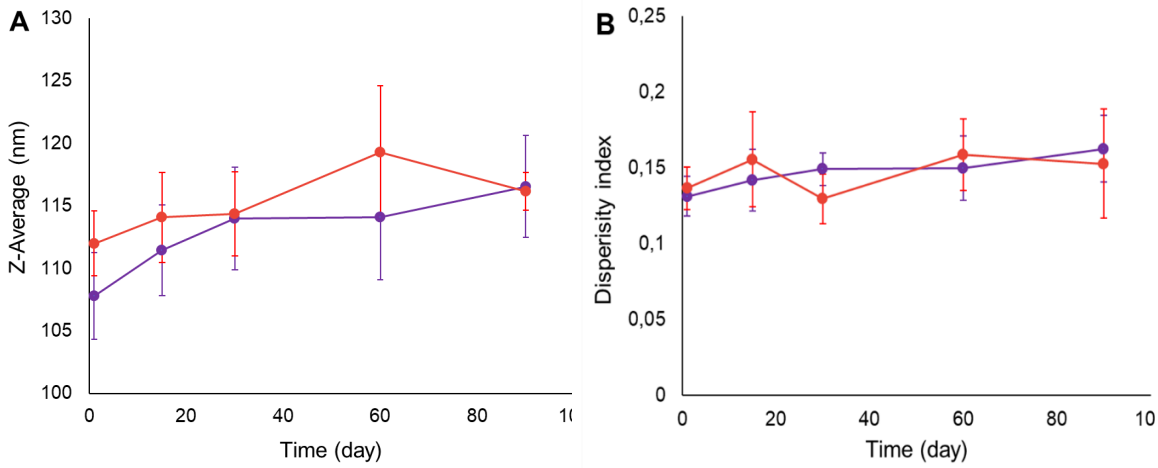

Figure 32. Size stability evaluation of TE_{EI} (purple line) and TE-GEN_{EI} (red line). Panel (A) shows Z-Average while panel (B) displays Dispersity index time course. Samples were stored at 4°C and protected from light and each data is the mean of 6 determinations ± s.d.

Z-potential stabilty

The stability of the Z-potential over a 60-day period was also investigated in order to associate the possible occurrence of instability phenomena with alterations in the Z-potential value. The results are shown in the Figure 33. As can be seen, the parameter undergoes fluctuations over time, which can be attributed to the dynamic nature of vesicular systems. A slight tendency towards more negative values with the course of time is recognisable.

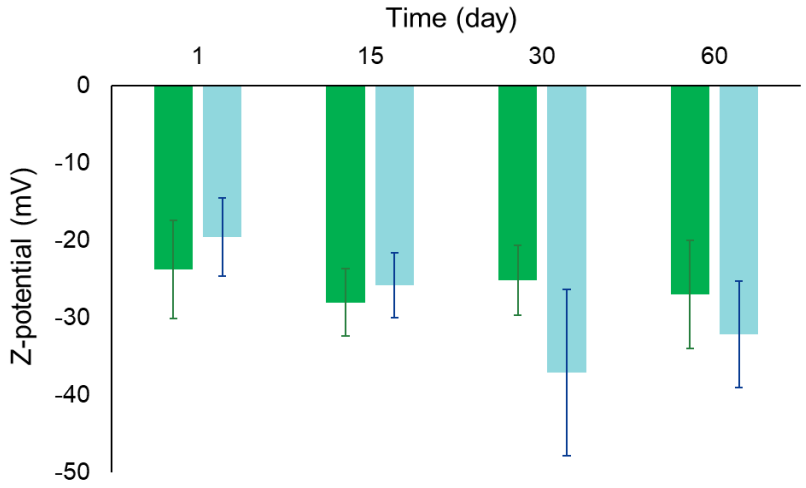

Figure 33. Z-potential stability evaluation of TE_{EI} (green bars) and TE-GEN_{EI} (blue bars). Samples were stored at 4°C and protected from light and each data is the mean of 4 determinations ± s.d.

Chemical stability

The result of the study highlighted the ability of TE to protect the associated active compound from degradation. Indeed, after 90 days of storage at 4°C, the formulations (TE-GEN_{EI}) still had, averagely, 95% of the initial GEN content.

8.2.6. TRANSETHOSOMAL GEL PREPARATION AND CHARACTERIZATION

In order allow cutaneous application of the formulations, it was decided to gelify the colloidal dispersion by addition of X-Gum as thickening agent. Thus, TE gels were prepared by direct addition of X-Gum to colloidal dispersion (TE_{EI}) kept under magnetic stirring until the complete dispersion of the polysaccharide. 3 different X-Gum concentration were evaluated (i.e. 0.5, 0.75 and 1 % w/w) to select the one with the most favourable characteristics. As demonstrated in Figure 34, homogeneous systems were produced for each of the three concentrations, with both viscosity and opacity exhibiting a notable increase in relation to the amount of X-Gum incorporated.

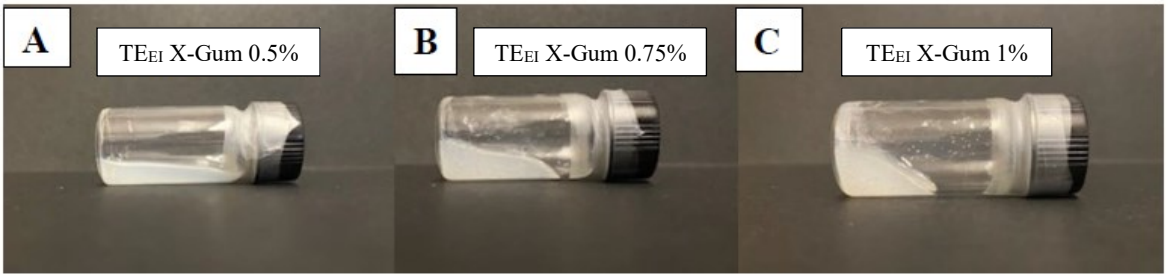

Figure 34. TE gels prepared from TE_{EI} by the addition of different amounts of X-Gum: 0.5 % (A), 0.75 % (B) and 1 % (C).

The optimal composition was identified based on the results of spreadability and leakage assays, the results of which are summarized in Table 23.

Table 23. Spreadability and leakage test results of reported formulations.

Formulation	X-Gum % (w/w)	Spreadability[1] (g cm/s)	Leakage[2] (cm)
TE_{EI} gel	0.5 %	21.75 ± 0.5	3.23 ± 0.42
	0.75 %	20.83 ± 0.29	1.84 ± 0.51
	1 %	18.67 ± 0.29	0.77 ± 0.06

[1]:calculated as reported in Equation (1); [2]: running distance along the slide; data are the mean of 3 independent measurements ± s.d.

As expected, an increase in the percentage of X-Gum corresponded to decreased leakage and spreadability values. The X-Gum concentration selected for subsequent studies is 0.5 % w/w, for which a higher spreadability value corresponds.

8.2.7. RHEOLOGICAL ANALYSIS

The formulations were characterized rheologically, comparing TE loaded or unloaded with GEN, with the corresponding gelified forms: TE_{EI}-gel and TE-GEN_{EI}-gel. Analyses were performed at two different temperatures: 25 °C and 37 °C, in order to assess the behaviour

at room temperature and under physiological conditions. Figure 35 shows viscosity curves obtained for all tested formulations.

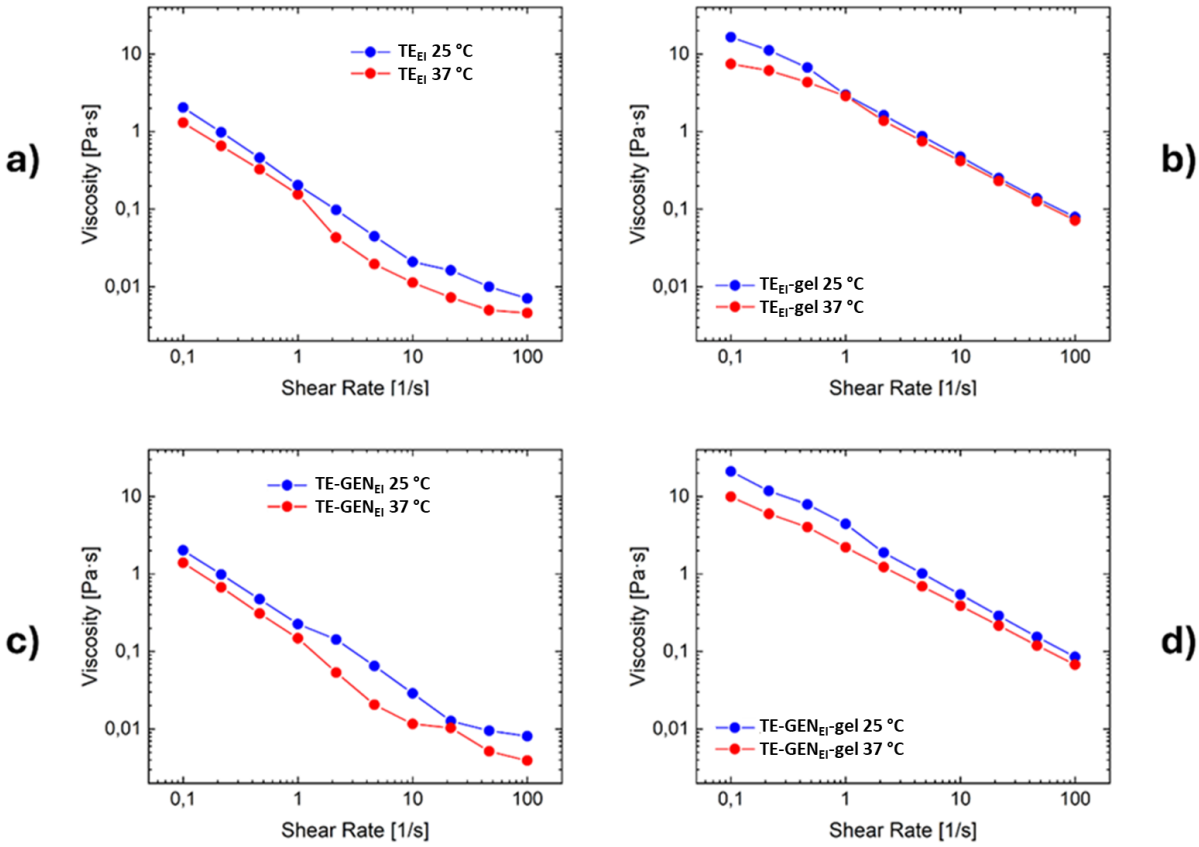

Figure 35. Viscosity curves analysed for TE_{EI} (a), TE_{EI}-gel (b), TE-GEN_{EI} (c), and TE-GEN_{EI}-gel (d). The blue curves refer to the measurement carried out at 25°C, while the red curves at a temperature of 37°C.

It is evident that in case of formulation gelified by X-Gum, the viscosity tends to increase about 10 times for any value of shear rate. Furthermore, as expected, a slight decrease in viscosity is observed with increasing of the temperature from 25 °C to 37 °C.

8.2.8. SAXS ANALYSIS

In order to further characterize the formulations, and get an insight into the internal supramolecular organisation, SAXS measurements were performed. The measurements were carried out at 2 different temperatures: 25 °C and 37 °C, in order to compare the behaviour of the formulation at room temperature and under physiological conditions. The formulations submitted for analysis are: TE_{EI}, TE-GEN_{EI}, TE_{EI}-gel and TE-GEN_{EI}-gel. SAXS diffraction spectra are shown in Figure 36.

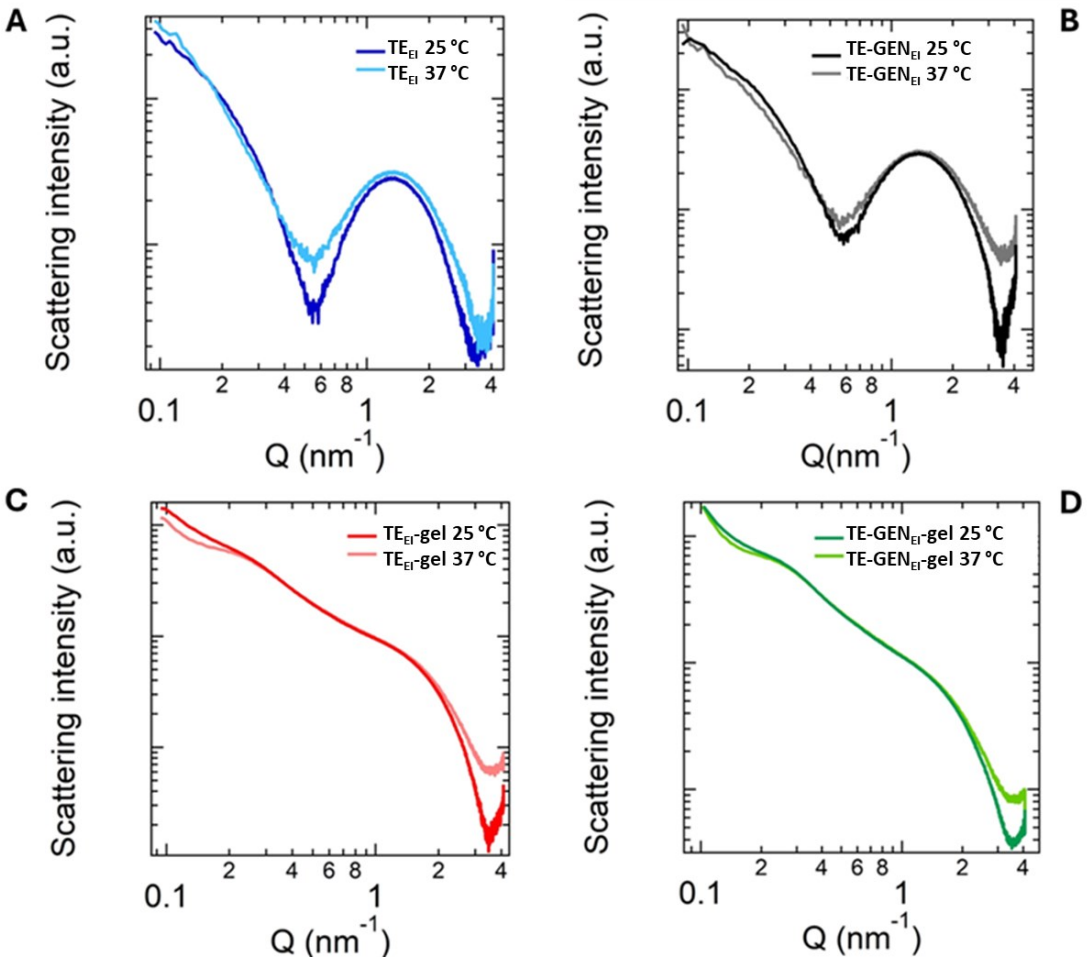

Figure 36. SAXS diffraction spectra of TE_{EI} (A), TE-GEN_{EI} (B), TE_{EI}-gel (C), and TE-GEN_{EI}-gel (D). Analyses were performed at 25 °C and 37 °C.

The results show that there are no differences in the measurements taken at the two different temperatures, demonstrating that the supramolecular organisation remains intact both under storage conditions at room temperature and in contact with skin and internal structures. No particular differences were observed between scattering profiles of GEN-loaded and unloaded formulations either, demonstrating that the addition of the drug does not alter the structural properties of the delivery system. In both TE_{EI} and TE-GEN_{EI} (Figure 36A and 36B) SAXS profile is that typical of vesicles having a lipid bilayer. In particular, there is an evident broad band centred at a position of approximately 1.5 nm^{-1}, corresponding to a distance of approximately 4.2 nm, which corresponds to the thickness of the lipid bilayer. In Figure 36C and Figure 36D we can see that the addition of X-Gum results in a significant change in the SAXS profile. It could be the sum of two profiles: at a higher angle, there is the contribution of the lipid bilayer, while at a lower angle, the presence of the thickening factor is noticeable. It can be therefore assumed that the vesicles were completely embedded within the polymeric network of the X-Gum.

8.2.9. ANTIOXIDANT ACTIVITY EVALUATION

The in vitro PCL assay allowed the evaluation of the antioxidant activity of gelified and non-gelified TE-GEN$_{EI}$. For comparison, the antioxidant activity of free GEN in ethanol solution (SOL GEN) and of the empty formulations (i.e. TE$_{EI}$ and TE$_{EI}$-gel) was also evaluated. The results obtained by applying the analytical protocol ACL (antioxidant capacity of lipid-soluble compounds) are shown in Table 24, and expressed as μmol Te/g.

Table 24. Antioxidant activity of indicated formulations as resulted from PCL test.

Formulation	ACL (μmol Te/g)	ACL (μmol Te/g) – blank[2]
GEN	200.53 ± 13.74	
SOL GEN	0.071 ± 0.005	
TE-GEN$_{EI}$	0.137 ± 0.004	0.068 ± 0.0037
TE$_{EI}$	0.070 ± 0.005	
TE-GEN$_{EI}$-gel	0.123 ± 0.005	0.062 ± 0.0047
TE$_{EI}$-gel	0.061 ± 0.003	

[1]: Antioxidant Capacity of lipid soluble compounds; [2]:blank is considered ACL signal of correspondent empty formulations (TE$_{EI}$ for TE-GEN$_{EI}$ and TE$_{EI}$ gel for TE-GEN$_{EI}$-gel). Data are the mean of 3 independent experiments ± s.d.

The results confirm the strong antioxidant activity of GEN (200 μmol Te/g), which is essentially related to the polyphenolic structure of isoflavones (chapter 1.4.4).

Interestingly, even empty formulations (i.e. TE$_{EI}$ and TE$_{EI}$-gel) possess some, although modest, antioxidant activity, attributable to the presence of TW80 and PC in the composition. Therefore, part of the signal produced by the formulations TE-GEN$_{EI}$ and TE-GEN$_{EI}$-gel is attributable to the vehicle. In order to highlight the contribution of GEN, in the right column of the table is reported the antioxidant activity value of the formulations subtracted from the "blank", represented by the signal of the corresponding empty formulation (TE$_{EI}$ for TE-GEN$_{EI}$ and TE$_{EI}$-gel for TE-GEN$_{EI}$-gel). It was found that GEN antioxidant contribution in loaded formulations TE-GEN$_{EI}$ and TE-GEN$_{EI}$-gel is not significantly different with the antioxidant activity of SOL GEN, (the two-tailed P values are 0.5111 and 0.1980 respectively), meaning that the vehicle does not mask the activity of the drug. Consequently, even when delivered in vesicular nanosystems, GEN is just as available to exert its antioxidant action as when free in solution. Even between TE-GEN$_{EI}$ and TE-GEN$_{EI}$-gel, no statistically significant difference was found (the two-tailed P value is 0.3035), confirming that both systems maintain the antioxidant profile of GEN.

Worth noting is that the antioxidant activity obtained for SOL GEN, TE-GEN$_{EI}$ and TE-GEN$_{EI}$-gel is in line with the percentage of active molecule present in the formulation.

8.2.10. IN VIVO STUDIES

In vivo studies were carried out on human volunteers to first test the possible irritating effect of the vesicular gel (TE-GEN$_{EI}$-gel) on the skin, but also to assess the capacity of the nanosystem as a drug delivery system. A X-Gum GEN gel (GEN-gel), was employed as a comparison. Precisely, GEN-gel was produced by dispersion of GEN in water, followed by addition of X-Gum under magnetic stirring. The formulation possesses the same amount of GEN and X-Gum as the TE-GEN$_{EI}$-gel.

Patch test

First, a patch test was conducted to evaluate the irritation potential of the selected formulations when applied in a single dose on intact human skin. The number of edematous and erythematous reactions caused by the GEN-gel and TE-GEN$_{EI}$-gel was recorded for each experimental time and results are presented in Table 25 as mean Irritation Index (IIM).

Table 25. Number of oedematous and erythematous reactions caused by tested formulations, expressed as mean Irritation Index (IIM).

Reactions	**GEN-gel.**	**TE-GEN$_{EI}$-gel**
IIM erythematous 15 min	0.05	0.05
IIM edematous 15 min	0.00	0.00
IIM erythematous 1 h	0.05	0.05
IIM edematous 1 h	0.00	0.00
IIM erythematous 24 h	0.00	0.00
IIM edematous 24 h	0.00	0.00

The results indicate that both formulations can be classified as non-irritant when applied to human skin.

Tape stripping

After confirmation of the non-irritating effect of the formulations on human skin, a tape stripping study was performed on 20 healthy volunteers to assess the potentiality of the TE-GEN$_{EI}$-gel formulation to promote permeation of the active molecule through the skin. Again, GEN-gel was employed as comparison. The results obtained are presented in the Figure 37, which shows the amount of GEN found in *stratum corneum* superficial layers (quantified in the extracts from the tapes) at the different time points (1-3-6 h).

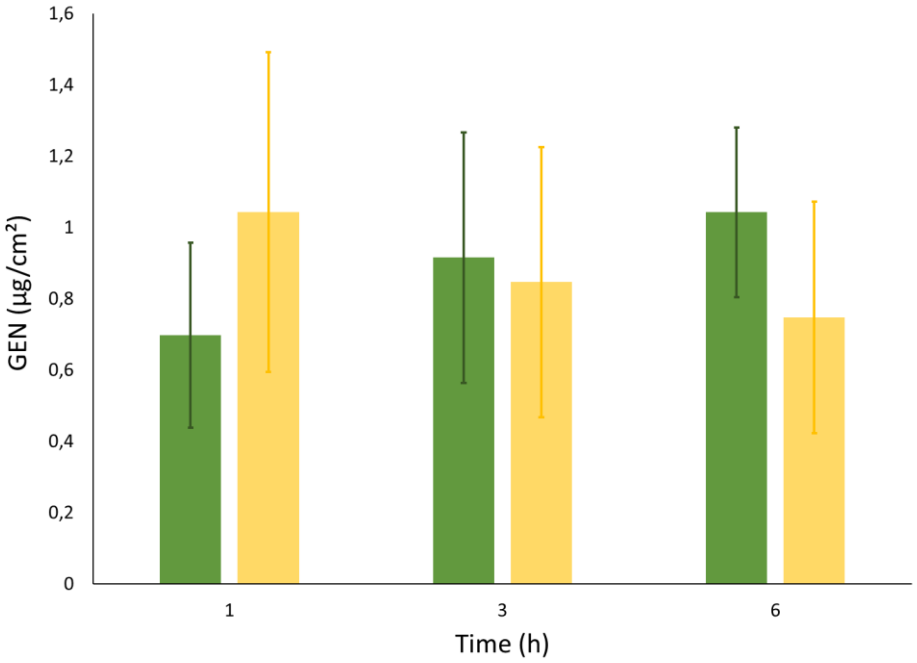

Figure 37. Amount of GEN permeated from TE-GEN$_{EI}$-gel (green) and GEN-gel (yellow) at different time points (1, 3 and 6 h). Data were obtained from tape stripping performed on 20 healthy volunteers.

As can be seen from the graph, it is possible to recognise opposite trends for the two formulations. In the case of the TE-GEN$_{EI}$-gel, we see a gradual increase in the amount of permeated GEN over time; on the contrary, in the case of the GEN-gel, we observe a maximum of GEN after the first hour, which tends to decrease towards the sixth hour.

It can be deduced that in the case of the GEN-gel formulation, there is an initial accumulation of GEN in the superficial layers, but the amount detected tends to decrease over time due to the progressive degradation of the active compound. In fact, as the test is conducted under non-occlusive conditions, the formulation is exposed to the external environment and therefore to light. Since GEN is a photosensitive molecule [173,174], when delivered in X-Gum-gel formulation, it is left unprotected and rapidly degrades, which corresponds to a possible loss of activity in the long term.

In the case of the TE-GEN$_{EI}$-gel formulation, in the opposite, to have found a low amount of GEN in the first time point is attributable to the fast penetration of the vesicles more deeply into the skin. Indeed, it must be taken into account that with tape stripping, the GEN found in the most superficial layers of the *stratum corneum* is quantified. It can therefore be assumed that during the first time interval, TE reach the deeper layers of the *stratum corneum* or living epidermis, where, forming a depot, they gradually release GEN, whose content in the superficial layers tends then to increase over time. In addition, unlike in the case of GEN-

gel, since the drug has penetrated deeper and is shielded by vesicular structures, it will not be susceptible to photodegradation.

Taken together, these results demonstrate the potential of TE-GEN$_{EI}$-gel as a sustained-release system, of relevance for prolonged-protective action required for the prevention against UV-induced skin damage.

9. CONCLUSIONS AND FUTURE PERSPECTIVES

The work presented highlighted the potential of lipid-based nanosystems, in particular ET, TE and SP, for the delivery of active compounds of natural origin through the skin. Thanks to these nanotechnologies, it has been possible to overcome problems related to the solubility and permeability of drugs, while achieving sustained-release systems that are easy to apply to the skin and minimally invasive.

The formulations under investigation were all composed of biocompatible, non-toxic excipients and their production did not involve the use of organic solvents other than ethanol. This benefits not only the safety of the formulation, but also the greater sustainability of manufacture, as toxic or difficult-to-dispose-of residues are avoided.

The preparation methods did not involve the use of extensive heating or prolonged high energy. For instance, the water injection and ethanol injection methods for the production of ET and TE were carried out entirely at room temperature. This benefits first of all, lower consumption for research and, in perspective, industrial production. Moreover, it ensures that the drugs are protected from degradation during the preparation steps. This is particularly important when working with natural compounds, which are generally thermo-sensitive.

In the light of the results obtained for each specific project, the following conclusions can be drawn.

Project 1 highlighted the potentiality of ET for both CUR and PIP delivery. The nanosystem was found to effectively encapsulate both active compounds and achieve a control over their release, as well as promote permeation in vitro. The antioxidant activity test indicated a potential synergistic effect of the combination of the two formulations (i.e. ET-CUR and ET-PIP), later confirmed by ex vivo experiments. Taken together, the results suggest a promising potential of ET as a platform for prolonged transdermal delivery of active compounds, which showed advantages over simple drug solutions and thus better protection against pollutant stressors to prevent skin ageing in the long term.

The SP formulation studied in Project 2 emerges as a versatile and efficient delivery system for natural antioxidants such as CUR and PIP. The data presented reveal a potential of the formulation in promoting the permeation of CUR through the skin, also favoured by the association with PIP. Furthermore, the efficacy demonstrated in ex vivo models suggests the potential use in advanced skin care products designed to protect against damage caused by

exposure to environmental pollution. As a future perspective, a possible long-term study efficacy of the SP formulation could then be proposed, to confirm the protective effects of CUR- and PIP-loaded SP against also other environmental stressors, including UV radiation, ozone, and cigarette smoke to which we are exposed in our daily lives.

Project 3 showed that the ethanol injection method could be more advantageous than the water injection method for the production of ET, because it resulted in smaller vesicle size and enhanced entrapment capacity. GOS was efficiently loaded into ET nanosystems, which were confirmed to be able to control its release and promote its diffusion in vitro. The results obtained from antioxidant activity tests and in vitro tests on melanoma cell line also showed the potential of ET-GOS_{EI}, also in viscous form, for the treatment of cutaneous melanoma. Further studies will certainly be undertaken to confirm the efficacy of the ET-GOS_{EI}-0.5%gel formulation on melanoma and possibly other skin diseases associated with oxidative stress.

In Project 4, on the other hand, the preformulatory study led to the selection of TE produced by the ethanol injection method as the most appropriate vehicle for GEN delivery. The formulation showed stability over 90 days and efficacy in promoting the permeation of the drug in vitro. The antioxidant activity test confirmed the action of GEN, even when delivered within TE and in the gelified formulation. The promising results of the in vivo tests pave the way for a possible and safe use of TE-GEN_{EI}-gel as a photo- and chemo-protective formulation against UV-induced skin damage. Additional studies are currently planned to confirm the protective efficacy both in vitro and in vivo.

The results collected in this thesis may represent a starting point for future research. Considering the worrying increase in pollution at global level and the persistence of skin disorders related to it, or associated to the deleterious action of UV radiation, the formulations proposed here may represent valid and *green* alternatives to the products currently on the market. The phytocompounds investigated present promising potential for both dermatological and cosmetic applications, and thanks to nanotechnology, and in particular lipid-based drug delivery systems, it has been possible to successfully deliver them. Certainly, further in vitro and in vivo evaluations are necessary to confirm the effectiveness of the formulations, and then move on to clinical trials, to validate the clinical efficacy and safety of these innovative dermatological products.

In addition, the proposed formulations have all the requirements to make the industrial transfer possible, due to the low-cost materials and almost no toxic waste (except for analytical procedures). Furthermore, the production methods are, as previously mentioned,

easy and low energy consuming. Undoubtedly, in-depth scale-up studies are needed, especially for SP production, that in this work has only been investigated in small volumes. While, as regard ET and TE, ongoing studies are already confirming the scalability of their preparation method and even the feasibility of producing them in continuous, exploiting also different technologies.

10. BIBLIOGRAPHY

[1] E. Proksch, J.M. Brandner, J.M. Jensen, The skin: an indispensable barrier, Exp Dermatol 17 (2008) 1063–1072. https://doi.org/10.1111/J.1600-0625.2008.00786.X.

[2] H.A.E. Benson, A.C. Watkinson, Transdermal and Topical Drug Delivery: Principles and Practice, Transdermal and Topical Drug Delivery: Principles and Practice (2012). https://doi.org/10.1002/9781118140505.

[3] L. Ventrelli, L. Marsilio Strambini, G. Barillaro, Microneedles for Transdermal Biosensing: Current Picture and Future Direction, Adv Healthc Mater 4 (2015) 2606–2640. https://doi.org/10.1002/ADHM.201500450.

[4] O. Arda, N. Göksügür, Y. Tüzün, Basic histological structure and functions of facial skin, Clin Dermatol 32 (2014) 3–13. https://doi.org/10.1016/J.CLINDERMATOL.2013.05.021.

[5] W.D. Losquadro, Anatomy of the Skin and the Pathogenesis of Nonmelanoma Skin Cancer, Facial Plast Surg Clin North Am 25 (2017) 283–289. https://doi.org/10.1016/J.FSC.2017.03.001.

[6] E. Esposito, A. Pecorelli, F. Ferrara, M. AnnLila, G. Valacchi, Feeding the Body Through the Skin: Ethosomes and Transethosomes as a New Topical Delivery System for Bioactive Compounds, Annu Rev Food Sci Technol 15 (2024) 53–78. https://doi.org/10.1146/ANNUREV-FOOD-072023-034528/CITE/REFWORKS.

[7] A. Baroni, E. Buommino, V. De Gregorio, E. Ruocco, V. Ruocco, R. Wolf, Structure and function of the epidermis related to barrier properties, Clin Dermatol 30 (2012) 257–262. https://doi.org/10.1016/J.CLINDERMATOL.2011.08.007.

[8] N. Akombaetwa, A.B. Ilangala, L. Thom, P.B. Memvanga, B.A. Witika, A.B. Buya, Current Advances in Lipid Nanosystems Intended for Topical and Transdermal Drug Delivery Applications, Pharmaceutics 2023, Vol. 15, Page 656 15 (2023) 656. https://doi.org/10.3390/PHARMACEUTICS15020656.

[9] L. Bartosova, J. Bajgar, Transdermal drug delivery in vitro using diffusion cells, Curr Med Chem 19 (2012) 4671–4677. https://doi.org/10.2174/092986712803306358.

[10] K.M.G. Taylor, M.E. Aulton, eds., Aulton's Pharmaceutics - the design and manufacture of medicines, 5th ed., Elsevier, 2018.

[11] M. Sala, R. Diab, A. Elaissari, H. Fessi, Lipid nanocarriers as skin drug delivery systems: Properties, mechanisms of skin interactions and medical applications, Int J Pharm 535 (2018) 1–17. https://doi.org/10.1016/J.IJPHARM.2017.10.046.

[12] A.C. Paiva-Santos, A.L. Silva, C. Guerra, D. Peixoto, M. Pereira-Silva, M. Zeinali, F. Mascarenhas-Melo, R. Castro, F. Veiga, Ethosomes as Nanocarriers for the Development of Skin Delivery Formulations, Pharm Res 38 (2021) 947–970. https://doi.org/10.1007/S11095-021-03053-5/FIGURES/5.

[13] E. Esposito, C. Nastruzzi, M. Sguizzato, R. Cortesi, Nanomedicines to Treat Skin Pathologies with Natural Molecules, Curr Pharm Des 25 (2019) 2323–2337. https://doi.org/10.2174/1381612825666190709210703.

[14] Y.Q. Yu, X. Yang, X.F. Wu, Y. Bin Fan, Enhancing Permeation of Drug Molecules Across the Skin via Delivery in Nanocarriers: Novel Strategies for Effective Transdermal Applications, Front Bioeng Biotechnol 9 (2021) 646554. https://doi.org/10.3389/FBIOE.2021.646554/BIBTEX.

[15] M.R. Prausnitz, R. Langer, Transdermal drug delivery, Nature Biotechnology 2008 26:11 26 (2008) 1261–1268. https://doi.org/10.1038/nbt.1504.

[16] L.A. Delouise, Applications of nanotechnology in dermatology, J Invest Dermatol 132 (2012) 964–975. https://doi.org/10.1038/JID.2011.425.

[17] W. Najahi-Missaoui, R.D. Arnold, B.S. Cummings, Safe Nanoparticles: Are We There Yet?, International Journal of Molecular Sciences 2021, Vol. 22, Page 385 22 (2020) 385. https://doi.org/10.3390/IJMS22010385.

[18] M. Sguizzato, E. Esposito, R. Cortesi, Lipid-Based Nanosystems as a Tool to Overcome Skin Barrier, International Journal of Molecular Sciences 2021, Vol. 22, Page 8319 22 (2021) 8319. https://doi.org/10.3390/IJMS22158319.

[19] E. Esposito, M. Drechsler, C. Nastruzzi, R. Cortesi, Cubic Phases, Cubosomes and Ethosomes for Cutaneous Application, Curr Pharm Des 22 (2016) 5382–5399. https://doi.org/10.2174/1381612822666160726123227.

[20] E. Touitou, N. Dayan, L. Bergelson, B. Godin, M. Eliaz, Ethosomes - Novel vesicular carriers for enhanced delivery: Characterization and skin penetration properties, Journal of Controlled Release 65 (2000) 403–418. https://doi.org/10.1016/S0168-3659(99)00222-9.

[21] D.B. Yarosh, Liposomes in investigative dermatology, Photodermatol Photoimmunol Photomed 17 (2001) 203–212. https://doi.org/10.1111/J.1600-0781.2001.170501.X.

[22] A. Ascenso, S. Raposo, C. Batista, P. Cardoso, T. Mendes, F.G. Praça, M.V.L.B. Bentley, S. Simões, Development, characterization, and skin delivery studies of related ultradeformable vesicles: transfersomes, ethosomes, and transethosomes, Int J Nanomedicine 10 (2015) 5837–5851. https://doi.org/10.2147/IJN.S86186.

[23] M. Emanet, G. Ciofani, Ethosomes as Promising Transdermal Delivery Systems of Natural-Derived Active Compounds, Adv Nanobiomed Res 3 (2023) 2300020. https://doi.org/10.1002/ANBR.202300020.

[24] C.K. Song, P. Balakrishnan, C.K. Shim, S.J. Chung, S. Chong, D.D. Kim, A novel vesicular carrier, transethosome, for enhanced skin delivery of voriconazole: characterization and in vitro/in vivo evaluation, Colloids Surf B Biointerfaces 92 (2012) 299–304. https://doi.org/10.1016/J.COLSURFB.2011.12.004.

[25] M. Sguizzato, F. Ferrara, S.S. Hallan, A. Baldisserotto, M. Drechsler, M. Malatesta, M. Costanzo, R. Cortesi, C. Puglia, G. Valacchi, E. Esposito, Ethosomes and transethosomes for mangiferin transdermal delivery, Antioxidants 10 (2021) 768. https://doi.org/10.3390/ANTIOX10050768/S1.

[26] M. Costanzo, E. Esposito, M. Sguizzato, M.A. Lacavalla, M. Drechsler, G. Valacchi, C. Zancanaro, M. Malatesta, Formulative Study and Intracellular Fate Evaluation of Ethosomes and Transethosomes for Vitamin D3 Delivery, International Journal of Molecular Sciences 2021, Vol. 22, Page 5341 22 (2021) 5341. https://doi.org/10.3390/IJMS22105341.

[27] E. Esposito, L. Calderan, A. Galvan, E. Cappellozza, M. Drechsler, P. Mariani, A. Pepe, M. Sguizzato, E. Vigato, E. Dalla Pozza, M. Malatesta, Ex Vivo Evaluation of Ethosomes and Transethosomes Applied on Human Skin: A Comparative Study, International Journal of Molecular Sciences 2022, Vol. 23, Page 15112 23 (2022) 15112. https://doi.org/10.3390/IJMS232315112.

[28] S. Milak, A. Zimmer, Glycerol monooleate liquid crystalline phases used in drug delivery systems, Int J Pharm 478 (2015) 569–587. https://doi.org/10.1016/J.IJPHARM.2014.11.072.

[29] C. V. Kulkarni, W. Wachter, G. Iglesias-Salto, S. Engelskirchen, S. Ahualli, Monoolein: a magic lipid?, Physical Chemistry Chemical Physics 13 (2011) 3004–3021. https://doi.org/10.1039/C0CP01539C.

[30] V.P. Chavda, S. Dyawanapelly, S. Dawre, I. Ferreira-Faria, R. Bezbaruah, N. Rani Gogoi, P. Kolimi, D.J. Dave, A.C. Paiva-Santos, L.K. Vora, Lyotropic liquid crystalline phases: Drug delivery and biomedical applications, Int J Pharm 647 (2023) 123546. https://doi.org/10.1016/J.IJPHARM.2023.123546.

[31] G. Blanco-Fernández, B. Blanco-Fernandez, A. Fernández-Ferreiro, F.J. Otero-Espinar, Lipidic lyotropic liquid crystals: Insights on biomedical applications, Adv Colloid Interface Sci 313 (2023) 102867. https://doi.org/10.1016/J.CIS.2023.102867.

[32] A.V.P. Silvestrini, A.L. Caron, J. Viegas, F.G. Praça, M.V.L.B. Bentley, Advances in lyotropic liquid crystal systems for skin drug delivery, Expert Opin Drug Deliv 17 (2020) 1781–1805. https://doi.org/10.1080/17425247.2020.1819979.

[33] L.B. Lopes, M.T. J Garcia, M.V. Lb Bentley, Chemical penetration enhancers, Ther Deliv 6 (2015) 1053–1061. https://doi.org/10.4155/TDE.15.61.

[34] M. Chountoulesi, S. Pispas, I.K. Tseti, C. Demetzos, Lyotropic Liquid Crystalline Nanostructures as Drug Delivery Systems and Vaccine Platforms, Pharmaceuticals 2022, Vol. 15, Page 429 15 (2022) 429. https://doi.org/10.3390/PH15040429.

[35] C. Puglia, M.R. Lauro, G.G. Tirendi, G.E. Fassari, C. Carbone, F. Bonina, G. Puglisi, Modern drug delivery strategies applied to natural active compounds, Expert Opin Drug Deliv 14 (2017) 755–768. https://doi.org/10.1080/17425247.2017.1234452.

[36] P. Ganesan, D.K. Choi, Current application of phytocompound-based nanocosmeceuticals for beauty and skin therapy, Int J Nanomedicine 11 (2016) 1987–2007. https://doi.org/10.2147/IJN.S104701.

[37] R.A. Sharma, A.J. Gescher, W.P. Steward, Curcumin: the story so far, Eur J Cancer 41 (2005) 1955–1968. https://doi.org/10.1016/J.EJCA.2005.05.009.

[38] A.R. Vaughn, A. Branum, R.K. Sivamani, Effects of Turmeric (Curcuma longa) on Skin Health: A Systematic Review of the Clinical Evidence, Phytother Res 30 (2016) 1243–1264. https://doi.org/10.1002/PTR.5640.

[39] S. Prasad, A.K. Tyagi, B.B. Aggarwal, Recent developments in delivery, bioavailability, absorption and metabolism of curcumin: the golden pigment from golden spice, Cancer Res Treat 46 (2014) 2–18. https://doi.org/10.4143/CRT.2014.46.1.2.

[40] S.J. Hewlings, D.S. Kalman, Curcumin: A Review of Its Effects on Human Health, Foods 2017, Vol. 6, Page 92 6 (2017) 92. https://doi.org/10.3390/FOODS6100092.

[41] S. V. Jovanovic, S. Steenken, C.W. Boone, M.G. Simic, H-Atom Transfer Is A Preferred Antioxidant Mechanism of Curcumin, J Am Chem Soc 121 (1999) 9677–9681. https://doi.org/10.1021/JA991446M.

[42] V.P. Menon, A.R. Sudheer, Antioxidant and anti-inflammatory properties of curcumin, Adv Exp Med Biol 595 (2007) 105–125. https://doi.org/10.1007/978-0-387-46401-5_3.

[43] L. Vollono, M. Falconi, R. Gaziano, F. Iacovelli, E. Dika, C. Terracciano, L. Bianchi, E. Campione, Potential of Curcumin in Skin Disorders, Nutrients 11 (2019). https://doi.org/10.3390/NU11092169.

[44] I.U. Haq, M. Imran, M. Nadeem, T. Tufail, T.A. Gondal, M.S. Mubarak, Piperine: A review of its biological effects, Phytother Res 35 (2021) 680–700. https://doi.org/10.1002/PTR.6855.

[45] P. Gohil, A. Mehta, Molecular targets of pepper as bioavailability enhancer, Orient Pharm Exp Med 9 (2009) 269–276. https://doi.org/10.3742/OPEM.2009.9.4.269.

[46] M. Imran, M. Samal, A. Qadir, A. Ali, S.R. Mir, A critical review on the extraction and pharmacotherapeutic activity of piperine, Polim Med 52 (2022) 29–34. https://doi.org/10.17219/PIM/145512.

[47] S. Arora, B. Singh, S. Kumar, A. Kumar, A. Singh, C. Singh, Piperine loaded drug delivery systems for improved biomedical applications: Current status and future directions, Health Sciences Review 9 (2023) 100138. https://doi.org/10.1016/J.HSR.2023.100138.

[48] K. Kesarwani, R. Gupta, Bioavailability enhancers of herbal origin: an overview, Asian Pac J Trop Biomed 3 (2013) 253–266. https://doi.org/10.1016/S2221-1691(13)60060-X.

[49] H. Lu, H. Gong, J. Du, W. Gao, J. Xu, X. Cai, Y. Yang, H. Xiao, Piperine ameliorates psoriatic skin inflammation by inhibiting the phosphorylation of STAT3, Int Immunopharmacol 119 (2023) 110221. https://doi.org/10.1016/J.INTIMP.2023.110221.

[50] A. Das, A.B. Ahmed, Natural permeation enhancer for transdermal drug delivery system and permeation evaluation: a review, Asian Journal of Pharmaceutical and Clinical Research 10 (2017) 5–9. https://doi.org/10.22159/AJPCR.2017.V10I9.19389.

[51] G. Jejurkar, M. Chavan, Therapeutic benefits of gossypin as an emerging phytoconstituents of Hibiscus spp.: a critical review, Future Journal of Pharmaceutical Sciences 2023 9:1 9 (2023) 1–13. https://doi.org/10.1186/S43094-023-00547-4.

[52] B. Song, X. Shen, C. Tong, S. Zhang, Q. Chen, Y. Li, S. Li, Gossypin: A flavonoid with diverse pharmacological effects, Chem Biol Drug Des 101 (2023) 131–137. https://doi.org/10.1111/CBDD.14152.

[53] S. Bhaskaran, K. V. Dileep, S.S. Deepa, C. Sadasivan, M. Klausner, N.K. Krishnegowda, R.R. Tekmal, J.L. VandeBerg, H.B. Nair, Gossypin as a novel selective dual inhibitor of V-RAF murine sarcoma viral oncogene homolog B1 and cyclin-dependent kinase 4 for melanoma, Mol Cancer Ther 12 (2013) 361–372. https://doi.org/10.1158/1535-7163.MCT-12-0965.

[54] J. Rajkumar, G. V. Radha, S. Ganapaty, Topical drug delivery of gossypin from proniosomal gel formulations: in vitro efficacy against human melanoma cells, International Journal of Applied Pharmaceutics 13 (2021) 144–152. https://doi.org/10.22159/IJAP.2021V13I1.39609.

[55] J. Sharifi-Rad, C. Quispe, M. Imran, A. Rauf, M. Nadeem, T.A. Gondal, B. Ahmad, M. Atif, M.S. Mubarak, O. Sytar, O.M. Zhilina, E.R. Garsiya, A. Smeriglio, D. Trombetta, D.G. Pons, M. Martorell, S.M. Cardoso, A.F.A. Razis, U. Sunusi, R.M. Kamal, L.S. Rotariu, M. Butnariu, A.O. Docea, D. Calina, Genistein: An Integrative Overview of Its Mode of Action, Pharmacological Properties, and Health Benefits, Oxid Med Cell Longev 2021 (2021) 3268136. https://doi.org/10.1155/2021/3268136.

[56] R.R. Yeligar, K.K. Sarwa, M. Chandrakar, M.S. Jangde, Nanotechnology-Based Delivery of Genistein to Overcome Physicochemical Hindrance and Enhance Therapeutic Response in Skin Cancer, BioNanoScience 2023 13:3 13 (2023) 1339–1358. https://doi.org/10.1007/S12668-023-01118-W.

[57] A. Arora, M.G. Nair, G.M. Strasburg, Antioxidant activities of isoflavones and their biological metabolites in a liposomal system, Arch Biochem Biophys 356 (1998) 133–141. https://doi.org/10.1006/ABBI.1998.0783.

[58] M.B. Ruiz-Larrea, A.R. Mohan, G. Paganga, N.J. Miller, G.P. Bolwell, C.A. Rice-Evans, Antioxidant activity of phytoestrogenic isoflavones, Free Radic Res 26 (1997) 63–70. https://doi.org/10.3109/10715769709097785.

[59] H. Wei, R. Saladi, Y. Lu, Y. Wang, S.R. Palep, J. Moore, R. Phelps, E. Shyong, M.G. Lebwohl, Isoflavone genistein: photoprotection and clinical implications in dermatology, J Nutr 133 (2003). https://doi.org/10.1093/JN/133.11.3811S.

[60] S.S. Hallan, M. Sguizzato, P. Mariani, R. Cortesi, N. Huang, F. Simelière, N. Marchetti, M. Drechsler, T. Ruzgas, E. Esposito, Design and Characterization of Ethosomes for Transdermal Delivery of Caffeic Acid, Pharmaceutics 12 (2020) 1–18. https://doi.org/10.3390/PHARMACEUTICS12080740.

[61] F. Ferrara, M. Benedusi, M. Sguizzato, R. Cortesi, A. Baldisserotto, R. Buzzi, G. Valacchi, E. Esposito, Ethosomes and Transethosomes as Cutaneous Delivery Systems for Quercetin: A Preliminary Study on Melanoma Cells, Pharmaceutics 14 (2022) 1038. https://doi.org/10.3390/PHARMACEUTICS14051038/S1.

[62] Mingfu Wang, Jiangang Li, Meera Rangarajan, Yu Shao, Edmond J. LaVoie, and Tzou-Chi Huang, Chi-Tang Ho*, Antioxidative Phenolic Compounds from Sage (Salvia officinalis), J Agric Food Chem 46 (1998) 4869–4873. https://doi.org/10.1021/JF980614B.

[63] I. Popov, G. Lewin, Antioxidative homeostasis: characterization by means of chemiluminescent technique, Methods Enzymol 300 (1999) 437–456. https://doi.org/10.1016/S0076-6879(99)00149-4.

[64] F. Ferrara, B. Woodby, A. Pecorelli, M.L. Schiavone, E. Pambianchi, N. Messano, J.P. Therrien, H. Choudhary, G. Valacchi, Additive effect of combined pollutants to UV induced skin OxInflammation damage. Evaluating the protective topical application of a cosmeceutical mixture formulation, Redox Biol 34 (2020) 101481. https://doi.org/10.1016/J.REDOX.2020.101481.

[65] S. Vertuani, P. Ziosi, N. Solaroli, V. Buzzoni, M. Carli, E. Lucchi, L. Valgimigli, G. Baratto, S. Manfredini, Determination of antioxidant efficacy of cosmetic formulations by non-invasive measurements, Skin Res Technol 9 (2003) 245–253. https://doi.org/10.1034/J.1600-0846.2003.00018.X.

[66] T. Münzel, A. Daiber, Environmental Stressors and Their Impact on Health and Disease with Focus on Oxidative Stress, Antioxid Redox Signal 28 (2018) 735–740. https://doi.org/10.1089/ARS.2017.7488.

[67] M. Nawaz, J. Sun, S. Shabbir, W.A. Khattak, G. Ren, X. Nie, Y. Bo, Q. Javed, D. Du, C. Sonne, A review of plants strategies to resist biotic and abiotic environmental stressors, Sci Total Environ 900 (2023). https://doi.org/10.1016/J.SCITOTENV.2023.165832.

[68] C. Parrado, S. Mercado-Saenz, A. Perez-Davo, Y. Gilaberte, S. Gonzalez, A. Juarranz, Environmental Stressors on Skin Aging. Mechanistic Insights, Front Pharmacol 10 (2019). https://doi.org/10.3389/FPHAR.2019.00759.

[69] K.O. Shin, Y. Uchida, K. Park, Diesel Particulate Extract Accelerates Premature Skin Aging in Human Fibroblasts via Ceramide-1-Phosphate-Mediated Signaling Pathway, International Journal of Molecular Sciences 2022, Vol. 23, Page 2691 23 (2022) 2691. https://doi.org/10.3390/IJMS23052691.

[70] G. Valacchi, E. Pambianchi, S. Coco, A. Pulliero, A. Izzotti, MicroRNA Alterations Induced in Human Skin by Diesel Fumes, Ozone, and UV Radiation, Journal of Personalized Medicine 2022, Vol. 12, Page 176 12 (2022) 176. https://doi.org/10.3390/JPM12020176.

[71] Z. Celebi Sozener, Ü. Özbey Yücel, S. Altiner, B. Ozdel Oztürk, P. Cerci, M. Türk, B. Gorgülü Akin, M. Akdis, I. Yilmaz, C. Ozdemir, D. Mungan, C.A. Akdis, The External Exposome and Allergies: From the Perspective of the Epithelial Barrier Hypothesis, Frontiers in Allergy 3 (2022). https://doi.org/10.3389/FALGY.2022.887672.

[72] A. V. Nguyen, A.M. Soulika, The Dynamics of the Skin's Immune System, International Journal of Molecular Sciences 2019, Vol. 20, Page 1811 20 (2019) 1811. https://doi.org/10.3390/IJMS20081811.

[73] S. Fuloria, J. Mehta, A. Chandel, M. Sekar, N.N.I.M. Rani, M.Y. Begum, V. Subramaniyan, K. Chidambaram, L. Thangavelu, R. Nordin, Y.S. Wu, K. V. Sathasivam, P.T. Lum, D.U. Meenakshi, V. Kumarasamy, A.K. Azad, N.K. Fuloria, A Comprehensive Review on the Therapeutic Potential of Curcuma longa Linn. in Relation to its Major Active Constituent Curcumin, Front Pharmacol 13 (2022) 820806. https://doi.org/10.3389/FPHAR.2022.820806/BIBTEX.

[74] S.S. Yadav, M.K. Singh, S. Hussain, P. Dwivedi, S. Khattri, K. Singh, Therapeutic spectrum of piperine for clinical practice: a scoping review, Crit Rev Food Sci Nutr 63 (2023) 5813–5840. https://doi.org/10.1080/10408398.2021.2024792.

[75] A. Giordano, G. Tommonaro, Curcumin and Cancer, Nutrients 2019, Vol. 11, Page 2376 11 (2019) 2376. https://doi.org/10.3390/NU11102376.

[76] S.I. Sohn, A. Priya, B. Balasubramaniam, P. Muthuramalingam, C. Sivasankar, A. Selvaraj, A. Valliammai, R. Jothi, S. Pandian, Biomedical applications and bioavailability of curcumin—an updated overview, Pharmaceutics 13 (2021) 2102. https://doi.org/10.3390/PHARMACEUTICS13122102/S1.

[77] N. Ghobadi, A. Asoodeh, Co-administration of curcumin with other phytochemicals improves anticancer activity by regulating multiple molecular targets, Phytotherapy Research 37 (2023) 1688–1702. https://doi.org/10.1002/PTR.7794.

[78] K. Wdowiak, R. Pietrzak, E. Tykarska, J. Cielecka-Piontek, Hot-Melt Extrusion as an Effective Technique for Obtaining an Amorphous System of Curcumin and Piperine with Improved Properties Essential for Their Better Biological Activities, Molecules 28 (2023) 3848. https://doi.org/10.3390/MOLECULES28093848/S1.

[79] L. Shi, W. Xun, W. Peng, H. Hu, T. Cao, G. Hou, Effect of the Single and Combined Use of Curcumin and Piperine on Growth Performance, Intestinal Barrier Function, and Antioxidant Capacity of Weaned Wuzhishan Piglets, Front Vet Sci 7 (2020) 554891. https://doi.org/10.3389/FVETS.2020.00418/BIBTEX.

[80] K. Srinivasan, Black Pepper and its Pungent Principle-Piperine: A Review of Diverse Physiological Effects, Crit Rev Food Sci Nutr 47 (2007) 735–748. https://doi.org/10.1080/10408390601062054.

[81] N. Atal, K.L. Bedi, Bioenhancers: Revolutionary concept to market, J Ayurveda Integr Med 1 (2010) 96–99. https://doi.org/10.4103/0975-9476.65073.

[82] C. Jantarat, P. Sirathanarun, S. Boonmee, W. Meechoosin, H. Wangpittaya, Effect of Piperine on Skin Permeation of Curcumin from a Bacterially Derived Cellulose-Composite Double-Layer Membrane for Transdermal Curcumin Delivery, Scientia Pharmaceutica 2018, Vol. 86, Page 39 86 (2018) 39. https://doi.org/10.3390/SCIPHARM86030039.

[83] H. Abolhassani, M.S. Safavi, S. Handali, M. Nosrati, S.A. Shojaosadati, Synergistic Effect of Self-Assembled Curcumin and Piperine Co-Loaded Human Serum Albumin Nanoparticles on Suppressing Cancer Cells, Drug Dev Ind Pharm 46 (2020) 1647–1655. https://doi.org/10.1080/03639045.2020.1820032.

[84] S. Ahmad, A. Hafeez, Formulation and Development of Curcumin–Piperine-Loaded S-SNEDDS for the Treatment of Alzheimer's Disease, Mol Neurobiol 60 (2023) 1067–1082. https://doi.org/10.1007/S12035-022-03089-7/FIGURES/9.

[85] E. Esposito, L. Ravani, P. Mariani, C. Contado, M. Drechsler, C. Puglia, R. Cortesi, Curcumin containing monoolein aqueous dispersions: A preformulative study, Materials Science and Engineering: C 33 (2013) 4923–4934. https://doi.org/10.1016/J.MSEC.2013.08.017.

[86] F.A.S. Politi, S.G. Carvalho, C.F. Rodero, K.P. dos Santos, A.B. Meneguin, R. Sorrechia, L.A. Chiavacci, M. Chorilli, Piperine-loaded nanoparticles incorporated into hyaluronic acid/sodium alginate-based membranes for the treatment of inflammatory skin diseases, Int J Biol Macromol 227 (2023) 736–748. https://doi.org/10.1016/J.IJBIOMAC.2022.12.147.

[87] B. Kumar, P.K. Sahoo, S. Manchanda, Curcumin Loaded Ethosomal Gel for Improved Topical Delivery: Formulation, Characterization and Ex-vivo Studies, Pharm Nanotechnol 9 (2021) 281–287. https://doi.org/10.2174/2211738509666210208225826.

[88] P. Upadhyay, D. Singh, S. Upadhyay, Vesicular Approach Review on Nanocarriers bearing Curcumin and Applications, Recent Adv Drug Deliv Formul 16 (2022) 256–269. https://doi.org/10.2174/2667387816666220404092415.

[89] M.R. Peram, S. Jalalpure, V. Kumbar, S. Patil, S. Joshi, K. Bhat, P. Diwan, Factorial design based curcumin ethosomal nanocarriers for the skin cancer delivery: in vitro evaluation, J Liposome Res 29 (2019) 291–311. https://doi.org/10.1080/08982104.2018.1556292.

[90] P. Kumar, D.K. Sharma, M.S. Ashawat, Topical creams of piperine loaded lipid nanocarriers for management of atopic dermatitis: development, characterization, and in vivo investigation using BALB/c mice model, J Liposome Res 32 (2022) 62–73. https://doi.org/10.1080/08982104.2021.1880436.

[91] T.-I. Hyeon, K.-S. Yoon, Ethosome Containing Ceramide as a Skin Carrier of Active Ingredients, Curr Drug Deliv 20 (2022) 927–942. https://doi.org/10.2174/1567201819666220720123737.

[92] S. Pozos-Nonato, C.L. Domínguez-Delgado, K.A. Campos-Santander, A.A. Benavides, S.M. Pacheco-Ortin, R.I. Higuera-Piedrahita, G. Resendiz-González, E.M. Molina-Trinidad, Novel Nanotechnological Strategies for Skin Anti-aging, Curr Pharm Biotechnol 24 (2022) 1397–1419. https://doi.org/10.2174/1389201024666221223095315.

[93] B. Lin, W. Wang, W. Ba, H. Li, J. Fan, Preparation and partial pharmacodynamic studies of luliconazole ethosomes, Clin Exp Pharmacol Physiol 49 (2022) 549–557. https://doi.org/10.1111/1440-1681.13623.

[94] A.A. Aljohani, M.A. Alanazi, L.A. Munahhi, J.D. Hamroon, Y. Mortagi, M. Qushawy, G.M. Soliman, Binary ethosomes for the enhanced topical delivery and antifungal efficacy of ketoconazole, OpenNano 11 (2023) 100145. https://doi.org/10.1016/J.ONANO.2023.100145.

[95] S.H. Abd El-Alim, A.A. Kassem, M. Basha, A. Salama, Comparative study of liposomes, ethosomes and transfersomes as carriers for enhancing the transdermal delivery of diflunisal: In vitro and in vivo evaluation, Int J Pharm 563 (2019) 293–303. https://doi.org/10.1016/J.IJPHARM.2019.04.001.

[96] S.B. Syed, H. Arya, I.H. Fu, T.K. Yeh, L. Periyasamy, H.P. Hsieh, M.S. Coumar, Targeting P-glycoprotein: Investigation of piperine analogs for overcoming drug resistance in cancer, Scientific Reports 2017 7:1 7 (2017) 1–18. https://doi.org/10.1038/s41598-017-08062-2.

[97] M.D. Ciuca, R.C. Racovita, Curcumin: Overview of Extraction Methods, Health Benefits, and Encapsulation and Delivery Using Microemulsions and Nanoemulsions, International Journal of Molecular Sciences 2023, Vol. 24, Page 8874 24 (2023) 8874. https://doi.org/10.3390/IJMS24108874.

[98] V. Patial, S. Mahesh, S. Sharma, K. Pratap, D. Singh, Y.S. Padwad, Synergistic effect of curcumin and piperine in suppression of DENA-induced hepatocellular carcinoma in rats, Environ Toxicol Pharmacol 40 (2015) 445–452. https://doi.org/10.1016/J.ETAP.2015.07.012.

[99] Y. Panahi, M.S. Hosseini, N. Khalili, E. Naimi, M. Majeed, A. Sahebkar, Antioxidant and anti-inflammatory effects of curcuminoid-piperine combination in subjects with metabolic syndrome: A randomized controlled trial and an updated meta-analysis, Clin Nutr 34 (2015) 1101–1108. https://doi.org/10.1016/J.CLNU.2014.12.019.

[100] E. Medicines Agency, Draft guideline on quality and equivalence of topical products, (n.d.). www.ema.europa.eu/contact (accessed November 1, 2024).

[101] P. Costa, J.M. Sousa Lobo, Modeling and comparison of dissolution profiles, European Journal of Pharmaceutical Sciences 13 (2001) 123–133. https://doi.org/10.1016/S0928-0987(01)00095-1.

[102] X. Liu, H. Liu, J. Liu, Z. He, C. Ding, G. Huang, W. Zhou, L. Zhou, Preparation of a ligustrazine ethosome patch and its evaluation in vitro and in vivo, Int J Nanomedicine 6 (2011) 241–247. https://doi.org/10.2147/IJN.S16044.

[103] A. Haq, B. Goodyear, D. Ameen, V. Joshi, B. Michniak-Kohn, Strat-M® synthetic membrane: Permeability comparison to human cadaver skin, Int J Pharm 547 (2018) 432–437. https://doi.org/10.1016/J.IJPHARM.2018.06.012.

[104] S.F. Ng, J. Rouse, D. Sanderson, G. Eccleston, A Comparative Study of Transmembrane Diffusion and Permeation of Ibuprofen across Synthetic Membranes Using Franz Diffusion Cells, Pharmaceutics 2010, Vol. 2, Pages 209-223 2 (2010) 209–223. https://doi.org/10.3390/PHARMACEUTICS2020209.

[105] ⟨1724⟩ Semisolid Drug Products—Performance Tests, (n.d.). https://doi.org/10.31003/USPNF_M5695_02_01.

[106] D. McDaniel, P. Farris, G. Valacchi, Atmospheric skin aging—Contributors and inhibitors, J Cosmet Dermatol 17 (2018) 124–137. https://doi.org/10.1111/JOCD.12518.

[107] A. Pecorelli, B. Woodby, R. Prieux, G. Valacchi, Involvement of 4-hydroxy-2-nonenal in pollution-induced skin damage, BioFactors 45 (2019) 536–547. https://doi.org/10.1002/BIOF.1513.

[108] K.I. Priyadarsini, D.K. Maity, G.H. Naik, M.S. Kumar, M.K. Unnikrishnan, J.G. Satav, H. Mohan, Role of phenolic O-H and methylene hydrogen on the free radical reactions and antioxidant activity of curcumin, Free Radic Biol Med 35 (2003) 475–484. https://doi.org/10.1016/S0891-5849(03)00325-3.

[109] R. Mittal, R.L. Gupta, In vitro antioxidant activity of piperine, Methods Find Exp Clin Pharmacol 22 (2000) 271–274. https://doi.org/10.1358/MF.2000.22.5.796644.

[110] G. Bocheva, R.M. Slominski, A.T. Slominski, Environmental Air Pollutants Affecting Skin Functions with Systemic Implications, International Journal of Molecular Sciences 2023, Vol. 24, Page 10502 24 (2023) 10502. https://doi.org/10.3390/IJMS241310502.

[111] R. Prieux, M. Eeman, B. Rothen-Rutishauser, G. Valacchi, Mimicking cigarette smoke exposure to assess cutaneous toxicity, Toxicology in Vitro 62 (2020) 104664. https://doi.org/10.1016/J.TIV.2019.104664.

[112] D.S. Hieda, L. Anastacio da Costa Carvalho, B. Vaz de Mello, E.A. de Oliveira, S. Romano de Assis, J. Wu, L. Du-Thumm, C.L. Viana da Silva, D.A. Roubicek, S.S. Maria-Engler, S. Berlanga de Moraes Barros, Air Particulate Matter Induces Skin Barrier Dysfunction and Water Transport Alteration on a Reconstructed Human Epidermis Model, J Invest Dermatol 140 (2020) 2343-2352.e3. https://doi.org/10.1016/J.JID.2020.03.971.

[113] J. Ivarsson, A. Pecorelli, M.A. Lila, G. Valacchi, Blueberry Supplementation and Skin Health, Antioxidants 2023, Vol. 12, Page 1261 12 (2023) 1261. https://doi.org/10.3390/ANTIOX12061261.

[114] E. Pambianchi, F. Ferrara, A. Pecorelli, B. Woodby, M. Grace, J.P. Therrien, M.A. Lila, G. Valacchi, Blueberry Extracts as a Novel Approach to Prevent Ozone-Induced Cutaneous Inflammasome Activation, Oxid Med Cell Longev 2020 (2020) 9571490. https://doi.org/10.1155/2020/9571490.

[115] X. Zhu, X. Zeng, X. Zhang, W. Cao, Y. Wang, H. Chen, T. Wang, H.I. Tsai, R. Zhang, D. Chang, S. He, L. Mei, X. Shi, The effects of quercetin-loaded PLGA-TPGS nanoparticles on ultraviolet B-induced skin damages in vivo, Nanomedicine 12 (2016) 623–632. https://doi.org/10.1016/J.NANO.2015.10.016.

[116] P. Liczbiński, J. Michałowicz, B. Bukowska, Molecular mechanism of curcumin action in signaling pathways: Review of the latest research, Phytotherapy Research 34 (2020) 1992–2005. https://doi.org/10.1002/PTR.6663.

[117] M.R. Islam, A. Rauf, S. Akash, S.I. Trisha, A.H. Nasim, M. Akter, P.S. Dhar, H.A. Ogaly, H.A. Hemeg, P. Wilairatana, M. Thiruvengadam, Targeted therapies of curcumin focus on its therapeutic benefits in cancers and human health: Molecular signaling pathway-based approaches and future perspectives, Biomedicine & Pharmacotherapy 170 (2024) 116034. https://doi.org/10.1016/J.BIOPHA.2023.116034.

[118] S. Singh, B.B. Aggarwal, Activation of transcription factor NF-κB is suppressed by curcumin (diferulolylmethane), Journal of Biological Chemistry 270 (1995) 24995–25000. https://doi.org/10.1074/JBC.270.42.24995/ASSET/3CC831F6-C3B1-459A-BEDB-E7ABA0F34F94/MAIN.ASSETS/GR7.JPG.

[119] J. Huang, Q. Yi, Y. You, Y. Chen, T. Niu, Y. Li, J. Zhang, X. Ji, G. Xu, W. Zou, F. Ji, W. Luo, Curcumin suppresses oxidative stress via regulation of ROS/NF-κB signaling pathway to protect retinal vascular endothelial cell in diabetic retinopathy, Mol Cell Toxicol 17 (2021) 367–376. https://doi.org/10.1007/S13273-021-00144-7/FIGURES/4.

[120] C.R. Pradeep, G. Kuttan, Piperine is a potent inhibitor of nuclear factor-κB (NF-κB), c-Fos, CREB, ATF-2 and proinflammatory cytokine gene expression in B16F-10 melanoma cells, Int Immunopharmacol 4 (2004) 1795–1803. https://doi.org/10.1016/J.INTIMP.2004.08.005.

[121] P. Saha, S. Durugkar, S. Jain, P.A. Shantanu, S.R. Panda, A. Jala, S. Gokhale, P. Sharma, V.G.M. Naidu, Piperine Attenuates Cigarette Smoke-Induced Oxidative Stress, Lung Inflammation, and Epithelial–Mesenchymal Transition by Modulating the SIRT1/Nrf2 Axis, Int J Mol Sci 23 (2022) 14722. https://doi.org/10.3390/IJMS232314722/S1.

[122] S.M. Pilkington, S. Bulfone-Paus, C.E.M. Griffiths, R.E.B. Watson, Inflammaging and the Skin, Journal of Investigative Dermatology 141 (2021) 1087–1095. https://doi.org/10.1016/J.JID.2020.11.006.

[123] P. Pittayapruek, J. Meephansan, O. Prapapan, M. Komine, M. Ohtsuki, Role of Matrix Metalloproteinases in Photoaging and Photocarcinogenesis, International Journal of Molecular Sciences 2016, Vol. 17, Page 868 17 (2016) 868. https://doi.org/10.3390/IJMS17060868.

[124] M. Panchatcharam, S. Miriyala, V.S. Gayathri, L. Suguna, Curcumin improves wound healing by modulating collagen and decreasing reactive oxygen species, Mol Cell Biochem 290 (2006) 87–96. https://doi.org/10.1007/S11010-006-9170-2/METRICS.

[125] D. Kumar, M. Kumar, C. Saravanan, S.K. Singh, Curcumin: a potential candidate for matrix metalloproteinase inhibitors, Expert Opin Ther Targets 16 (2012) 959–972. https://doi.org/10.1517/14728222.2012.710603.

[126] A. Field, Discovering Statistics Using Spss, London, UK, 2009.

[127] G. Valacchi, C. Sticozzi, A. Pecorelli, F. Cervellati, C. Cervellati, E. Maioli, Cutaneous responses to environmental stressors, Ann N Y Acad Sci 1271 (2012) 75–81. https://doi.org/10.1111/J.1749-6632.2012.06724.X.

[128] X. Gu, Z. Li, J. Su, Air pollution and skin diseases: A comprehensive evaluation of the associated mechanism, Ecotoxicol Environ Saf 278 (2024). https://doi.org/10.1016/J.ECOENV.2024.116429.

[129] S. Steiner, C. Bisig, A. Petri-Fink, B. Rothen-Rutishauser, Diesel exhaust: current knowledge of adverse effects and underlying cellular mechanisms, Archives of Toxicology 2016 90:7 90 (2016) 1541–1553. https://doi.org/10.1007/S00204-016-1736-5.

[130] C.A. Weitekamp, L.B. Kerr, L. Dishaw, J. Nichols, M. Lein, M.J. Stewart, A systematic review of the health effects associated with the inhalation of particle-filtered and whole diesel exhaust, Inhal Toxicol 32 (2020) 1–13. https://doi.org/10.1080/08958378.2020.1725187.

[131] K.E. Kim, D. Cho, H.J. Park, Air pollution and skin diseases: Adverse effects of airborne particulate matter on various skin diseases, Life Sci 152 (2016) 126–134. https://doi.org/10.1016/J.LFS.2016.03.039.

[132] F. Papaccio, A. D'arino, S. Caputo, B. Bellei, Focus on the Contribution of Oxidative Stress in Skin Aging, Antioxidants (Basel) 11 (2022). https://doi.org/10.3390/ANTIOX11061121.

[133] J.M. Jaffri, Reactive Oxygen Species and Antioxidant System in Selected Skin Disorders, Malays J Med Sci 30 (2023) 7–20. https://doi.org/10.21315/MJMS2023.30.1.2.

[134] M. Rakotoarisoa, B. Angelov, V.M. Garamus, A. Angelova, Curcumin- and Fish Oil-Loaded Spongosome and Cubosome Nanoparticles with Neuroprotective Potential against H 2 O 2 -Induced Oxidative Stress in Differentiated Human SH-SY5Y Cells, ACS Omega 4 (2019) 3061–3073. https://doi.org/10.1021/ACSOMEGA.8B03101/ASSET/IMAGES/MEDIUM/AO-2018-031015_M002.GIF.

[135] M. Rakotoarisoa, B. Angelov, M. Drechsler, V. Nicolas, T. Bizien, Y.E. Gorshkova, Y. Deng, A. Angelova, Liquid crystalline lipid nanoparticles for combined delivery of curcumin, fish oil and BDNF: In vitro neuroprotective potential in a cellular model of tunicamycin-induced endoplasmic reticulum stress, Smart Mater Med 3 (2022) 274–288. https://doi.org/10.1016/J.SMAIM.2022.03.001.

[136] G. Valacchi, F. Virgili, C. Cervellati, A. Pecorelli, OxInflammation: From Subclinical Condition to Pathological Biomarker, Front Physiol 9 (2018). https://doi.org/10.3389/FPHYS.2018.00858.

[137] Z. Wu, X. Tang, S. Liu, S. Li, X. Zhao, Y. Wang, X. Wang, H. Li, Mechanism underlying joint loading and controlled release of β-carotene and curcumin by octenylsuccinated Gastrodia elata starch aggregates, Food Research International 172 (2023) 113136. https://doi.org/10.1016/J.FOODRES.2023.113136.

[138] F. Ferrara, A. Pecorelli, E. Pambianchi, S. White, H. Choudhary, A. Casoni, G. Valacchi, Vitamin C compounds mixture prevents skin barrier alterations and inflammatory responses upon real life multi pollutant exposure, Exp Dermatol 33 (2024). https://doi.org/10.1111/EXD.15000.

[139] C. Baudouin, M. Charveron, R. Tarroux, Y. Gall, Environmental pollutants and skin cancer, Cell Biol Toxicol 18 (2002) 341–348. https://doi.org/10.1023/A:1019540316060.

[140] E. Esposito, C. Sticozzi, L. Ravani, M. Drechsler, X.M. Muresan, F. Cervellati, R. Cortesi, G. Valacchi, Effect of new curcumin-containing nanostructured lipid dispersions on human keratinocytes proliferative responses, Exp Dermatol 24 (2015). https://doi.org/10.1111/exd.12696.

[141] M. Sguizzato, M. Drechsler, A. Baldisserotto, R. Cortesi, E. Esposito, Antioxidant-containing monoolein aqueous dispersions: a preliminary study, Drug Deliv Transl Res 12 (2022) 1873–1880. https://doi.org/10.1007/S13346-022-01119-4.

[142] E. Esposito, R. Cortesi, M. Drechsler, L. Paccamiccio, P. Mariani, C. Contado, E. Stellin, E. Menegatti, F. Bonina, C. Puglia, Cubosome dispersions as delivery systems for percutaneous administration of indomethacin, Pharm Res 22 (2005). https://doi.org/10.1007/s11095-005-8176-x.

[143] B. Angelov, A. Angelova, R. Mutafchieva, S. Lesieur, U. Vainio, V.M. Garamus, G. V. Jensen, J.S. Pedersen, SAXS investigation of a cubic to a sponge (L3) phase transition in self-assembled lipid nanocarriers, Physical Chemistry Chemical Physics 13 (2011) 3073–3081. https://doi.org/10.1039/C0CP01029D.

[144] P. Mariani, V. Luzzati, H. Delacroix, Cubic phases of lipid-containing systems. Structure analysis and biological implications, J Mol Biol 204 (1988) 165–189. https://doi.org/10.1016/0022-2836(88)90607-9.

[145] J. Gustafsson, T. Nylander, M. Almgren, Phase Behavior and Aggregate Structure in Aqueous Mixtures of Sodium Cholate and Glycerol Monooleate, J Colloid Interface Sci 211 (1999) 326–335. https://doi.org/10.1006/JCIS.1998.5996.

[146] M. Rakotoarisoa, B. Angelov, S. Espinoza, K. Khakurel, T. Bizien, M. Drechsler, A. Angelova, Composition-Switchable Liquid Crystalline Nanostructures as Green Formulations of Curcumin and Fish Oil, ACS Sustain Chem Eng 9 (2021) 14821–14835. https://doi.org/10.1021/ACSSUSCHEMENG.1C04706/ASSET/IMAGES/MEDIUM/SC1C04706_0009.GIF.

[147] V. Luzzati, R. Vargas, P. Mariani, A. Gulik, H. Delacroix, Cubic phases of lipid-containing systems. Elements of a theory and biological connotations, J Mol Biol 229 (1993) 540–551. https://doi.org/10.1006/JMBI.1993.1053.

[148] S. Mazzoni, L.R.S. Barbosa, S.S. Funari, R. Itri, P. Mariani, Cytochrome-c Affects the Monoolein Polymorphism: Consequences for Stability and Loading Efficiency of Drug Delivery Systems, Langmuir 32 (2016) 873–881. https://doi.org/10.1021/ACS.LANGMUIR.5B03507.

[149] N.P. Aditya, M. Shim, I. Lee, Y. Lee, M.H. Im, S. Ko, Curcumin and genistein coloaded nanostructured lipid carriers: in vitro digestion and antiprostate cancer activity, J Agric Food Chem 61 (2013) 1878–1883. https://doi.org/10.1021/JF305143K.

[150] A. Sandilands, C. Sutherland, A.D. Irvine, W.H.I. McLean, Filaggrin in the frontline: role in skin barrier function and disease, J Cell Sci 122 (2009) 1285–1294. https://doi.org/10.1242/JCS.033969.

[151] G.F. Murphy, T.C. Flynn, R.H. Rice, G.S. Pinkus, Involucrin expression in normal and neoplastic human skin: a marker for keratinocyte differentiation, J Invest Dermatol 82 (1984) 453–457. https://doi.org/10.1111/1523-1747.EP12260945.

[152] L. Gardeazabal, A. Izeta, Elastin and collagen fibres in cutaneous wound healing, Exp Dermatol 33 (2024) e15052. https://doi.org/10.1111/EXD.15052.

[153] M. Arnold, D. Singh, M. Laversanne, J. Vignat, S. Vaccarella, F. Meheus, A.E. Cust, E. De Vries, D.C. Whiteman, F. Bray, Global Burden of Cutaneous Melanoma in 2020 and Projections to 2040, JAMA Dermatol 158 (2022) 495–503. https://doi.org/10.1001/JAMADERMATOL.2022.0160.

[154] D. Schadendorf, A.C.J. van Akkooi, C. Berking, K.G. Griewank, R. Gutzmer, A. Hauschild, A. Stang, A. Roesch, S. Ugurel, Melanoma, The Lancet 392 (2018) 971–984.

https://doi.org/10.1016/S0140-6736(18)31559-9/ASSET/8F42AA0D-C695-48AF-BE1A-49DF35F0B891/MAIN.ASSETS/GR4.SML.

[155] G.C. Leonardi, L. Falzone, R. Salemi, A. Zanghì, D.A. Spandidos, J.A. Mccubrey, S. Candido, M. Libra, Cutaneous melanoma: From pathogenesis to therapy (Review), Int J Oncol 52 (2018) 1071–1080. https://doi.org/10.3892/IJO.2018.4287.

[156] M. Benedusi, H. Lee, Y. Lim, G. Valacchi, Oxidative State in Cutaneous Melanoma Progression: A Question of Balance, Antioxidants 2024, Vol. 13, Page 1058 13 (2024) 1058. https://doi.org/10.3390/ANTIOX13091058.

[157] I. Kozar, C. Margue, S. Rothengatter, C. Haan, S. Kreis, Many ways to resistance: How melanoma cells evade targeted therapies, Biochimica et Biophysica Acta (BBA) - Reviews on Cancer 1871 (2019) 313–322. https://doi.org/10.1016/J.BBCAN.2019.02.002.

[158] P. Sitarek, T. Kowalczyk, J. Wieczfinska, A. Merecz-Sadowska, K. Górski, T. Śliwiński, E. Skała, Plant Extracts as a Natural Source of Bioactive Compounds and Potential Remedy for the Treatment of Certain Skin Diseases, Curr Pharm Des 26 (2020) 2859–2875. https://doi.org/10.2174/1381612826666200417160049.

[159] Y.E. Yoon, Y.J. Jung, S.J. Lee, The Anticancer Activities of Natural Terpenoids That Inhibit Both Melanoma and Non-Melanoma Skin Cancers, Int J Mol Sci 25 (2024). https://doi.org/10.3390/IJMS25084423.

[160] S. Choi, B. Kang, E. Yang, K. Kim, M.K. Kwak, P.S. Chang, H.S. Jung, Precise control of liposome size using characteristic time depends on solvent type and membrane properties, Scientific Reports 2023 13:1 13 (2023) 1–12. https://doi.org/10.1038/s41598-023-31895-z.

[161] E.M. Nsengiyumva, P. Alexandridis, Xanthan gum in aqueous solutions: Fundamentals and applications, Int J Biol Macromol 216 (2022) 583–604. https://doi.org/10.1016/J.IJBIOMAC.2022.06.189.

[162] M. Sguizzato, F. Ferrara, P. Mariani, A. Pepe, R. Cortesi, N. Huang, F. Simelière, P. Boldrini, A. Baldisserotto, G. Valacchi, E. Esposito, “Plurethosome” as vesicular system for cutaneous administration of mangiferin: Formulative study and 3D skin tissue evaluation, Pharmaceutics 13 (2021) 1124. https://doi.org/10.3390/PHARMACEUTICS13081124/S1.

[163] J.A. Nichols, S.K. Katiyar, Skin photoprotection by natural polyphenols: anti-inflammatory, antioxidant and DNA repair mechanisms, Arch Dermatol Res 302 (2010) 71–83. https://doi.org/10.1007/S00403-009-1001-3.

[164] J. D’Orazio, S. Jarrett, A. Amaro-Ortiz, T. Scott, UV radiation and the skin, Int J Mol Sci 14 (2013) 12222–12248. https://doi.org/10.3390/IJMS140612222.

[165] B. Armstrong, A. Kricker, How much melanoma is caused by sun exposure?, Melanoma Res 3 (1993) 395–402. https://doi.org/10.1097/00008390-199311000-00002.

[166] V. Madan, J.T. Lear, R.M. Szeimies, Non-melanoma skin cancer, Lancet 375 (2010) 673–685. https://doi.org/10.1016/S0140-6736(09)61196-X.

[167] A.-R. Ciuciulete, A.E. Stepan, B.C. Andreiana, C.E. Simionescu, Non-Melanoma Skin Cancer: Statistical Associations between Clinical Parameters, Curr Health Sci J 48 (2022) 110–115. https://doi.org/10.12865/CHSJ.48.01.16.

[168] M. Zambrano-Román, J.R. Padilla-Gutiérrez, Y. Valle, J.F. Muñoz-Valle, E. Valdés-Alvarado, Non-Melanoma Skin Cancer: A Genetic Update and Future Perspectives, Cancers 2022, Vol. 14, Page 2371 14 (2022) 2371. https://doi.org/10.3390/CANCERS14102371.

[169] A.C. Chen, G.M. Halliday, D.L. Damian, Non-melanoma skin cancer: Carcinogenesis and chemoprevention, Pathology 45 (2013) 331–341. https://doi.org/10.1097/PAT.0b013e32835f515c.

[170] Z.R. Huang, C.F. Hung, Y.K. Lin, J.Y. Fang, In vitro and in vivo evaluation of topical delivery and potential dermal use of soy isoflavones genistein and daidzein, Int J Pharm 364 (2008) 36–44. https://doi.org/10.1016/J.IJPHARM.2008.08.002.

[171] J.Y. Lin, J.A. Tournas, J.A. Burch, N.A. Monteiro-Riviere, J. Zielinski, Topical isoflavones provide effective photoprotection to skin, Photodermatol Photoimmunol Photomed 24 (2008) 61–66. https://doi.org/10.1111/J.1600-0781.2008.00329.X.

[172] E. Proksch, pH in nature, humans and skin, J Dermatol 45 (2018) 1044–1052. https://doi.org/10.1111/1346-8138.14489.

[173] Y. Xiao, C.T. Ho, Y. Chen, Y. Wang, Z. Wei, M. Dong, Q. Huang, Synthesis, Characterization, and Evaluation of Genistein-Loaded Zein/Carboxymethyl Chitosan Nanoparticles with Improved Water Dispersibility, Enhanced Antioxidant Activity, and Controlled Release Property, Foods 2020, Vol. 9, Page 1604 9 (2020) 1604. https://doi.org/10.3390/FOODS9111604.

[174] K. Spanou, A.I. Barbosa, A. Detsi, S.A. Costa Lima, S. Reis, Development and characterization of gel-like matrix containing genistein for skin application, J Drug Deliv Sci Technol 90 (2023) 105119. https://doi.org/10.1016/J.JDDST.2023.105119.

La borsa di dottorato cofinanziata con risorse del
Programma Operativo Nazionale Ricerca e Innovazione 2014-2020 (CCI 2014IT16M2OP005),
risorse Fondo Sociale Europeo REACT-EU, Azione I.1 “Dottorati Innovativi con caratterizzazione industriale”, Azione IV.4 “Dottorati e contratti di ricerca su tematiche dell’innovazione” e Azione IV.5 “Dottorati su tematiche Green”